A hydrodynamic study on floating export cable systems

Using finite element method modelling to study the hydrodynamic behaviour and optimise the design of floating export cable systems

Graduation thesis

M.A. (Marnix) Weiler

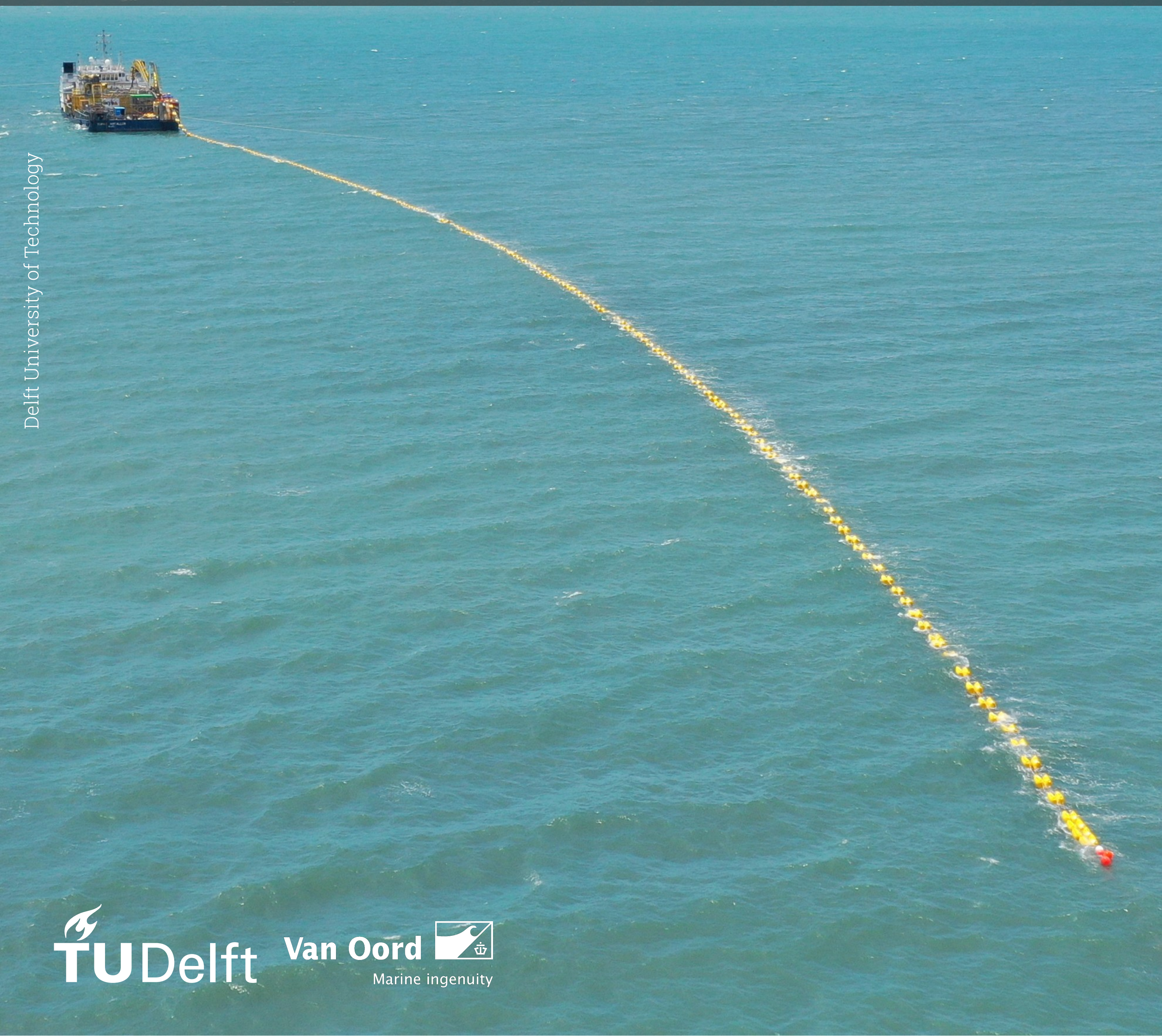

Delft University of Technology

A hydrodynamic study on floating export cable systems

Using finite element method modelling to study the hydrodynamic behaviour and optimise the design of floating export cable systems

by

M.A. (Marnix) Weiler

in fulfillment of the requirements to obtain the degree

Master of Science

Department of Hydraulic Engineering
Faculty of Civil Engineering and Geosciences
Delft University of Technology

to be defended publicly on the 16th of February 2023, at 15:45 PM.

Student number:	4391837	
Thesis committee:	dr. ir. A. (Alessandro) Antonini	TU Delft, chair
	dr. J.O. (Oriol) Colomés Gené	TU Delft
	ir. B.D. (Bas) van den Berg	Van Oord DMC
	ir. R.H. (Robin) de Jong	Van Oord DMC

An electronic version of this thesis is available at `http://repository.tudelft.nl/`

Cover images:
Photos of a floating export cable system taken during the float-out installation procedure
by Van Oord in the Greater Changhua project, Taiwan

Preface

This graduation thesis report is the result of the final stage of my MSc Civil Engineering at Delft University of Technology and closes my time as a student in Delft. This thesis is executed in partial fulfillment of the Hydraulic Engineering master program at the TU Delft and was conducted in cooperation with Van Oord Dredging and Marine Contractors. I am thankful to the TU Delft for giving this opportunity to arrange this joined project and thankful to Van Oord to actually make it happen.

I can truly say that it was a challenge. As a student specialised in coastal - and river engineering, I had little knowledge on structural dynamics and finite-element-method modelling before I started, which turned out to be crucial in researching these offshore systems. Besides that, floating export cable systems were a brand new research subject that had (as far as I can retrieve) never been studied before in the academic world. Until now. This made it though but exciting as well to get the chance to pioneer in the pioneering industry of offshore renewable energies and learn on engineering disciplines in addition to by bachelor program in civil engineering and master in hydraulic engineering.

First of all, I would like to thank my supervisors from the TU Delft: Alessandro Antonini, Assistant Professor in Coastal Engineering, and Oriol Colomés Gené, Assistant Professor in Offshore Engineering. I remember the enthousiasm of Alessandro for the research topic, when I asked him to be my supervisor. I would like to express my gratitude for his time and efforts, even during holidays, and his patience with my somewhat long emails ;). I want to thank Oriol in particular for his time and assistance during the extra, useful discussions we had together on the finite-element-method model. He made me see the mathematical charm and ingenuity of the finite-element-method, that I will for sure use in my upcoming career on whatever the application may be.

Secondly, I would like to thank my supervisors from Van Oord: Bas van den Berg, lead engineer of the pipelines and cables team, and Robin de Jong, part of that team and my daily supervisor. Both of them, but especially Robin as daily supervisor and expert in 'float-out' operations, have given me insight in this innovative installation method. During weekly discussions and other moments, they have given professional guidance with their 'marine ingenuity' and introduced me to Van Oord as a great, inspiring company.

Lastly, I would like to thank family and friends, giving emotional support during my research and providing required distraction in order not to get gobbled up too much in the research project. Gratitude goes in particular to my dad, who gave massive support acting as personal study counsellor and 'fellow researcher', and my mom where I could always come home and relax. During my studies I have made friends with fellow students from my student house, study association, student association, student political party and elsewhere, who really have made me a '*Delft engineer*'. That is something I want to thank them for and something that I am proud of.

I hope you will enjoy reading!

M.A. (Marnix) Weiler
Rotterdam, February 2023

To my grandfather,
who stood out as a scientist in history but preferred to become a civil engineer.

Summary

The market for offshore renewable energies has recently grown significantly and is expected to continue to grow in the future. Export cables are transporting generated energy from an offshore energy farm to shore. During their installation in shallow waters and intertidal areas, Van Oord uses an innovative method of '*float-outs*' since cable-laying vessels can not operate in these areas due to their draught. During float-outs the cable is pulled to shore while floating, supported by inflatable floaters. Understanding the hydrodynamic behaviour of these cable-floater-systems (CFS's) is important, to be able to relate the hydraulic environment to the cable stresses and determine the maximum allowed hydraulic conditions for these procedures. The software package OrcaFlex, used by Van Oord, has appeared to be insufficient and gives untrustworthy results, namely really high peak axial tension and compression forces in the cable. In this research, the CFS is studied with three methods to explain these extreme forces and improve the CFS design.

With the first method, the CFS is modelled as an Euler Bernoulli Beam (EBB) on a continuous elastic foundation in which the mass and stiffness of the floaters is spread over the beam length between two floaters. In this analytical model, straight, accessible formulas showed that the CFS is a really stiff dynamic system, dominated by the buoyancy stiffness of the floaters. This is caused, first of all, by the relatively big dimensions and small spacing of the floaters and secondly by the big length of the CFS. As a consequence, the natural frequencies are relatively high and in the same range as the wave frequency spectrum. This lead to this research' hypothesis that the extreme, internal stresses in the cable-floater-system are caused by resonance taking place between the external wave forcing and the CFS itself.

With the second method, the CFS is modelled with the finite-element-method as a long system of EBB's, each of them reaching from node to node with a length dependent on the chosen grid size. At the nodes that correspond to floater locations, floaters are modelled as 'lumped masses', acting at a certain point as a discrete foundation. This model is made in two versions, (1) in the vertical direction and (2) in the horizontal direction. In the vertical direction, the natural frequencies are again in the range of wave frequencies and are barely increasing for higher modes. The explanation for both of these observations is given by the local oscillations in the modal shapes occurring in between floaters. A parametric study on floater spacing shows that the length of these oscillations is determined by the floater spacing. Since the original floater spacing is small, it causes small wave lengths and high frequencies. In the horizontal direction, floater buoyancy stiffness is absent causing the natural frequencies to be significantly smaller, far outside the range of wave frequencies, and differences in natural frequencies for consecutive modes to be bigger.

With the third method, dynamic analyses are done in OrcaFlex with cases varying in wave frequency and presence/absence of a current in order to test the hypothesis of resonance. It can be concluded that the CFS is really sensitive to Stokes drift when an other current is absent. This causes a different positioning of the CFS and a mean axial tension in the cable decreasing in wave direction. Consequently, the hydrodynamic behaviour of the CFS is changing throughout its length. Therefore, extreme axial forces near both CFS boundaries should to be explained differently. Near the cable end most closest from where waves originate, the Stokes drift induced axial tension causes the CFS to be unable to move vertically in waves. Consequently, no interaction between wave and CFS, necessary for resonance, is taking place. The most extreme axial forces (tension and compression) occur for the highest wave frequency, since the Stokes drift is then largest. Near the other cable end, the mean axial tension is close to zero and the most extreme axial forces (tension and compression) occur for resonance conditions with wave frequency equal to natural frequency. This is confirmed by a study on floater's buoyancy energy with results in frequency domain and a comparison of local oscillations in modal shapes and OrcaFlex results.

The results do not fully confirm the hypothesis, but do give answer to the first part of the research question. Regarding the second part on the optimisation of a CFS design, one could focus on eliminating the chance on the occurrence of resonance, by increasing the floater spacing or decreasing the floater dimensions, or focus on decreasing the impact of resonance by increasing the floater's drag area in vertical direction.

Contents

List of Figures

List of Tables

Nomenclature

List of Abbreviations

BC Boundary Condition

CALM Catenary Anchor Leg Mooring

CFD Computational Fluid Dynamics

CFS Cable-Floater-System

DOF Degree Of Freedom

EBB Euler Bernoulli Beam

EQM Equation of Motion

FEM Finite Element Method

HDD Horizontal Directional Drilling

IC Interface Condition

IMU Inertial Measurement Unit

OTEC Ocean Thermal Energy Conversion

SPM Single Point Mooring

List of Greek Letters

α, δ, γ Rotational DOF's in OrcaFlex models

Δ_f The distance between adjacent floaters (floater spacing)

λ_i Eigenvalue of a matrix

Ω_e The spatial domain of one element

ω_i Angular natural frequency

ϕ_i Eigenvector of a matrix

ρ_c Density of the cable

ρ_w Density of sea water

θ Rotational (pitch) DOF of the CFS model

List of Symbols

$\hat{x}$ the position along the horizontal axis of the elemental scale coordinate system

A_c Cross-section area of the cable

b_{ij}^e Bending stiffness input value for elemental stiffness matrix

C_A Added mass coefficient of the CFS

C_D Drag coefficient of the CFS

D_c Diameter of the cable

D_f Diameter of an inflatable cylinder, part of the floater

d_f Draught of the floater

d_{ij}^e Floater buoyancy stiffness input value for elemental stiffness matrix

E Total amount of elements in the FEM model

e Reference to a specific element in in the FEM model

E_c Elastic modulus of the cable

E_{ff} The amount of elements between two adjacent floaters

f_i Specific natural frequency in vector with all natural frequencies

$f_{Ma=0}$ Natural frequency excluding added mass

f_{Ma} Natural frequency including added mass

f_{nat} Natural frequency in general, not of a specific eigenmode

g Gravitational acceleration constant

h Longitudinal length of one element in the FEM model (grid size)

i The row number (vertical direction) of the element matrix

I_c Second moment of inertia of the cable

J Bending stiffness in the cable

j The column number (horizontal direction) of the element matrix

$k_{d,\theta}$ Spring coefficient representing buoyancy of the floater in rotational direction

$k_{d,f}$ Spring coefficient representing buoyancy of the floater

$k_{d,u}$ Spring coefficient representing buoyancy of the floater in vertical direction

L_f	Length of the floater, longitudinal to the cable direction
L_{arc}	Arc length position along the modelled cable in OrcaFlex
L_{cfs}	Total length of the CFS
M	Total mass per unit length of the CFS
M_a	Total added mass per unit length
m_f	Structural mass of the floater
M_s	Total structural mass per unit length
$m_{a,c}$	Added mass of the cable per unit length
$m_{a,f}$	Added mass of the floater per unit length
MM_e	External moment on the floater
MM_r	Righting, stabilising moment of the floater
N	Total amount of nodes in the FEM model
n	Order of eigenmode
n	Reference to a specific node in in the FEM model
Q	Total amount of DOF's
$q(x)$	Forces term in the equation of motion
S^e	Internal force in an element
T	Current-induced axial tension
t	time
T_p	Indication for wave period of the Airy wave in OrcaFlex
t^e_{ij}	Tensional stiffness input value for elemental stiffness matrix
T_{nat}	Natural period
T_{sim}	Simulation period in OrcaFlex
T_w	Wave period of a modelled Airy wave
u_c	Constant (tidal) current velocity
$v(x)$	The test function or weight function
w	vertical, translational degree of freedom of the CFS model
W_f	Width of the floater
w_i	Vector with all variables of DOF's for one element
x	the position along the longitudinal x-axis, parallel to the CFS model
X, Y, Z	Translational DOF's in OrcaFlex models
y_{max}	Maximum deflection of CFS in horizontal direction due to distributed current load

Part I

Topic study & conceptual models

1 Introduction

This first chapter starts with Section 1.1 that explains the societal and engineering relevance of this research topic. Next, in Section 1.2 a short description is given on the software package OrcaFlex. In Section 1.3 a scientific background is given of research on similar structures using the results of a literature review. With all this information the problem is defined in Section 1.4. In the research approach, Section 1.5, it is described how this problem is tackled. This includes the research objective, the research questions and the methodology. Finally, in Section 1.6 it is explained how this report is built up in the reading guide.

1.1. Growing energy demand and installation of offshore cables

At the moment the world is at the start of an energy transition in which the energy supply is slowly changing from fossil sources to renewable sources. At the same time the world's population and the energy consumption per capita are growing. This causes an enormous growth in the demand for renewable energy. Whereas the energy demand is growing, the amount of available space onshore is decreasing due to the already mentioned growth of the world population but also due to urbanisation and industrialisation. Explained by the fact that coastal and delta regions are the most urbanized areas on earth, in these regions the developments of increasing energy demand and decreasing onshore space availability are conflicting the most. As water is close by and offers an abundance of space, governments conclude that an increasing amount of energy will have to be generated offshore. At the moment, all across the globe offshore wind turbines are installed and in the future also other energy sources (like solar -, wave -, tidal energy and ocean thermal energy conversion (OTEC)) could be an important offshore energy source. In order to transport all this generated energy to shore an extensive electricity cable grid is necessary. Within an energy farm, inter-array cables transport the energy to an offshore converter platform. From this platform an export cable is transporting energy to shore. For all areas with a large water depth, cable laying vessels (CLV) are used to install these cables. In Figure 1.1 one can find an example which is the Nexus owned by Van Oord. For nearshore areas the water depth is decreasing which make these areas inaccessible for a CLV. Other methods should be invented in order to cross these shallow areas. Marine contractor Van Oord is using an installation method which is called a '*float-out*' cable installation operation.

During a float-out a cable is pulled from the CLV, that is moored at a certain position, towards the shore by a smaller scale working barge. In order to make it float, the cable is carried by a floater for every few meters of cable length. In Figure 1.2 one can find some photos of these floaters. When the barge has reached its final position, the cable is connected to the end point. This is often a Horizontal Directional Drilling pipeline (HDD) located at the waterfront and is bridging the waterfront. Afterwards, the cable is pulled in from the CLV through the water onto land. Finally, the floaters are removed from the cable, the cable is lowered to the sea bed, buried into the sea bed and covered with sediment and rock to protect it. During this operation the cable line is temporarily floating in an offshore environment of (tidal) currents, waves and wind. The float out installation operation takes between one and two days and the cable length is between one and two kilometres. However, this spatial scale is increasing. For future projects a length up to 3.5 kilometres is desired, but this causes an increase in the loads on the cable as well. The influence of environmental parameters like waves and currents on the motions and internal stresses of the cable should be modelled with care and precision in preparation of a float out cable installation.

Figure 1.1: Cable-laying vessel 'Nexus' owned by Van Oord (Van Oord, n.d.-b)

Figure 1.2: Images of a float out operation (van der Mout, 2017) (Van Oord, n.d.-a)

1.2. Orcaflex software

Up to this moment Van Oord has been using the software package 'Orcaflex' from Orcina for creating these models. "Orcaflex is the world's leading package for the dynamic analysis of offshore marine systems." (Orcina, n.d.) Orcaflex is being used for a broad range of offshore applications, for example vessels, turbines, lines, buoys and connections (hooks and winches). Orcaflex can model external, environmental conditions like currents, wind, the seabed and water characteristics like temperature, density and viscosity as input (Orcina, n.d.). The analysis that Orcaflex can perform is both static analysis and dynamic analysis. The dynamic analysis can be done both in frequency domain and time domain. With these analyses, results can be generated concerning the system modes, fatigue in the system, positions, curvature, stresses and much more. OrcaFlex is modelling (the dynamics of) structures with the finite-element-method (FEM) in a hydraulic environment using computational fluid dynamics (CFD) theory. FEM is a modelling technique in which a structure is discretised in non-overlapping components with a simple geometry. Each of these components, finite elements, are expressed separately in a number of degrees of freedom and their response to loads is computed. The response of the whole structure is modelled by assembling and connecting all elements. (Lin, n.d.). CFD "is the process of mathematically modelling a physical phenomenon involving fluid flow and solving it numerically using the computational process." (Simscale, n.d.). Orcaflex is connecting the structural and fluid disciplines by using FEM and CFD.

However, in the run-up to this research issues have also been encountered with OrcaFlex. First of all, it was found out that OrcaFlex is not succeeding in correctly analysing the natural modes of a cable-floater-system (CFS) because of linearisation of the buoyancy force of the floater. However, the natural modes of the system, including the natural frequencies and modes of the system, are crucial in understanding the dynamic behaviour of the system. Secondly, Van Oord has doubts about the reliability of the OrcaFlex model results regarding the forces in the cable. Simulation results showed high forces and showed compression forces which were not expected. This leads to the problem statement which is defined in Section 1.4.

1.3. Literature on similar floating structures

The float-out cable installation is an innovative method for cable installations and has only been used by a few companies in the offshore working field. Therefore, as far as could be verified no research has been done on the physics of a CFS. However, similar, long, slender, flexible, floating structures do exist in various applications. The best comparison can be made with floating hoses and floating pipelines. Floating hoses are applied in the oil industry. From an offshore oil field, oil is transported to shore with a tanker. If harbours or jetties are not present, or the draft of the vessel is too big, often a Single Point Mooring (SPM) system is used. The tanker is moored to a Catenary Anchor Leg Mooring (CALM) and via a floating hose the oil is transported from the tanker to the CALM buoy, downward to the bottom and via a pipeline to shore. Applications of floating pipelines can be found for example in the dredging industry to transport dredged sediment from a dredging vessel to a sediment dumping location. An important difference between these structures and the floating export cables is the goal and the perspective when the design is made. These floating oil hoses and dredging pipelines are designed specifically for floating conditions and environment as that is their main function. However, the primary goal of an export cable is to transport electricity. The design conditions are based on this goal and on a subsurface, buried environment and not on floating conditions.

By many researchers wave-structure-interaction is described with the Morison equation. The Morison equation is a semi-empirical equation defined by (Morison, Johnson, & Schaaf, 1950) and determines “the force by unbroken surface waves on a cylindrical object.” It “is made up of two components, namely a drag force … and a virtual mass force” (Morison et al., 1950). The Morison equation was improved by (Zhang, Chen, Zhang, Zhang, & Zhang, 2015) for the application of floating hoses based on a partially immersed cylinder model which lead to an increase in accuracy of 15 % compared to the conventional Morison equation. By doing experiments (Xu, Dong, Zhao, Ma, & Ma, 2013) analysed the influence of the drag coefficient in the Morison equation on motion responses of a floating pipe and its mooring forces in random waves. (Li, Gui, & Teng, 2007) compared results of a numerical model to experimental model of a straight floating pipe in regular waves and formulated values for the tangential drag coefficient C_t and the normal drag coefficient C_n. (Fu, Xu, Hu, & Zhang, 2013) did experimental investigation of a floating -, a semi-submerged - and a fully submerged cylinder in an environment with both waves and currents simultaneously and researched the effect of various parameters on its drag coefficient and added mass coefficient.

By means of model tests and analytical study (Donoghue & Halliwell, 1990) found a relation between the response of a buoy in waves and the bending moments and axial forces in a floating hose-string connected to the buoy. It was “... found that the dynamic axial forces on the hose-string are determined … by the surge response of the buoy in waves. The dynamic vertical bending moment on the hose … mostly depends on the heave response of the buoy in waves” (Donoghue & Halliwell, 1990). Similar research was done by (Brown & Elliott, 1988) who presented a mathematical model able “to predict the stresses and motion of a realistic hose-string attached to a buoy which undergoes heaving and pitching motions of various sea states.” (Sundar, Sundaravadivelu, & Purushotham, 1988) did experimental research on moored floating pipe breakwaters in random waves and proved via statistical analysis that the heave motions, surge motions and peak mooring forces follow the Rayleigh distribution. (Teng & Li, 1991) came up with a linearisation method “which enables the force spectrum on an inclined cylinder to be calculated … from the wave spectrum in presence of a current.” (Papathanasiou, Karperaki, Theotokoglou, & Belibassakis, 2015) developed a high order finite element model for large floating bodies in an inhomogeneous shallow water environment on which the energy conservation principle was tested.

Conclusion
Concluding on this literature is that there has been done research on similar structures but not yet on the CFS. This leads to the problem definition in the next section.

1.4. Problem definition

In multiple projects Van Oord has used Orcaflex to model the behaviour of cables during a float out cable installation. Main goal of these simulations is to determine the maximum environmental conditions up to which it is safe and responsible to carry out the operation. In these computations there are set acceptance criteria, e.g. maximum allowable axial tension or minimum bending radius of the cable. A variety of incoming wave periods, wave directions, current velocities and current directions are chosen and for all these combinations the maximum allowable significant wave height is computed. The combination which gives the smallest significant wave height is governing. In particular the high frequency waves appear to be causing exceedance of the maximum allowed tension and minimum allowed tension (compression) in the cable. For the projects that have been done the governing maximum significant wave height for the float-out operation was 0 to 0.25 meter (Van Oord, 2020a) (Van Oord, 2021). Van Oord has doubts whether the high tension and compression forces on the cable, resulting in these low maximum wave heights, are computed correctly by OrcaFlex. On top of that, with the goal of getting more clarity on the unusual results, a modal analysis for the cable-floater-systems could not be done correctly in OrcaFlex (see Section 1.2).

These low maximum wave heights result in an extremely low workability, since there are presumably only a few days per year for which the acceptance criteria are met and installation is possible. Besides that, as these operations are likely to take more than one day, the amount of time intervals which are suitable for deployment even reduces further. For Van Oord this is a major issue, because this low workability can cause a construction project to delay in time and project costs to increase. In order to optimise the installation method in terms of safety, speed and workability a better understanding of the hydrodynamic behaviour of the CFS is necessary. However, up to this moment little to no research has been done on the interaction between waves/currents and these systems (see Section 1.3). It is this knowledge gap that will be addressed in this research thesis.

1.5. Research approach

1.5.1. Research objective and scope

The objective for this research is defined in the following way:

To gain understanding on the hydrodynamic behaviour, structural behaviour and modelling methods of floating export cables during float out cable installations with potential optimisation of the design of the cable-floater-system in mind.

This thesis objective is twofold. The main goal is the academic objective to gain understanding on the behaviour of floating export cables in waves and currents. In this thesis the focus will be on the hydrodynamic forcing of waves and currents on the floating export cable structure and its dynamic structural response. In order to study this hydrodynamic forcing and response and to gain insights, different types of models are used. This research is limited to the use of analytical models and FEM models. The FEM software package Orcaflex will be used since this software is also used by Van Oord and all their existing floating cable models are created in this format. Using the OrcaFlex software, existing models will be studied and new models are made. Simulations will only be done in time domain as this is also the common method within Van Oord to do simulations in OrcaFlex. In these simulations wave frequency will be the most important input parameter and less attention will be given to the effects of wave height, wave direction and currents on the cable structure. In particular, high frequency waves will be researched. Besides OrcaFlex, a new script in Python is made that can create a FEM model of the CFS as an alternative for OrcaFlex. It is made in order to do modal analyses on the CFS in the vertical direction and on the second place also in the horizontal direction. Modal analysis means that the model analyses the natural response of the structure characterised by natural frequencies and modal shapes. Simulations in time are not possible with these models and motions and forces of/in the structure can not be computed with this model.

The second part of the thesis objective is the goal to optimise the design of the CFS. This goal is subordinate to and more the result of the academic objective. Only after gaining new insights on the behaviour of floating export cables, these insights can be applied in order to achieve this second goal. Improvements for the CFS design will be suggested on a conceptual level, rather than on a detailed design level. Besides that, these recommendations will not address the installation procedures or operational guidelines.

1.5.2. Research questions and a hypothesis

In the literature review in Section 1.3 the current knowledge gap was adressed in the research and understanding on the hydrodynamic behaviour of floating export cable systems. In Section 1.5.1 the objective was set and the scope of the project was defined. Taking this objective, this scope and this knowledge gap into account, the following main research question was formulated:

"Which explanation can be given for extreme internal stresses in the cable-floater-system under wave and current loads using dynamic modelling methods and to which improvements of the design of the cable-floater-system does this explanation lead?"

In an early stage of the research, simple conceptual models showed that the natural frequencies of the CFS are within the range that the wave frequencies in the environment of the CFS are as well. See Section 3.3.2. In addition to the main research question this has lead to a hypothesis, a potential answer to the research question, that is tested in this research. The hypothesis is the following:

The extreme internal stresses in the cable-floater-system are caused by resonance taking place in vertical direction between the external forcing of waves and the cable-floater-system itself.

Based on the formulated main research question and hypothesis, the following research sub-questions were formulated:

1. *How can an export cable, a floater and a cable-floater-system as a whole in water be modelled for hydrodynamic and structural analysis?*
2. *How can the natural frequencies and modal shapes of a cable-floater system be approximated?*
3. *Which physical phenomena are occurring when resonance between a floating structure and hydraulic waves are taking place?*
4. *On which parameters do the internal stresses in an export cable, part of a cable-floater-system depend?*

1.5.3. Methodology

In order to answer the research question different methods are used. These are mentioned below:

1. Literature study: academic research papers, university courses and theses in the same field of research are studied to gain knowledge on the common behaviour of similar structures and the best methods to model this type of structures.
2. A new FEM model: first the script is created to generate a FEM model representing the CFS. Next FEM models are created that represent the CFS in different cases. Finally, the modal behaviour of the CFS is analysed for these different cases.
3. OrcaFlex: results are studied of dynamic analyses done by Van Oord already. Models of the CFS are created and adapted to make them better applicable for this research. Next dynamic analyses in time domain are done with these models. Finally, the (hydro)dynamic behaviour of the CFS is analysed for the modelled cases.
4. A further analysis on results of FEM model and OrcaFlex complementing each other with the goal to gain understanding of the real CFS and to optimise the CFS design.

1.6. Reading guide

In the same sequence as the methodology was described above, this research report is build up. Similar to the four steps in the methodology, there are four main parts I I, II, III and IV. In Part I, in Chapter 2 a literature study is reported upon. Besides that, in Chapter 3 the results of a first conceptual model are presented and analysed. Next, in Part II the new FEM model is reported. First in Chapter 4 the build-up of the FEM model is explained and afterwards in Chapter 5 the results are presented, analysed and concluded upon. Thereafter, in Part III the Orcaflex models are treated. Similar to the FEM model, first in Chapter 6 the set-up of the OrcaFlex model is explained. In Chapter 7 the results of the OrcaFlex are presented and analysed in various ways and concluded upon. Finally, in Part IV there is reflected upon the research. This is done by a discussion in Chapter 8 on both modelling methods, the gained CFS understanding and an optimisation of the CFS design. Afterwards, conclusions and recommendations are given on the research in respectively Chapter 9 and 10. As attachment to the report, in Part V the references and appendices of the research are included.

2
Literature study on dynamic modelling

In Chapter 1 the relevance of this research was clarified with a topic introduction, a literature review and problem definition. Next, the research approach was described and made clear that the research involves dynamic modelling in multiple ways. In order to create a new model correctly and understand results of existing models, relevant literature is studied in this chapter. The theory on the physics of an Euler-Bernoulli beam (EBB) will be discussed, as well as the mathematical modelling of an EBB and the derivation of its natural frequency. Finally, in Section 2.4 several hydrodynamic phenomena are explained which are relevant for the dynamic modelling and require a more in-depth explanation. The goal of the literature study is to gain knowledge on how a dynamic model for the cable-floater-system (CFS) can be made in order to perform modal analysis.

2.1. Introduction to dynamics of structures

2.1.1. Different types of dynamic systems

In order to model the cable-floater-system (CFS) the fundamental theory of structural dynamics was studied. A general distinction can be made into different types of models (Spijkers, Vrouwenvelder, & Klaver, 2006):

- Rigid bodies
- Discrete dynamic systems (mass-spring systems): with 1, 2, 3, ..., n degrees of freedom
- Continuous dynamic systems: string, bar, beam, plate and a half space.

Firstly, in this research the focus will be on the forces on the structure and resultant motions of part of the structure requiring a certain flexibility of the modelled structure. As a rigid body assumes no deformation due to external forces / loads, this modelling approach is not suitable.

Secondly, in mass-spring systems the most simple form consists of one body. This body has a mass and can move in a predefined number of directions. These are called the degrees of freedom (DOF's). Just like a rigid body the maximum number of degrees of freedom is six (three translational degrees and three rotational degrees). Apart from a mass resulting in inertia of the body, there are forces acting on the body. These are categorised in a spring force, interacting with the displacement of the body, a damping force, interacting with the velocity of the body and an external force, often called 'loads'. In practice these mass-spring systems do not consist of one body but are a connected system of bodies. Important to notice is the fact that in a dynamic system the bodies are considered as discrete points having a certain distance from each other. These systems are also being called discrete dynamic systems or lumped mass systems. With the aim of modelling a floating cable, a discrete dynamic system is a modelling approach that would require a relatively small computation time. The model consists of many elements and can be adapted from a very basic, crude model to an extensive, detailed model. Besides that, the system could be modelled only in the horizontal plane or vertical plane or it could be chosen to model in 3D for a more extensive model. This modelling approach is especially suitable when it is desired to model the whole cable and study the behaviour of the cable as a whole.

Thirdly, the counterpart of a discrete dynamic system is a continuous dynamic system, also being called distributed parameter systems. Whereas in a discrete dynamic system mass is assigned to discrete points, in a continuous dynamic system the mass is continuously distributed along a line, on a plane or in a volume element. The most simple form of a continuous dynamic system is a string. In this model, the mass is distributed along a line, the system is assumed to have no bending stiffness and only models axial forces (so it can not deal with normal forces). In a bar and a beam the mass is distributed along a plane. The difference between the two is that in a bar only normal force and axial force is taken into account. In a beam besides these two, also bending moment is included. In a plate the mass is distributed in a volume element in which one dimension is small compared to other two dimensions. Therefore, the structure has a bending stiffness in two planes. In a elastic half-space the mass is distributed in a volume element in which all dimensions are of similar magnitude. The result is a structure that has a bending stiffness in three planes.

To sum up, all different types of dynamic models are discussed. In the next section the choice is made and explained for one model type: a continuous EBB. After studying the continuous EBB and modelling the CFS with this approach, in Section 2.3 also a discrete model is set up.

2.1.2. Motivation for the model choice of a beam

In reality the cable is a continuous structure which does not have a mass at certain locations but all along the structure. That's why a continuous dynamic system is a better representation of the real cable than a discrete system. Besides that, peaks in internal stresses occur locally in the cable. Focusing on internal stresses in the cable, the bending stiffness is of significant importance. Therefore the model of a string or a bar is not suitable. Studying the spatial dimensions of a floating cable, it can be concluded that one dimension, the (longitudinal) length is significantly bigger than the other two dimensions (height and width / radius). It can be concluded that a half space model or plate model are not necessary and would only cause computation times to increase. Since the bending stiffness also needs to be included, a beam model is concluded to be the most suitable. The cable has a continuous character, but the floaters have a discrete character and therefore do not fit in a continuous model. With the considerations on the different types of dynamic models made above, it was chosen to further elaborate on the continuous dynamic model of a beam as a first step. A separate solution in order to include the floaters will also be found.

There are multiple methods to model the structural behaviour of a beam. The two main theories are the Euler-Bernoulli beam (EBB) theory and the Timoshenko beam theory (Simone, 2011). The difference between the two theories is that the Timoshenko beam theory takes into account shear deformation, whereas the EBB theory neglects the effects of shear deformation. This shear deformation occurs when a beam is bending and in a cross section in the beam a bending moment is present. To counteract this bending moment there will be a tension force at either the upper or under side of the beam and a compression force at the other side. These forces in opposite direction cause a shear stress and a shear deformation as a result. The cross section in the beam is in fact rotating. Studying a cross section in an EBB, it is assumed that this cross section is rotating due to bending only. This means that the cross section plane remains normal to the longitudinal axis of the beam. In a Timoshenko beam it is assumed that the rotation of the cross section is caused by bending as well as shear deformation. As the beam is higher the effect of shear deformation grows. That's why a Timoshenko beam is often used for thick structures. Considering the cable dimensions one can conclude that the height is really small compared to the length. Therefore, in this research an EBB model will be used to model the cable in the CFS.

2.2. A continuous Euler-Bernoulli beam model

2.2.1. The set-up of the continuous model

The most simple EBB model is a 1D model with one DOF, the vertical direction w. The system itself is defined by the x-axis, which is in the parallel, longitudinal direction of the beam. In Figure 2.1 the coordinate system is shown. Besides that the EBB model is a continuous model. This means that the structural characteristics along the beam (the x-direction) are constant. Or in other words, that the CFS is homogeneous. The CFS consists of two main elements: the cable and the floaters. For the cable, it is therefore assumed that the diameter, density, axial stiffness and bending stiffness are the same throughout the full cable length. For the floaters it is assumed that the distance from floater to floater, the floater spacing, is small compared to the wave length. With a wave length bigger than three times the floater spacing, the change of CFS characteristics in space can be ignored and the structure is approached as being a continuous structure (Metrikine, 2022). The consequence is that the floater's structural parameters are 'smeared out' / spread over the distance between two adjacent floaters (floater spacing). This is done by dividing the structural floater parameter by the floater spacing. See Section 2.2.3.

Figure 2.1: Coordinate system of the Euler-Bernoulli model

In a dynamic model the equation(s) of motion (EQM) describe(s) the motion of the system, see Section 2.2.3 below. In this model there are four important terms, being mass, stiffness, damping and external forces. Damping and external forcing will not be included in this continuous model, because these do not influence the natural frequency. Concerning the mass, there is structural mass of the cable and the floater. As mentioned above these are expressed in one term as a constant mass per unit length in x-direction. The mass of the floaters is expressed as mass per unit length by dividing by the floater spacing. Afterwards it is added to the structural cable mass. Besides structural mass there is added mass of the structure. The concept of added mass is more elaborately explained in Section 2.4.1.

Concerning the stiffness, there is bending stiffness caused by the cable, constant and continuous over the cable length. Besides that, the change in buoyancy force of the floaters adds stiffness to the dynamic system as well. See an elaborate determination of the spring coefficient in Section 2.4.2. Lastly, there is an axial tension in the cable caused by (tidal) current, that also adds stiffness to the system. The relation between the current velocity and the axial tension in the cable is determined in Section 2.4.4. To sum up, there is one total contribution on mass of the CFS and there are three separate contributions on stiffness of the CFS.

2.2.2. Simplifications and assumptions

All simplifications and assumptions used in the model are summarized below:

- The cable is modelled as an EBB.
- The cable structure is assumed to be homogeneous. All structural characteristics of the cable (bending stiffness, axial stiffness, density and cross-section area) are constant in a cross sectional area of the cable and in longitudinal (x)-direction.
- It is assumed that the wave lengths in the hydraulic environment are larger than three times the floater spacing. This entails that the floater lumped mass characteristics are equally spread over the floater's spacing. This makes the system a continuous system, with structural characteristics that are constant in longitudinal direction.
- In this model only the motions of the structure in the vertical direction are of interest. This simplifies the CFS to a 1D dynamic system.

- At both ends the cable is connected to a vessel. This boundary is modelled as a simply supported (pinned-pinned) boundary condition. This means that it is assumed that vertical displacement is zero at these locations and the rotation is not restricted.
- Effects of damping have not been taken into account. This means that it is assumed that the structural system does not loose energy in time. Besides that external forcing are not included. The reason is that both parameters do not influence the natural frequency of the system.
- At the real project sites, the water depth is often small and variable and during low water in a tidal cycle some parts of the cable are above the water level and dry on sand banks. These changes in water depth in space and time are neglected in this model. The water depth is assumed to be constant and deep water wave conditions are assumed, meaning that the water depth is assumed to be significantly larger than the wave height (wave height : water depth < 1 : 20).
- The current acting on the CFS is assumed to be constant in time and space and from a direction perpendicular to the longitudinal x-axis of the CFS. See an extensive explanation in Section 2.4.4.
- Based on the study of images shot and videos recorded during float-out-installation procedures in Changhua, it is assumed that the cable remains below the water surface at all times. See more explanation in Section 2.4.2.
- The spring coefficient, representing the change in buoyancy force of the floater, is linearised. This means that the change in water piercing area of the floater is neglected. In other words, the floater dimensions are simplified in the model. See an elaborate explanation on the definition of the spring coefficient in Section 2.4.2.

2.2.3. The equations of motion for four basic Euler-Bernoulli beam models

When the CFS is modelled with an EBB model, the model consists of different elements. In order to fully understand the model and to interpret the results in the correct manner, the EBB model is build up gradually. Four elementary EBB models have been studied first: model I, model II, model III and model IV. In the list below a corresponding numbering is used. It mentions the different system contributions and the EQM's, Equation 2.1 until 2.4. In Figure 2.2 the four model schemes are sketched. Model IV will be continued with in the next chapter, because it is the most accurate representation of the real dynamic system of the floating cable-floater-system. The four basic EBB models that are being studied, are:

I A simply supported EBB:

'bending stiffness' + 'inertia'

$$J * \frac{\partial^4 w(x,t)}{\partial x^4} + M_s * \frac{\partial^2 w(x,t)}{\partial t^2} = 0 \tag{2.1}$$

II A simply supported EBB on a continuous elastic (Winkler) foundation:

'bending stiffness' + 'inertia' + 'buoyancy stiffness'

$$J * \frac{\partial^4 w(x,t)}{\partial x^4} + M_s * \frac{\partial^2 w(x,t)}{\partial t^2} + K * w(x,t) = 0 \tag{2.2}$$

III A simply supported EBB with axial tension:

'bending stiffness' + 'inertia' + 'tensional stiffness'

$$J * \frac{\partial^4 w(x,t)}{\partial x^4} + M_s * \frac{\partial^2 w(x,t)}{\partial t^2} - T * \frac{\partial^2 w(x,t)}{\partial x^2} = 0 \tag{2.3}$$

IV A simply supported EBB with axial tension on a continuous elastic (Winkler) foundation:

'bending stiffness' + 'inertia' + 'tensional stiffness' + 'buoyancy stiffness'

$$J * \frac{\partial^4 w(x,t)}{\partial x^4} + M_s * \frac{\partial^2 w(x,t)}{\partial t^2} - T * \frac{\partial^2 w(x,t)}{\partial x^2} + K * w(x,t) = 0 \tag{2.4}$$

In the Equations 2.1 until 2.4 there are several elements summed up below. Notice that in the definition of the mass for the cable and the floater, the added mass of the water is not yet included. The added mass will be included in the next section. The main EQM elements are:

- Bending stiffness: $J = E_c I_c$
- Structural mass per unit length: $M_s = \rho_c A_c + \frac{m_f}{\Delta_f}$
- Spring coefficient: $K = \frac{k_{d,f}}{\Delta} = \frac{2 D_f \rho_w g L_f}{\Delta_f}$
- Axial tension: T

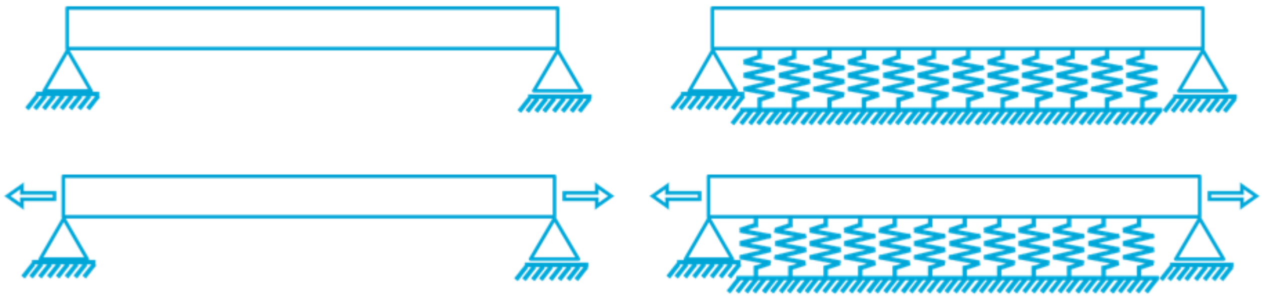

Figure 2.2: Schemes of four elementary Euler-Bernoulli models: from left to right, top to bottom: model I, II, III and IV

2.2.4. Natural frequencies for four elementary models

Using the EQM's, Equation 2.1 to 2.4, the boundary conditions and general formulas for $w(x,t)$, expressions can be found for the natural frequencies. These expressions can also be found in literature (Blevins, 2016). The definitions for the natural frequency of model I until IV are stated below in Equation 2.5 until 2.8 respectively. In these formulas n is the order of eigenmode.

$$f_{nat} = \sqrt{\frac{n^4 \pi^2 J}{4 M_s L_{cfs}^4}} \qquad \text{with: } n = 1, 2, 3, ... \tag{2.5}$$

$$f_{nat} = \sqrt{\frac{n^4 \pi^2 J}{4 M_s L_{cfs}^4} + \frac{K}{4 \pi^2 M_s}} \qquad \text{with: } n = 1, 2, 3, ... \tag{2.6}$$

$$f_{nat} = \sqrt{\frac{n^4 \pi^2 J}{4 M_s L_{cfs}^4} + \frac{n^2 T}{4 M_s L_{cfs}^2}} \qquad \text{with: } n = 1, 2, 3, ... \tag{2.7}$$

$$f_{nat} = \sqrt{\frac{n^4 \pi^2 J}{4 M_s L_{cfs}^4} + \frac{n^2 T}{4 M_s L_{cfs}^2} + \frac{K}{4 \pi^2 M_s}} \qquad \text{with: } n = 1, 2, 3, ... \tag{2.8}$$

In the equations above, the effect of the added mass of water is not yet included. "Natural frequencies of a structure in fluid are smaller than those in a vacuum by a factor:" (Blevins, 2016)

$$\frac{f_{Ma}}{f_{Ma=0}} = \frac{1}{\sqrt{1 + M_a / M_s}} \tag{2.9}$$

The added mass of the system M_a consists of added mass of the cable $m_{a,c}$ and added mass of the floater $m_{a,f}$. The cable is considered as a continuous cylinder shape with diameter D_c. The shape of the floater is simplified to a spheroid shape. The formulas for determining the added mass per unit length for cable and floater are stated in Section 2.4.1 in respectively Equation 2.16 and 2.17. Combining the added massses per unit length of both elements, a continuous added mass value is found by Equation 2.10:

$$M_a = m_{a,c} + \frac{L_f}{\Delta_f} * m_{a,f} \tag{2.10}$$

2.2.5. Conclusions on the continuous Euler-Bernoulli beam model

In conclusion on Section 2.1 and 2.2, with the aim to do modal analysis on the CFS, the structure can modelled relatively simply with the dynamic model of a simply supported EBB with axial tension on a continuous elastic foundation. By using quite a lot of simplifications and assumptions, a continuous dynamic model can be defined that is described with one single EQM. The fact that the system is described with one equation is a big difference with the models that are used elsewhere in this research. However, nearly all the assumptions and simplifications that were made for this first model (Section 2.2.2) are also required for the other models used in this research. The results for the four basic models are presented and reflected upon in Chapter 3.

2.3. A discrete Euler-Bernoulli beam model

In Section 2.2 the CFS was considered as a beam with a constant, continuous spring underneath as an elastic foundation. However, to model the CFS in more detail it can also be chosen to create a more advanced discrete EBB model with a periodic elastic foundation instead. In this section an adapted EBB model is presented. In Section 2.3.1 the differences are presented between the EBB model with a continuous elastic foundation and the EBB model with a discrete elastic foundation. Next, in Section 2.3.2 the basis of the discrete model is presented. Afterwards, in Section 2.3.3 the method is explained how to extend the model to the full CFS length. Lastly, in Section 2.3.4 there is concluded on the discrete model.

2.3.1. Differences between the discrete model and the continuous model

The physical principles and mathematical methods are similar for both the discrete model and continuous model. However, there are also differences. The two main differences between the modelling approaches are explained below. Afterwards some more practical differences, advantages and disadvantages are mentioned.

In the continuous model the cable can be modelled as one EBB from begin to end of the cable. All the beam's characteristics like the dimensions, density, axial stiffness, bending stiffness, added mass etc, are assumed to be constant along the entire beam. Modelling the cable as one body means that there is only one EQM (if we take into account one DOF). In a discrete model, the cable is separated into smaller segments, reaching from floater to floater or smaller when more detail is desired. Each of these segments are in fact a separate EBB and each segment therefore has its own EQM for each DOF that the segment has. See these EQM's in Equation 2.11 and Equation 2.12.

In the continuous model the floater's characteristics of buoyancy and (added) mass were spread ('smeared out') over the EBB in order to make the structure a continuous structure. In the discrete model the cable of the CFS is still modelled as a continuous EBB, but the floater's characteristics are located at the floater location (at the transition between one segment and the next segment) instead of along one beam. Modelling the floater characteristics in this way is a more realistic representation of the real CFS. Whereas the spring force representing buoyancy was present in the EQM of the continuous model, in the discrete model the spring force is present in the interface conditions (IC's). See Figure 2.3.

So in conclusion, the discrete model is more advanced and is a more realistic representation of the CFS. For example, local hydrodynamic behaviour occurring at or between floaters could be studied with a discrete model but not with a continuous model. On the contrary, the discrete model has a lot more EQM's. Therefore it is a more computationally demanding approach compared to the continuous model. The CFS has a large length ($L_{cfs} \approx 1000$ m) and the floaters are relatively close to each other ($\Delta_f \approx 2$ m). That's why a lot of segments ($N \approx 500$) are needed if one wants to model every floater of the CFS individually. More segments in the model means more EQM's to solve and therefore longer computation times.

2.3.2. A start on the discrete model

In Figure 2.3 one can find a schematic figure of the basis of the discrete EBB model consisting of two segments. This basis model contains two segments of which the vertical displacement is described by w_1 and w_2. In a similar way as in Section 2.2.3 the EQM's can be formulated, see Equation 2.11 and 2.12.

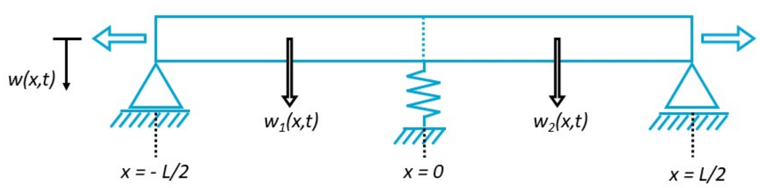

Figure 2.3: Schematic figure of the basis of the discrete Euler-Bernoulli beam model

$$J * \frac{\partial^4 w_1}{\partial x^4} + M * \frac{\partial^2 w_1}{\partial t^2} - T * \frac{\partial^2 w_1}{\partial x^2} = 0 \tag{2.11}$$

$$J * \frac{\partial^4 w_2}{\partial x^4} + M * \frac{\partial^2 w_2}{\partial t^2} - T * \frac{\partial^2 w_2}{\partial x^2} = 0 \tag{2.12}$$

As these EQM are of fourth order, there are 2 x 4 = 8 BC's and IC's needed to solve these EQM. For the basis model of Figure 2.3 there are the following boundary conditions (BC's) at $x = -L/2$ and $x = L/2$ and IC's at $x = 0$:

$$w_1(x = -L/2, t) = 0 \qquad w_1(x = 0, t) = w_2(x = 0, t) \qquad w_2(x = L/2, t) = 0$$

$$\frac{\partial^2 w_1(x = -L/2, t)}{\partial x^2} = 0 \qquad \frac{\partial^2 w_1(x = 0, t)}{\partial x^2} = \frac{\partial^2 w_2(x = 0, t)}{\partial x^2} \qquad \frac{\partial^2 w_2(x = L/2, t)}{\partial x^2} = 0$$

$$\frac{\partial w_1(x = 0, t)}{\partial x} = \frac{\partial w_2(x = 0, t)}{\partial x}$$

$$J(\frac{\partial^3 w_1(x = 0, t)}{\partial x^3} - \frac{\partial^3 w_2(x = 0, t)}{\partial x^3}) = -K * w_1(x = 0, t)$$

The next step is to solve the EQM's, Equation 2.11 and 2.12, with these BC's and IC's. This is done with the help of a general solution, Equation 2.13. The result is an 8x8 matrix, indicated as H, being part of Equation 2.14 below. In this equation, C is a set of coefficients originating from the general solution Equation 2.13. With this equation not only the coefficients $A_1, B_1, C_1, D_1, A_2, B_2, C_2, D_2$ can be computed but also the eigenvalues of the matrix which represent the natural frequencies. Computing the determinant of matrix H and setting this equal to zero, the value of β can be found. Afterwards using the expression $\beta = \frac{\rho A}{E_c I_c}\Omega^2$ the values of Ω can be computed. These represent the natural frequencies.

$$W_j(x) = A_j * cosh(\beta x) + B_j * sinh(\beta x) + C_j * cos(\beta x) + D_j * sin(\beta x) \qquad \text{with j = 1, 2} \tag{2.13}$$

$$H \cdot C = \begin{pmatrix} h_{1,1} & h_{1,2} & ... & h_{1,8} \\ h_{2,1} & h_{2,2} & ... & h_{2,8} \\ ... & ... & ... & ... \\ h_{8,1} & h_{8,2} & ... & h_{8,8} \end{pmatrix} \cdot \begin{pmatrix} A_1 \\ B_1 \\ ... \\ D_2 \end{pmatrix} = \begin{pmatrix} 0 \\ 0 \\ ... \\ 0 \end{pmatrix} \tag{2.14}$$

2.3.3. Extension of the model to full cable length

Having explained the basis of the model in Section 2.3.2, in this section is shown how the model can be extended in such a way that the full length of the cable can be modelled. See Figure 2.4. As was already explained, one segment (w_j) represents one part of the cable from floater to floater. Therefore, if one wants to model the full CFS, the model should consist of N + 1 segments (N = number of floaters), requiring also N + 1 EQM's. In order to solve all these fourth order EQM's, there are needed 4 x (N+1) equations. With each segment extra there is one interface extra which gives four extra IC's. So for N EQM's, 4 x N IC's can be stated. For the last segment ("+1") there are four BC's, two for each boundary, that can be stated. In this way, there are 4 x (N + 1) BC's / IC's required to solve the N + 1 EQM's. Below one can find the generalized EQM, Equation 2.15 for a random segment j, corresponding to Figure 2.4. BC's and IC's can be derived in a similar way as in Section 2.3.2.

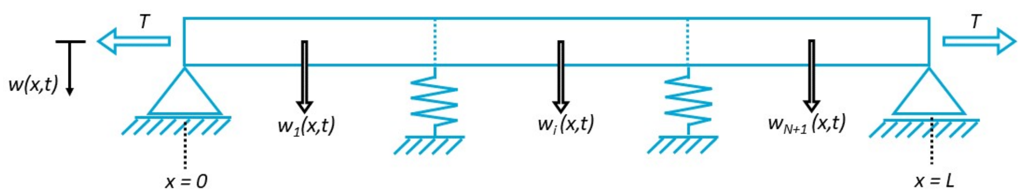

Figure 2.4: Schematic figure of the extended discrete Euler-Bernoulli beam model

$$J * \frac{\partial^4 w_j}{\partial x^4} + M * \frac{\partial^2 w_j}{\partial t^2} - T * \frac{\partial^2 w_j}{\partial x^2} = 0 \qquad \text{with j = 1, 2, ..., N+1} \tag{2.15}$$

2.3.4. Conclusions on the discrete Euler-Bernoulli beam model

Concluding on Section 2.3, this EBB model with a discrete foundation is a rather simple, analytical model which makes it easy to understand and set up. However, the computation time is increasing quickly when the number of segments and length of the model is extended. For each segment four extra coefficients (A_j, B_j, C_j, D_j) need to be solved, which is requiring four extra equations. The matrix H is then also increasing with four columns and four rows. Solving this bigger matrix to find the eigenvalues takes more computational time. This makes an analytical method is no longer the correct method to model the CFS in a discrete way. Therefore, in Chapter 4 a more intelligent method, the Finite Element Method (FEM), is introduced.

2.4. Hydrodynamic characteristics relevant for modal analysis

There are several characteristics in modelling the CFS that require a more detailed explanation. The scope of the continuous model (Section 2.2.1) and the FEM model (Chapter 4) is to do modal analysis in vertical direction. Therefore, the most important characteristics are described below, but do not provide a complete overview of the hydrodynamic behaviour of the CFS. The definitions derived below were used and were referred to already in setting up the continuous model. Also in the next Chapter 4 the definitions below are used again as input parameter for the FEM model. First in Section 2.4.1 until 2.4.4 a detailed explanation is given on the most important input parameters for both models, being added mass, the spring coefficient representing the floater buoyancy and the axial tension caused by currents. Afterwards the definitions of resonance, natural frequencies and modal shapes are briefly explained Section 2.4.5.

2.4.1. Definition of the added mass

The mass as input for the model consists of two kinds of masses, being its structural mass and the added mass of moving water. The structural mass was described already. Added mass is the extra inertia added to a dynamic system of a body that is moving through a certain volume / fluid. As a structural body and its surrounding volume can not occupy the same space, the volume needs to move when the body is moving. The inertia that the volume experiences when it is moving is expressed as the *added mass* or *virtual mass*. By excluding the added mass, the structure is being modelled as if it is in vacuum. However, in this research the structure is moving in water and to model this correctly the added mass of water should be added up to the structural mass resulting in the total mass. Considering the added mass in the CFS, a distinction should be made between the added mass of the cable and the added mass of the floater, since shapes are different. Besides that, a distinction should be made between the added mass in vertical (translational) direction and the added mass in rotational direction. In the continuous EBB model in Section 2.2 only the vertical direction is included. However, in setting up the FEM model in Chapter 4 also the rotational direction is included.

To compute added mass per unit length of the cable in vertical direction, the cable is assumed to have a cylindrical shape and can therefore be computed with Equation 2.16 (Newman, 2017). The rotational added mass for the cable does not need to be accounted for, since it is included using the shape functions.

$$m_{a,u,c} = \frac{\pi}{4}\rho_w D_c^2 \tag{2.16}$$

However, for the added mass of the floater both the vertical direction and rotational direction need to be defined since the (added) mass of the floater is a discrete, lumped mass. To compute the added mass of the floater, a spheroid shape is assumed. In this case, Equation 2.17 can be used to compute the vertical added mass per unit length and Equation 2.18 can be used to compute the rotational added mass per unit length (Newman, 2017):

$$m_{a,u,f} = \pi\rho_w a_f^2 \tag{2.17}$$
$$m_{a,\theta,f} = \frac{\pi}{8}\rho_w (a_f^2 - b_f^2)^2 \tag{2.18}$$

In these equations:

- $a_f = \frac{L_f}{2}$: half of the length of the floater
- $b_f = \frac{W_f}{2}$: half of the width of the floater

The length and width of the floater are assumed to be known. As the mass of the cable and floater do not change along the CFS, both added mass values are valid along the whole structure. However, an important difference between added mass of the cable and floater is that the cable added mass is present along the whole structure, whereas the floater added mass acts at discrete points. Besides that, in the continuous model (Section 2.2) the added mass of the floater and cable is a continuous characteristic and expressed per unit length [kg/m]. The FEM model (Chapter 4) is a discrete model in which the added mass of cable and floater is expressed in [kg] and should be multiplied by respectively the length of the cable element h and floater length L_f.

2.4.2. Definition of the vertical spring coefficient of the floater

When external wave forcing is excluded, there are two forces in vertical direction that should be considered for a model in vertical direction:

- The downward (positive) gravitational force of the structure (weight), defined as the mass of the structure multiplied by the gravitational acceleration. This force is constant in time for both the cable and the floater, because the volume and density of both elements do not change in time. The force also remains constant when the CFS is moving in vertical direction. Therefore, this gravitational force is not included in the EQM of the dynamic model.
- The upward (negative) buoyancy force, defined as the weight of the fluid that is being displaced by the structure (*Archimedes*). This buoyancy force therefore changes when the underwater volume of the CFS changes. This underwater volume is dependant on the vertical position of the CFS and that is why the buoyancy force has to be accounted for in the dynamic model. To fully understand this, the cable and the floater are treated separately below.

See Figure 1.2. Based on this photos and other footage that were taken during offshore operations, the assumption is made that the cable is fully submerged at all times. Alternatively, this is also reasonable assumption to make when the density of salt water and the density of the cable are compared. For a cable type CU1600SQ (often used by Van Oord), the density is $\rho_c = 16087$ kg/m^3, whereas the density of salt water ($\rho_w = 1025$ kg/m^3) is significantly smaller. Therefore, the cable will sink (*Archimedes*) and be submerged at all times as long as vertical displacements are relatively small. When the cable remains submerged, the submerged volume of the cable remains the same and therefore the buoyancy force of the cable will not change in space or time (*Archimedes*). On the contrary, the floaters are partially above and partially below the water surface. This means that with a vertical motion, that is studied in this model, the underwater volume of the floater changes. If this underwater volume changes, the upward buoyancy force changes as well. This dependency of the buoyancy force on the floater's vertical position can be included in the dynamic model by modelling it as a spring. In this model the spring coefficient is the relation between buoyancy force and vertical position of the floater. The spring coefficient represents the change in buoyancy force of the CFS and is defined below.

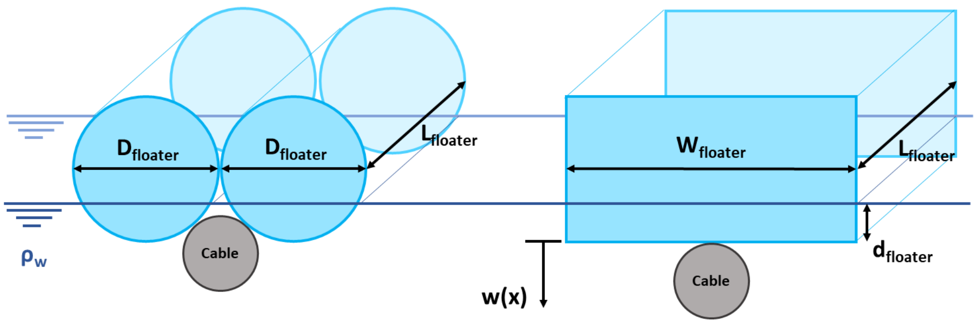

Figure 2.5: Schematisation of the original - (left) and simplified floater (right) in water

In the left of Figure 2.5 the floater is schematised and its dimensions are given symbols. Studying the shape of the floater, one can see that the floater width is not constant over the floater height. The consequence is that for a vertical movement of the floater w the change in buoyancy force is not proportional along the height of the floater. Therefore, the buoyancy force expressed as a function of the vertical floater position w is a non-linear function. When this force is implemented in the EQM describing the dynamic behaviour of the CFS this would also result in a non-linear differential equation, that are more computationally demanding to solve. The theory described in 2.2.1 and the hand formulas for the natural frequency would be insufficient to implement this non-linear behaviour and also the methods applied in Chapter 4 and 5 would need to be extended. This is beyond the scope of this research and therefore the shape of the floater is simplified in order to come up with a linear function on the buoyancy force and a constant spring coefficient. In order to come up with a linear expression for the spring force, the floater shape is simplified from two cylinders into one rectangular shape, see Figure 2.5. In this simplification it is assumed that the floater width is equal to two times the diameter of a single cylinder: $W_f = 2 \cdot D_f$. The draft of the floater when the system is in vertical static equilibrium is referred to with the symbol d_f. With this simplification and using the new dimensions, an expression for the (change in) buoyancy force can be defined. The buoyancy force of the floater is described by:

$$F_{b,f}(w,x) = -\rho_w \cdot g \cdot V_{sub} = -\rho_w \cdot g \cdot W_f L_f (d_f + w(x))$$

The buoyancy force is negative since it the direction is upward, in opposite direction of the positive axis of vertical displacement w. d_f is a constant value and therefore not contributing to the spring force of the system and removed from the equation. The part of the buoyancy force that is variable, is the spring force. Afterwards, using the general expression for a spring (force = spring coefficient x deflection) one can find the linearised spring coefficient representing the change in buoyancy force depending the vertical displacement of the floater.

$$F_{b,f,var}(w,x) = -\rho_w g W_f L_f \cdot w(x) = F_{spring} = -k_{d,f} \cdot w(x)$$

Finally, the linearised spring coefficient is:

$$k_{d,f} = \rho_w g W_f L_f = 2D_f \rho_w g L_f \tag{2.19}$$

2.4.3. Definition of the rotational spring coefficient of the floater

This section is irrelevant for the continuous model in Section 2.2 but is relevant for the set-up of the FEM model in Chapter 4, because in the FEM model also rotational DOF's are taken into account explicitly. As was explained in the previous section, it is only required to study the rotational spring coefficient of the floater buoyancy and not of the cable buoyancy, because the floater is partially submerged whereas the cable is assumed to be fully submerged at all times.

For the rotational stiffness, the sum of moments in the floater is studied instead of the vertical forces. This sum of moments consist of an external moment and a righting moment and the sum of these two moments should be zero in case of an equilibrium. The external moment is caused by loading and the exact formulation will not be treated here. The righting moment is a moment that is caused by the rotation of the floater itself. Namely, the rotation causes a change in the shape of the under water part of the floater and this causes a shift in the centre of the buoyancy relative to the centre of gravity. It is this force couple that is the righting moment. An equilibrium is again achieved when the righting moment is equal to the external moment (Journée, Massie, & Huijsmans, 2015):

$$MM_e = MM_r$$

The expression for the righting moment is Equation 2.20. It is assumed that the rotation angle θ are small. If this is the case then $sin(\theta) \approx \theta$. Therefore, a general expression for the righting moment as a function of the rotational stiffness $k_{D,\theta}$ and the rotation angle θ can be defined. The expression for the rotational stiffness is Equation 2.21.

$$MM_r = \rho_w g \nabla \overline{GN_\theta} \cdot \sin(\theta) \approx k_{D,\theta} \cdot \theta \tag{2.20}$$

$$k_{D,\theta} = \rho_w g \nabla \overline{GN_\theta} \tag{2.21}$$

In this equation, see also all symbols in Figure 2.6:

- $\nabla = L_f W_f d_f$: the displaced volume by the floater [m^3]
- $\overline{GN_\theta} = \overline{KB} + \overline{BN_\theta} - \overline{KG}$: the distance from the gravity centre G to the metacentre N_θ [m]
  - $\overline{KB} = d_f/2$: the distance from the keel point K to the buoyancy centre B [m]
  - $\overline{KG} = H_f/2$: the distance from the keel point K to the gravity centre G [m]
  - $\overline{BN_\theta}$: the distance from the buoyancy centre B to the meta-centre N_θ [m]

Distances $\overline{KB}$ and $\overline{KG}$ can easily be determined by computing the centre of the submerged floater's volume for the buoyancy centre B and the centre of the total floater's volume for the gravity centre G. The keel point K is situated in the middle of the bottom side of the floater. The third distance $\overline{BN_\theta}$ can be computed using the *Scribanti formula* (Journée et al., 2015). In this formula I_T is the moment of inertia of the water plane. Assuming a rectangular shape of the floater, I_T can be computed with formula below. Besides that, this formula can be simplified since with the assumption that rotation angles are small ($\theta < 10$ degrees).

$$\overline{BN_\theta} = \frac{I_T}{\nabla}\left(1 + \frac{1}{2}tan^2\theta\right) \approx \frac{I_T}{\nabla} \qquad \text{in which: } I_T = \frac{1}{12} \cdot W_f \cdot L_f^3 \tag{2.22}$$

The final expression for $k_{D,\theta}$, Equation 2.23, is found by substituting the expressions for $\overline{BN_\theta}$ and I_T into Equation 2.21. All spatial parameters that were mentioned, are found in Figure 2.6

$$k_{D,\theta} = \rho_w g \nabla \cdot \left(\overline{KB} - \overline{KG} + \frac{W_f^2}{12 D_f} \right) \tag{2.23}$$

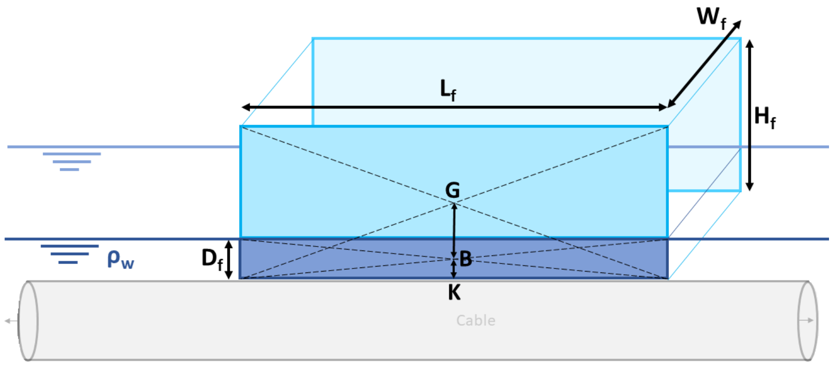

Figure 2.6: Schematisation of floater with four main dimensions and buoyancy centre B, gravity centre G and keel point K

2.4.4. Definition of the current induced axial tension in the cable

If the hydraulic environment surrounding the CFS is simplified, a distinction could be made between waves and currents. Whereas a wave causes a force on the CFS that is changing rapidly in time, the current can be seen as a force that has a more constant character. The current causes a constant axial tension in the cable and this axial tension adds stiffness to the system. If one imagines a beam under an axial pre-tension force that is moved from is original straight shape, it is easy to understand that the beam wants to move back into its straight shape due to the axial tension. Therefore, this current and the axial tension is relevant to study further below. A CFS is usually located in coastal waters where currents can be present from a range of different origins. In general, the dominating current in coastal waters is likely to be the current caused by astronomical tides. Other currents can be wind generated drift currents and currents due to nearshore processes such as rip currents, eddy currents and littoral currents, which are all occurring at a smaller scale (Det Norske Veritas, 2010). The maximum velocity of these currents varies in time and location, but are in the order from 0 to 1 m/s. The direction of this tidal current is about parallel to the shoreline. Since the CFS is oriented about perpendicular to the shoreline, it has been assumed in this model that the current direction is perpendicular to the longitudinal axis of the CFS. To compute the sectional force on the structure $f_N(t)$ in a flow the Morison formula can be used (Det Norske Veritas, 2010). See Equation 2.24. In this model it will be assumed that the current acceleration is zero and therefore the inertia part of the Morison force is also zero. This simplifies the expression to a constant drag force per unit length of cable caused by a constant current. In this equation C_D is the drag coefficient of the CFS which is dependent on roughness and dimensions and assumed to be known.

$$f_N(t) = f_{inertia}(t) + f_{drag}(t) = \rho_w(1 + C_A)A\frac{\partial u_c}{\partial t} + \frac{1}{2}\rho_w C_D D u_c|u_c| \quad \rightarrow \quad q_{y,c} = \frac{1}{2}\rho_w C_D D u_c|u_c| \tag{2.24}$$

Equation 2.24 gives the sectional force per unit length normal to the longitudinal axis of the CFS. This force can therefore be seen as a distributed load all along the CFS in the y direction. It is assumed that this distributed load is constant along the x-axis of the CFS and that the magnitude of the distributed load is constant in time. To compute the distributed load the diameter of the cable was used and therefore the additional drag area at locations of floaters is ignored. Simple static mechanics theory gives the relation between the distributed load, the bending stiffness, the total length and the axial tension force. See Equation 2.25 below and all the input parameters in Figure 2.7 that shows a top view of the EBB model. The resulting tension force T is used then in the continuous model and FEM model.

$$T = \sqrt{T_h^2 + T_v^2} = \sqrt{\left(\frac{q_{y,c} L_{cfs}^2}{8 y_{max}}\right)^2 + \left(\frac{q_{y,c} L_{cfs}}{2}\right)^2} \qquad \text{in which: } y_{max} = -\frac{5 q_{y,c} L_{cfs}^4}{384 J} \tag{2.25}$$

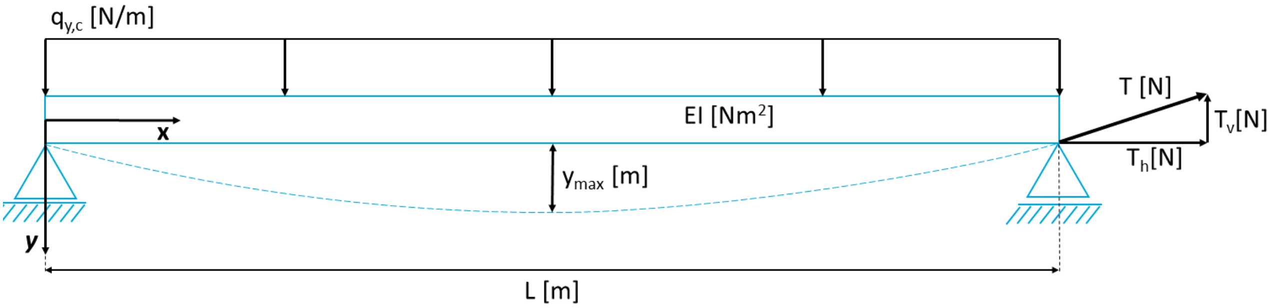

Figure 2.7: Distributed static load on an Euler-Bernoulli beam due to current and the axial tension force as result (top view)

2.4.5. Resonance, natural frequencies and modal shapes

Resonance can be described as the phenomenon of an amplifying vibration of an object, caused by an external, periodic force applied on the object at a frequency equal to the *natural frequency* of motion for the object. In the case of a floating, hydraulic structure, the relevant external, periodic force is the wave forcing originating from wind waves or swell waves. The object in this case is the CFS and its natural frequency of motion is the frequency in which the system moves after being set in motion by a instant short force. It is the frequency in which the object vibrates in a standing wave.

This natural frequency is not influenced by the external wave forcing, but is fully determined by the total mass and the total stiffness of the system and therefore is a characteristic of the system itself. A bigger mass means a bigger inertia of the system, that causes smaller accelerations and therefore results in smaller natural frequencies. A bigger stiffness means bigger (spring) forces acting on the system, that causes higher accelerations and therefore results in higher natural frequencies.

As said, the natural frequency is the frequency in which the object vibrates in a standing wave. A standing wave is the opposite of a propagating wave that moves over distance in a certain direction. A standing wave has certain locations were there is zero motion at all times (*nodes*) and locations in between with maximum amplitude (*anti-nodes*). However, since the number of nodes and anti-nodes can change. There exist multiple shapes of standing waves (called *modal shapes*), each of them having their own natural frequency value. See Figure 2.8. The first shape and corresponding natural frequency are called the 1st *mode*, the second shape and frequency are the 2nd mode etc. The number of modes is equal to the number of DOF's of the dynamic system. In this research modal analysis is done on several models, by which is meant that the natural frequencies and modal shapes are computed and analysed. This is not done for all modes but often only mode 1 to 10, which are most relevant from a physical point of view.

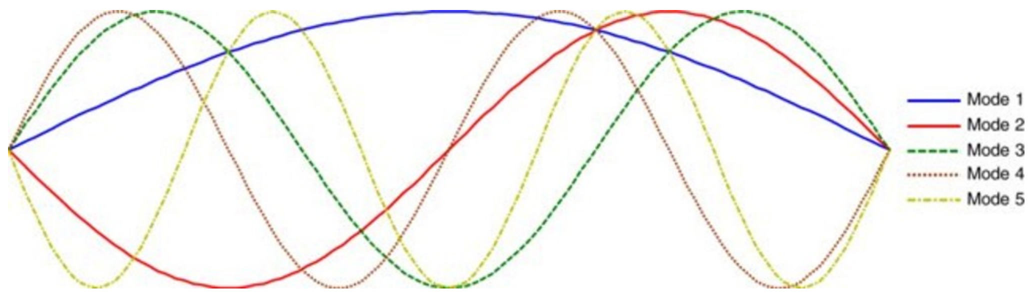

Figure 2.8: First five eigenmodes / modal shapes of a simply supported ('free') beam (Chellapilla, 2016)

3 Results of a continuous Euler Bernoulli Beam model

In the previous chapter several modelling methods were studied and applied on the cable-floater-system (CFS). This chapter starts with Section 3.1 reporting on all the input parameters of the CFS that are relevant for computing the natural frequencies of the continuous Euler Bernoulli Beam (EBB) model. Afterwards, in Section 3.2 the formulas for the continuous EBB model are used, the natural frequencies are computed and presented. Finally, in Section 3.3 a reflection is given on the results and conclusions are drawn regarding further modelling of the CFS.

3.1. Input parameters of the cable-floater-system

The data that characterises the model of the CFS in this research is part of the full set of specifications on the CFS, provided by Van Oord (LS Cable System Ltd., 2020) (Van Oord, 2020b). The full set of technical specifications on the CFS and environmental input parameters for all models used in this research can be found in Appendix A. In Table 3.1 on the left, the magnitudes of all terms in the natural frequency formulas, Equation 2.5 to 2.8, and added mass ratio, Equation 2.9 are included. The values of these input values are the result of using the hydrodynamic formulas as explained in Section 2.4 with the input parameters of Appendix A. With these parameters, the separate terms in Equation 2.5 to 2.8 can be computed. See Table 3.1 on the right. The term in which the bending stiffness is included and the term in which the tensional stiffness is included are a function of n, which is the mode number. The absolute value of these numbers is the most right column of Table 3.1 does not have a real physical meaning, since added mass is not included yet and they are only one term in a more elaborate formula. The relative magnitude will appear to be useful. See Section 3.3.

Table 3.1: Input parameters for natural frequency formulas on Euler-Bernoulli beam model with a continuous elastic foundation

Parameter:	Symbol:	Value:	Unity:	Term:	Symbol:	Value:
Structural mass CFS	M_s	156.6	kg/m	'Bending stiffness'	$\frac{n^4\pi^2 J}{4M_s L_{cfs}^4}$	1.97E-9 $\cdot n^4$
Added mass CFS	M_a	2924	kg/m			
Vertical spring coeff.	K	7.49	kN/m	'Buoyancy stiffness'	$\frac{K}{4\pi^2 M_s}$	1.21
Axial tension	T	11.9	kN			
Bending stiffness	J	170.000	kNm^2	'Tensional stiffness'	$\frac{n^2 T}{4M_s L_{cfs}^2}$	1.63E-5 $\cdot n^2$
Total length CFS	L_{cfs}	1080	m			

3.2. Natural frequency results

With the formulas for the different elementary models (Equation 2.5 to 2.8), the formula to include added mass, Equation 2.9, and the parameters and terms in Table 3.1 the natural frequencies can be computed. The natural frequencies of the first ten eigenmodes for all four models are enumerated below. In Table 3.2, the values with only structural mass are stated. The values including structural mass and added mass are in Table 3.3 and visualised in Figure 3.1. Be aware of the logarithmic scale on the y-axis.

Table 3.2: Values of natural frequencies and natural periods for four elementary models without added mass

Mode	Model I		Model II		Model III		Model IV	
n	f_{nat} [Hz]	T_{nat} [s]	f_{nat} [Hz]	T_{nat} [s]	f_{nat} [Hz]	T_{nat} [s]	f_{nat} [Hz]	T_{nat} [s]
1	4.44E-05	2.25E+04	1.10E+00	9.08E-01	4.04E-03	2.48E+02	1.10E+00	9.08E-01
2	1.78E-04	5.63E+03	1.10E+00	9.08E-01	8.08E-03	1.24E+02	1.10E+00	9.08E-01
3	3.99E-04	2.50E+03	1.10E+00	9.08E-01	1.21E-02	8.25E+01	1.10E+00	9.08E-01
4	7.10E-04	1.41E+03	1.10E+00	9.08E-01	1.62E-02	6.19E+01	1.10E+00	9.08E-01
5	1.11E-03	9.01E+02	1.10E+00	9.08E-01	2.02E-02	4.95E+01	1.10E+00	9.08E-01
6	1.60E-03	6.26E+02	1.10E+00	9.08E-01	2.43E-02	4.12E+01	1.10E+00	9.08E-01
7	2.17E-03	4.60E+02	1.10E+00	9.08E-01	2.83E-02	3.53E+01	1.10E+00	9.08E-01
8	2.84E-03	3.52E+02	1.10E+00	9.08E-01	3.24E-02	3.08E+01	1.10E+00	9.08E-01
9	3.59E-03	2.78E+02	1.10E+00	9.08E-01	3.65E-02	2.74E+01	1.10E+00	9.08E-01
10	4.44E-03	2.25E+02	1.10E+00	9.08E-01	4.06E-02	2.46E+01	1.10E+00	9.08E-01

Table 3.3: Values of natural frequencies and natural periods for four elementary models with added mass

Mode	Model I		Model II		Model III		Model IV	
n	f_{nat} [Hz]	T_{nat} [s]	f_{nat} [Hz]	T_{nat} [s]	f_{nat} [Hz]	T_{nat} [s]	f_{nat} [Hz]	T_{nat} [s]
1	1.00E-05	1.00E+05	2.48E-01	4.03E+00	9.10E-04	1.10E+03	2.48E-01	4.03E+00
2	4.00E-05	2.50E+04	2.48E-01	4.03E+00	1.82E-03	5.49E+02	2.48E-01	4.03E+00
3	9.00E-05	1.11E+04	2.48E-01	4.03E+00	2.73E-03	3.66E+02	2.48E-01	4.03E+00
4	1.60E-04	6.25E+03	2.48E-01	4.03E+00	3.64E-03	2.74E+02	2.48E-01	4.03E+00
5	2.50E-04	4.00E+03	2.48E-01	4.03E+00	4.56E-03	2.19E+02	2.48E-01	4.03E+00
6	3.60E-04	2.78E+03	2.48E-01	4.03E+00	5.47E-03	1.83E+02	2.48E-01	4.03E+00
7	4.90E-04	2.04E+03	2.48E-01	4.03E+00	6.39E-03	1.56E+02	2.48E-01	4.03E+00
8	6.40E-04	1.56E+03	2.48E-01	4.03E+00	7.31E-03	1.37E+02	2.48E-01	4.03E+00
9	8.10E-04	1.23E+03	2.48E-01	4.03E+00	8.23E-03	1.21E+02	2.48E-01	4.03E+00
10	1.00E-03	1.00E+03	2.48E-01	4.03E+00	9.16E-03	1.09E+02	2.48E-01	4.03E+00

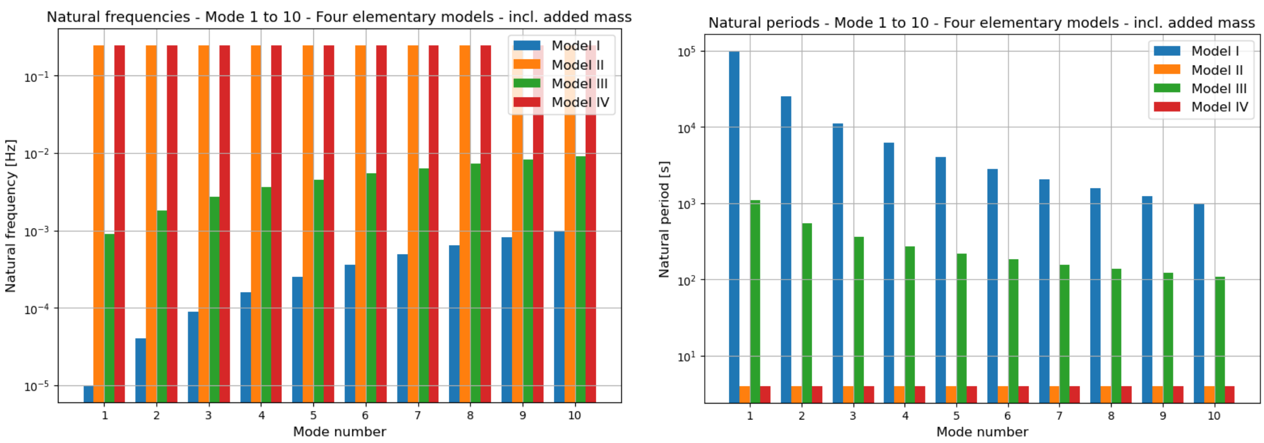

Figure 3.1: Natural frequencies and natural periods for eigenmode n =1-10 for four elementary models I, II, III and IV with added mass

3.3. Reflection on the results

If one studies the results, several remarks can be made. These are elaborated upon in the sections below. It has to be stressed that these values are the result of very crude computations using hand formulas and final conclusions can not be drawn yet.

3.3.1. Separate contributions of the buoyancy, axial tension and added mass

Observing Table 3.1 one can see a big difference in magnitude between the contributions of bending stiffness and tensional stiffness versus the contribution of buoyancy stiffness to the natural frequency. This explains the big differences between the natural frequencies for model I and III compared to model II and IV in Table 3.2 and 3.3. Whereas model I and III do not include the buoyancy stiffness, model 2 and 4 do include the buoyancy stiffness.

Per definition natural frequencies of higher order eigenmodes are higher than the natural frequencies of lower order eigenmodes. That's why one can see that the natural frequency values from model I and III are gradually increasing for higher eigenmodes. However, the natural frequencies of model II and IV are hardly increasing. This difference in behaviour is also caused by the relatively big buoyancy stiffness term, independent from mode number n. In the values for model I and III the influence of n, present in the bending stiffness term and tensional stiffness term, can be observed since values are increasing. The values for model II and IV are also increasing for increasing mode number, but this is hardly visible since the computation of the natural frequency is dominated by the high buoyancy stiffness term, that does not increase for higher n.

Comparing model I versus model III and model II versus model IV, one can conclude that in model III the influence of the axial tension is significant whereas it is negligibly small in model IV. Comparing I and III, the natural frequency is higher in model III and the rate of increase for increasing mode numbers is also higher, due to the fact that the tensional stiffness term increases for higher mode numbers.

The dominance of the model on the buoyancy stiffness is an important characteristic of the dynamics of the CFS and is caused by and depends mainly on two parameters. First of all, there is the magnitude of the buoyancy stiffness K, which is determined by the dimensions and the spacing of the floaters. More floaters, bigger floaters and/orsmaller floater spacing means more buoyancy, more stiffness in the system and higher natural frequencies. Secondly, the length of the system is relatively large, when compared to other dimensions of the CFS and compared to other civil or offshore structures. The bending stiffness term and tensional stiffness term are divided by the CFS length to respectively fourth order and second order. The consequence is that for a large CFS length these two terms decrease in magnitude. Subsequently the dominance of buoyancy stiffness term increases.

In order to study the effects of added mass, one can compare Table 3.2 with Table 3.3. It can quickly be concluded that for all models the computations including added mass show smaller natural frequencies compared to the computations excluding added mass. This can easily be explained by the fact that the added mass adds inertia to the dynamic system which results in an oppressive effect on the motions of the CFS. The conclusions made in sections above this section are valid for cases with and without added mass.

Conclusion

In conclusion, with the results of four different models and studying the contribution of separate elements it can be understood how the natural frequency of the CFS is build up and it can be concluded that the natural frequency is dominated by floater buoyancy stiffness being caused by the big length of the CFS and the floater dimensions and - spacing.

3.3.2. Interference with the wave frequency spectrum

When doing this analysis on natural frequencies of a dynamic system it is useful to compare these natural frequencies with the frequencies of external forcing acting on the CFS. When the natural frequencies and forcing frequencies are in the same range, resonance could occur. Resonance leads to high excitations of the system and could be a possible explanation of the large stresses in the cable, as explained already in Section 2.4.5. In this case, these external forces are the waves that have an oscillating character. In Figure 3.2 the wave frequency spectrum is shown for the offshore environment at the location of the Greater Changhua project of Van Oord, one of the projects in which the float-out method was applied. The wave frequency is on the horizontal axis and the wave spectral density is on the vertical axis. A higher spectral density means that there is more wave energy with this wave frequency. In this way it shows the wave climate of this location. This wave frequency spectrum was compared with the natural frequency values of the four elementary models. One can conclude that the natural frequencies of model II and IV including added mass are interfering with the wave frequency spectrum. This means that resonance phenomena are likely to occur. This hypothesis should be tested by modelling the CFS in more detail and research its natural frequencies in more detail.

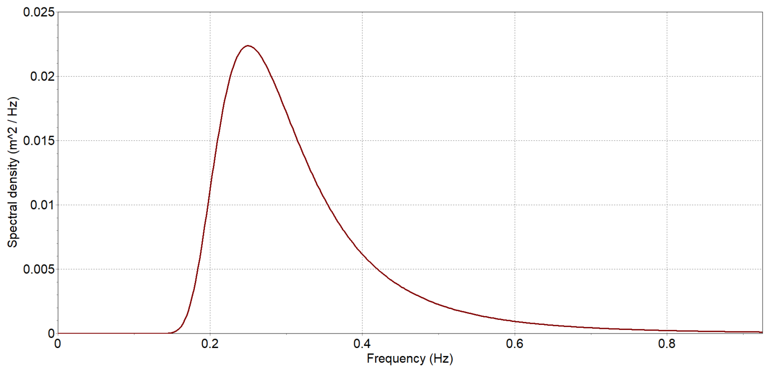

Figure 3.2: Wave frequency spectrum (JONSWAP) for the Van Oord Changhua project

3.3.3. Conclusions

The first important conclusion to make is that the floater's buoyancy is the biggest contribution to the natural frequency of the CFS. The buoyancy force of the floater acts as a spring, gives stiffness to the dynamic system and therefore increases the natural frequency. This dominance of the floater buoyancy will return often in the rest of the report. The axial tension also causes an increase in natural frequencies, in particular for higher mode natural frequencies, but has much less influence. Besides that, the added mass, increases the total mass in the dynamic system and therefore decreases the magnitude of the natural frequencies. A second important conclusion is that the natural frequencies of model II and model IV are in the same range as hydraulic wave frequencies.

This has lead to a hypothesis which will be tested in this research and is therefore an important topic throughout the whole report. The hypothesis is that the extreme internal stresses in the cable-floater-system are caused by resonance taking place between the wave forcing and the CFS itself. In order to test this hypothesis and research the dynamic behaviour of the CFS in more detail, a dynamic model is needed that approaches the floaters in a more realistic way. Therefore, an EBB model on a discrete elastic foundation is required. This model was already introduced in Section 2.3, but appeared to be really time consuming to model in an analytical way. Therefore, in the next Chapter 4 a finite-element-method model will be set-up.

Part II

Finite Element Method models

4
Set-up of the Finite Element Method model

The Finite Element Method (FEM) is a useful method to model the cable-floater-system (CFS) with the goal of studying the hydrodynamic behaviour. In this chapter the set-up of the FEM model is described. First of all, in Section 4.1 the spatial domain of the model is defined and discretised in small model elements and shape functions are introduced and determined. Afterwards, in Section 4.1.2 the dynamics of the system at a small scale are described in equations of motion (EQM's) of one element. Furthermore it is explained how to include the floater characteristics in Section 4.3. Next, in Section 4.4 the mathematical structure of the FEM model is assembled and in Section 4.5.2 the boundary conditions are added to this structure. Finally, adaptations for a model version in horizontal direction are explained in 4.6 and an overview of the simulated model cases is given in Section 4.7.

4.1. Definition and discretisation of the spatial domain

4.1.1. Introduction of the spatial domain and all used symbols

The Finite Element Method (FEM) is a systematic method to model a larger structure by dividing it into an equivalent system of many smaller structures or units (Colomes Gene, 2021). The same structural dynamics theory is used in the FEM models that was already explained in the previous Chapter 2.3. What differs is the method of building up the model of the full cable. As can be seen in Figure 4.1 below, the model consists of elements from 0 to E and indicated with parameter e. Besides that, there are $E+1$ nodes in the model including the boundaries. The nodes are numbered from 0 to N and are indicated with parameter n. Each element represents a piece of cable in between two nodes and has a length h. The floaters are all located at positions of nodes. Concerning the desired level of detail the number of elements between two floaters can be chosen. The minimum amount is one. In Section 5.1 it will be determined that 10 elements between two floaters give enough detail. The distance between two floaters is defined as Δ_f. The first and last node do not correspond to a floaters' location but are the boundaries of the CFS. See Section 4.5. In this model, only the degrees of freedom (DOF) of vertical motion u and the rotational motion θ will be studied along the horizontal axis x. See the DOF's including the x-coordinate indicated in bottom of Figure 4.1. The rotational motion θ is computed, because this influences the vertical motion u. θ is defined with the rotational axis horizontal and perpendicular to the cable length, often referred to as *pitch*.

Important to mention is that the floaters are modelled as discrete points, as in Chapter 2.3. This means that the horizontal length of the floater is neglected in studying the vertical motions along the CFS. However, the length (just like width and height) is taken into account in defining the buoyancy and added mass of the floater. The difference compared to the real situation is that in the model all the floaters' characteristics are assigned to one discrete point, which is a certain node in the FEM model. In reality, these characteristics are present along the whole length of the floater. When the number of elements between two floaters is higher than one, this means that there are more nodes than floaters. Therefore, in the model there are nodes that do have the floater characteristics attached and there are nodes that do not have any characteristics at all apart from their x-position along the horizontal axis and DOF's. All parameters that are used to define space, are mentioned in Table 4.1 below.

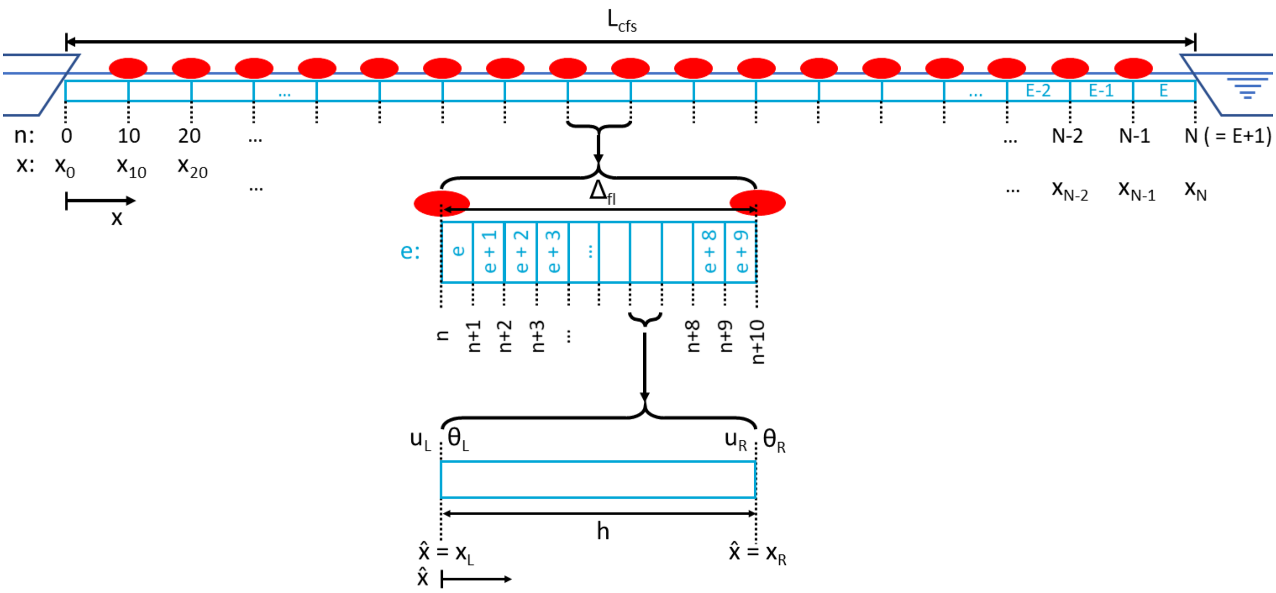

Figure 4.1: Overview of the finite-element-method model

Table 4.1: All parameters that define the spatial domain in the finite-element-method model, including symbol and unity

Symbol:	Unity:	Parameter:
x	m	the position along the horizontal axis of the structure
$\hat{x}$	m	the position along the horizontal axis of the elemental scale coordinate system
u	m	the vertical position of nodes above or below the horizontal x-axis
θ	rad	the rotation angle at the nodes' locations
e	-	refers to a specific element, between two nodes
E	-	the total number of elements in the CFS
n	-	refers to a specific node, on the border between two elements
N	-	the total number of nodes in the CFS
h	m	the longitudinal length of one element (element size)
E_{ff}	-	the amount of elements between two adjacent floaters
Δ_f	m	the longitudinal distance between two adjacent floaters (floater spacing)
L_{cfs}	m	the total length of the CFS

4.1.2. Determination of the shape functions in the elemental dynamic system

Before the structure can be dynamically described at the full system scale, first the dynamics of one model element are described. The dynamics of one element are described by the two nodes of this element on both sides. In other words, equations need to be derived for the 2 x 2 = 4 DOF's of one model element. See one element as well as the DOF's visualised in the bottom image of Figure 4.1. In modelling an element, the dynamics of the floaters is not yet included. Once the dynamics for one element is described, the effects of the floaters are included. To describe these DOF's in a systematic way, it is necessary to introduce so called *'shape functions'*. Shape functions are a mathematical tool and can assist to describe the relations between the DOF's of one element in the FEM model. With these relations for one element, the relations between physical system properties such as mass, stiffness, buoyancy and tension and the dynamic response of the system can be described correctly. In Appendix B, the concept of shape functions is explained in detail and the shape functions for the FEM model are derived. The end result being four shape functions are repeated here in Equation 4.1:

$$N_1(\hat{x}) = 1 - \frac{3}{h^2}\hat{x}^2 + \frac{2}{h^3}\hat{x}^3 \quad (4.1a) \qquad N_2(\hat{x}) = \hat{x} - \frac{2}{h}\hat{x}^2 + \frac{1}{h^2}\hat{x}^3 \quad (4.1b)$$

$$N_3(\hat{x}) = \frac{3}{h^2}\hat{x}^2 - \frac{2}{h^3}\hat{x}^3 \quad (4.1c) \qquad N_4(\hat{x}) = -\frac{1}{h}\hat{x}^2 + \frac{1}{h^2}\hat{x}^3 \quad (4.1d)$$

4.2. The equations of motion of one model element

Similar to the structures that were modelled in Chapter 2.3, the cable is modelled as a collection of Euler-Bernoulli Beams (EBB's) and the floaters are modelled as springs located at the interface between the EBB's. In this section the EQM's for one model element are formulated in order to make them suitable to be applied in the discretised spatial domain, that was defined in previous Section 4.1. This means that the original strong form of the EQM's is rewritten to a weak form of the EQM's in which the shape functions, that were determined in Section 4.1, are substituted.

4.2.1. The strong form of the equation of motion

The essence of the dynamic behaviour of the CFS is described with its EQM. Similar to Chapter 2.3, the EQM consists of three main parts being mass, stiffness and axial tension. The difference with the EQM's in Chapter 2.3 is that the model is significantly larger and that for each node EQM's are derived. In order to apply the Finite Element Method, the EQM is rewritten from its *strong form* into its *weak form*. The continuous strong form of the EQM is the conventional notation and states the conditions at every point over a domain that a solution must satisfy. In the solution continuity and differentiability have to be maintained. It is a (set of) differential equation(s) that must be respected at every point in the domain. See Equation 4.2 below. However, a weak form states the conditions that the solution must satisfy in an averaged, integral sense. See Equation 4.5 in Section 4.2.3. One could say that by rewriting the EQM's from the strong form into the weak form the spatial domain is mathematically discretised.

The strong form of the EQM is:

$$m\ddot{u}(x) + EIu''''(x) + Tu''(x) = q(x) \tag{4.2}$$

Multiplying all terms by the *weight function* or *test function* $v(x)$ and integrating over one element Ω_e gives:

$$\int_{\Omega_e} m\ddot{u}(\hat{x})v(\hat{x})\,d\Omega + \int_{\Omega_e} EIu''''(\hat{x})v(\hat{x})\,d\Omega + \int_{\Omega_e} Tu''(\hat{x})v(\hat{x})\,d\Omega = \int_{\Omega_e} q(\hat{x})v(\hat{x})\,d\Omega \qquad \forall v(x) \tag{4.3}$$

Important to stress is that the test function $v(x)$ is an arbitrary function, which means that Equation 4.3 has to hold for all possible functions $v(x)$.

4.2.2. Rewriting the strong form into weak form

In this section below, all terms, excluding the mass term, will be rewritten into the weak form. Afterwards, these seperate terms are combined into one general EQM in weak form. First, integrate by parts the bending stiffness term from Equation 4.3 with a fourth order derivative:

$$\begin{aligned}\int_{\Omega_e} EIu''''(x)v(\hat{x})\,d\Omega &= -\int_{\Omega_e} EIu'''(\hat{x})v'(\hat{x})\,d\Omega + EIu'''(\hat{x})v(\hat{x})\Big|_{\hat{x}=x_l}^{\hat{x}=x_r} \\ &= \int_{\Omega_e} EIu''(\hat{x})v''(\hat{x})\,d\Omega - EIu''(\hat{x})v'(\hat{x})\Big|_{\hat{x}=x_l}^{\hat{x}=x_r} + EIu'''(\hat{x})v(\hat{x})\Big|_{\hat{x}=x_l}^{\hat{x}=x_r}\end{aligned}$$

Secondly, integrating by parts the second order axial tension term from Equation 4.3 leads to:

$$\int_{\Omega_e} Tu''(\hat{x})v(\hat{x})\,d\Omega = -\int_{\Omega_e} Tu'(\hat{x})v'(\hat{x})\,d\Omega + Tu'(\hat{x})v(\hat{x})\Big|_{\hat{x}=x_l}^{\hat{x}=x_r}$$

In this equation the last term is equal to zero. This can be explained by studying the term in more detail. Since $u'(x) = \theta(x)$ the term can be rewritten. If the rotations are studied at one node, it is found the term is equal to zero:

$$Tu'(\hat{x})v(\hat{x})\Big|_{\hat{x}=x_l}^{\hat{x}=x_r} = Tu'(\hat{x})\Big|_{\hat{x}=x_l}^{\hat{x}=x_r} = Tu'(x_r) - Tu'(x_l) = T \cdot [u'(x_r) - u'(x_l)] = T \cdot [\theta(x_r) - \theta(x_l)] = T \cdot [0] = 0$$

On the right hand side of the equation there is the external forces term $q(\hat{x})$. When studying the external forces on the CFS, one can distinguish a few categories, being hydraulic forces due to currents and waves, wind forces and mooring forces. The mooring forces are in fact the forces present at the outer boundaries of the model and are assumed to be known. The CFS is a structure that is mostly below the water surface. Besides that, the density of air is one thousand times smaller than the density of water. Therefore, it is assumed that the wind forces are relatively small compared to the hydraulic forces and are not taken into account. Current forces have already been described in Section 2.4.4. In order to take account wave forcing in a correct way, more in-depth dynamic analysis instead of modal analysis is required. This is considered beyond the scope of this research.

4.2.3. The weak form of the equation of motion

The bending stiffness term and the axial tension term have been rewritten. These terms can be substituted into Equation 4.3. The weak form of the EQM for one system element becomes:

$$\begin{aligned} &\int_{\Omega_e} m\ddot{u}(\hat{x})v(\hat{x})\,d\Omega + \int_{\Omega_e} EIu''(\hat{x})v''(\hat{x})\,d\Omega - \int_{\Omega_e} Tu'(\hat{x})v'(\hat{x})\,d\Omega = \\ &\int_{\Omega_e} q(\hat{x})v(\hat{x})\,d\Omega + \left[EIu''(\hat{x})v'(\hat{x}) - EIu'''(\hat{x})v(\hat{x})\right]\Big|_{\hat{x}=x_l}^{\hat{x}=x_r} \end{aligned} \tag{4.4}$$

The equation is simplified by renaming the last two terms in the equation above:

$$P(\hat{x}) = EIu''(\hat{x}) \qquad Q(\hat{x}) = EIu'''(\hat{x})$$

Next,the shape functions are substituted into the weak form. To do so we substitute the test function $v(\hat{x})$ for the shape function $N_i(\hat{x})$ or a derivative of it:

$$v(\hat{x}) = N_i(\hat{x}) \qquad v'(\hat{x}) = N_i'(\hat{x}) \qquad v''(\hat{x}) = N_i''(\hat{x}) \qquad \text{for all degrees of freedom } i = 1, ..., Q$$

Besides that, in the EQM the following terms are replaced:

$$u(\hat{x}) = \sum_{j=1}^{N} N_j(\hat{x})w_i \qquad u''(\hat{x}) = \sum_{j=1}^{N} N_j''(\hat{x})w_i \qquad \ddot{u}(\hat{x}) = \sum_{j=1}^{N} N_j(x)\ddot{w}_i \qquad \text{in which: } w_i = \begin{bmatrix} u(x_l) \\ \theta(x_l) \\ u(x_r) \\ \theta(x_r) \end{bmatrix}$$

Finally, Equation 4.4 can be rewritten into the final weak form of the EQM for one element of the FEM model. See Equation 4.5 below:

$$\begin{aligned} &\sum_{j=1}^{N}\left[m\int_{\Omega_e} N_j(\hat{x})N_i(\hat{x})\,d\Omega\right]\ddot{w}_i + \sum_{j=1}^{N}\left[J\int_{\Omega_e} N_j''(\hat{x})N_i''(\hat{x})\,d\Omega\right]w_i + \sum_{j=1}^{N}\left[T\int_{\Omega_e} N_j'(\hat{x})N_i'(\hat{x})\,d\Omega\right]w_i \\ &= \int_{\Omega_e} q_(\hat{x})N_i(\hat{x})\,d\Omega + \left[P(\hat{x})N_i'(\hat{x}) - Q(\hat{x})N_i(\hat{x})\right]\Big|_{\hat{x}=x_L}^{\hat{x}=x_R} \end{aligned} \tag{4.5}$$

4.2.4. Explanation on the internal forces

The last term in Equation 4.5 is the internal forces term, which is referred to as S^e. When the values of x_l and x_r are substituted into the expression, the following equation is the result:

$$S_i^e = \left[P(\hat{x})N_i'(\hat{x}) - Q(\hat{x})N_i(\hat{x})\right]\Big|_{\hat{x}=x_l}^{\hat{x}=x_r} = \left[P(x_R)N_i'^e(x_r) - Q(x_r)N_i^e(x_r)\right] - \left[P(x_L)N_i'^e(x_l) - Q(x_l)N_i^e(x_l)\right]$$

If this equation S_i^e is computed for i = 1, ... 4, it is found that:

When $i = 1:$ $\quad S_1 = Q(x_l)$
When $i = 2:$ $\quad S_2 = -P(x_l)$
When $i = 3:$ $\quad S_3 = -Q(x_r)$
When $i = 4:$ $\quad S_4 = P(x_r)$

One can conclude that $S_1 = -S_3$ and $S_2 = -S_4$. These calculations can be repeated for all elements e. If these contributions of internal forces are added up for E elements in the system, these internal forces contributions will cancel and disappear from the equation. Only at the boundaries the internal forces need to be accounted for.

4.3. Including floater characteristics in the model set-up

In the previous Section 4.2, one element of the cable was described from one node to the next node. In between two elements, at the node locations, the floaters are located. Before the FEM model is assembled in Section 4.4, the contributions of the floaters to the EQM's of the nodes need to be formulated in equations in this section.

Based on the CFS design and the desired grid size, a floater is located at every node (except boundaries) or there are only floaters at certain nodes. A node has two DOF's and it is assumed that the floater is influencing both DOF's. Besides that, the floater has a structural mass and associated added mass that has influence on the behaviour of the cable. So, in total there are four aspects of the floater that influence the hydrodynamic behaviour of the CFS and that have to be included in the dynamic model:

- The structural mass of the floater m_f;
- The added mass of the floater moving in water $m_{a,f}$;
- The buoyancy force is modelled as a translational, vertical spring force as a function of vertical displacement u;
- The righting moment of the floater (ship stability), modelled as a rotational spring moment as a function of rotational motion θ.

Most terms in the EQM, being cable mass, cable bending stiffness and axial tension are present along the full length of one element and along the full length of the CFS. These terms are therefore modelled as an integral from left boundary x_l to the right boundary x_r of an element. See Equation 4.3. However, the four floater characteristics mentioned above are acting at discrete points, namely the nodes in between two elements. Therefore, these forces are not modelled using shape functions but modelled with a *Dirac Delta function*. A Dirac Delta function is a function that is non-zero for a (set of) narrow interval(s) along a certain axis, and zero for the rest of the domain on the axis. For the CFS, this is the x-axis longitudinal to the cable and the specific intervals are the floater's locations. At the scale of one element the x-axis is the local $\hat{x}$ axis and the floater's locations are $\hat{x} = x_l$ and $\hat{x} = x_r$. Therefore the forces term $q(\hat{x})$ becomes:

$q(\hat{x}) = P_0\delta(\hat{x} - x_l)$ in which: $P_0 = -k_{D,u}u(x_l)$ for vertical motions
$P_0 = -k_{D,\theta}\theta(x_l) = -k_{D,\theta}u'(x_l)$ for rotational motions

$q(\hat{x}) = P_0\delta(\hat{x} - x_r)$ in which: $P_0 = -k_{D,u}u(x_r)$ for vertical motions
$P_0 = -k_{D,\theta}\theta(x_r) = -k_{D,\theta}u'(x_r)$ for rotational motions

4.4. Assembling the model

In Section 4.2 the focus was on deriving the 'weak form' of the EQM, which is a format that is compatible to the FEM calculations. In this section the FEM model is in fact assembled. This entails that the EQM in its mathematical, weak form is used to rewrite the system into a set of elemental matrices. The main input of these matrices are the shape functions defined in Section 4.1.2 and the input parameters, of which the formulas are explained in Section 2.4 and technical specifications on the CFS in Appendix A.

Studying the four summations of shape function integrals in Equation 4.5, one can conclude that these are 4x4 matrices. The elemental mass matrix, elemental bending stiffness matrix, elemental discrete stiffness matrix and elemental axial tension matrix are labeled respectively M^e_{ij}, B^e_{ij}, D^e_{ij} and T^e_{ij}. As the matrices B^e_{ij}, D^e_{ij} and T^e_{ij} are all multiplied with the same matrix w_j these matrices are added up to one elemental stiffness matrix K^e_{ij}. For the sake of overview, the two terms on the right hand side are given the symbols of Q^e and S^e respectively. Q^e and S^e will not be defined since these are not relevant for this research. Expressing the elemental weak form with these parameters, Equation 4.5 finally becomes Equation 4.6:

$$
\begin{aligned}
M^e_{ij}\ddot{w}_i + B^e_{ij}w_i + D^e_{ij}w_i + T^e_{ij}w_i &= Q^e + S^e \\
M^e_{ij}\ddot{w}_i + [B^e_{ij} + D^e_{ij} + T^e_{ij}]w_i &= Q^e + S^e \\
M^e_{ij}\ddot{w}_i + K^e_{ij}w_i &= Q^e + S^e
\end{aligned}
\tag{4.6}
$$

Matrix M^e_{ij} is explained in Section 4.4.1 and matrix K^e_{ij} in Section 4.4.2. Afterwards, in Section 4.4.3 the full structure FEM model is assembled. In the build up of these two matrices a distinction needs to be made between input values that concern system elements and input values that concern system nodes. See the distinction in Table 4.2 below. All parameters related to the cable are continuous characteristics and are assigned to the elements. The shape functions are used to write the continuous CFS system into a dynamic system with a mass matrix and stiffness matrix that describes motions at the nodes. The consequence of doing this for each element are 4x4 elemental matrices, because per element there are two nodes each having two DOF's. Afterwards these elemental matrices imported into one global mass matrix and stiffness matrix. An elaborate explanation of this procedure is found below. On the contrary, all parameters related to the floater are discrete characteristics and are assigned already to a node. Shape functions are therefore not needed and soley the input values themselves are added to the elemental mass matrix and elemental stiffness matrix. Since these characteristics are not a matrix but single values, the floater input parameters are only present on the diagonal axis of the matrix.

Table 4.2: Model characteristics and a distinction between element and node

		Element characteristic	**Node characteristic**
Structural mass cable	m_c	x	
Added mass cable	$m_{a,u,c}$	x	
Structural mass floater	m_f		x
Added mass floater	$m_{a,u,f}$ and $m_{a,\theta,f}$		x
Bending stiffness	b	x	
Floater stiffness	d_u and d_θ		x
Axial tension	t	x	

4.4.1. Mass in the model

The format of the elemental mass matrix M^e_{ij} is stated below. The value of each matrix cell is computed with the same integral function but having another shape function for each index number i and j. This integral has the size of one element Ω_e. In formulating the shape functions, see Equation 4.1, it was assumed that the length of one element reaches from $\hat{x} = 0$ to $\hat{x} = h$. h is the distance between two nodes (the element size) and is known. The integral can be computed using these same values. Assuming that each element has the same diameter D_c, horizontal length h and structural density ρ_c, it can be concluded that the mass values concerning the cable can be used for all FEM model elements.

These values $m^e_{ij,c}$ are the base of the 4x4 elemental mass matrix M^e_{ij} and do not change for different CFS configurations. However, the mass values of the floater have to be added to this elemental matrix as well. The position of these values depend on the CFS configuration and the grid size that is chosen. As an example, if the elemental mass matrix would represent an element that on one side borders on a node with a floater, the elemental mass matrix would look like this:

$$M_{ij}^e = \begin{bmatrix} m_{11,c}^e + m_{u,f} & m_{12,c}^e & m_{13,c}^e & m_{14,c}^e \\ m_{21,c}^e & m_{22,c}^e + m_{\theta,f} & m_{23,c}^e & m_{24,c}^e \\ m_{31,c}^e & m_{32,c}^e & m_{33,c}^e & m_{34,c}^e \\ m_{41,c}^e & m_{42,c}^e & m_{43,c}^e & m_{44,c}^e \end{bmatrix} \quad \text{in which:} \quad \begin{cases} m_{ij,c}^e = (m_c + m_{a,u,c}) \int_{\Omega_e} N_j(\hat{x}) N_i(\hat{x}) d\Omega \\ m_{u,f} = m_f + m_{a,u,f} \\ m_{\theta,f} = m_f + m_{a,\theta,f} \end{cases}$$

4.4.2. Stiffness in the model

Similar to the mass matrix the stiffness matrix also has a 4x4 shape. It has three main contributions: bending stiffness, axial tension and the (discrete) floater stiffness. The bending stiffness B_{ij}^e and the axial tension T_{ij}^e have a continuous character and are therefore described with the shape functions. This results again in a 4x4 elemental stiffness matrix K_{ij}^e. Similar to the floater (added) mass the floater stiffness D_{ij}^e has a discrete character. Resembling the mass matrix, the integrals of the input values b_{ij}^e and t_{ij}^e of the elemental bending stiffness matrix and tension matrix are computed with the values of $\hat{x} = 0$ and $\hat{x} = h$.

$$B_{ij}^e = \begin{bmatrix} b_{11}^e & b_{12}^e & b_{13}^e & b_{14}^e \\ b_{21}^e & b_{22}^e & b_{23}^e & b_{24}^e \\ b_{31}^e & b_{32}^e & b_{33}^e & b_{34}^e \\ b_{41}^e & b_{42}^e & b_{43}^e & b_{44}^e \end{bmatrix} \qquad b_{ij}^e = J \int_{\Omega_e} N_j''(\hat{x}) N_i''(\hat{x}) d\Omega$$

$$T_{ij}^e = \begin{bmatrix} t_{11}^e & t_{12}^e & t_{13}^e & t_{14}^e \\ t_{21}^e & t_{22}^e & t_{23}^e & t_{24}^e \\ t_{31}^e & t_{32}^e & t_{33}^e & t_{34}^e \\ t_{41}^e & t_{42}^e & t_{43}^e & t_{44}^e \end{bmatrix} \qquad t_{ij}^e = T \int_{\Omega_e} N_j'(\hat{x}) N_i'(\hat{x}) d\Omega$$

$$d_u = k_{D,u} \qquad d_\theta = k_{D,\theta}$$

The bending stiffness matrix B_{ij}^e, the axial tension matrix T_{ij}^e and the input values of discrete buoyancy stiffness have been composed. The complete element stiffness matrix K_{ij}^e is achieved by summing up all characteristics. Similar to the floater mass, the position of the discrete stiffness values $d_{ij,u}^e$ and $d_{ij,\theta}^e$ depend on the CFS configuration and the grid size that is chosen. As an example, if the elemental stiffness matrix would represent an element that on one side borders on a node with a floater, the elemental stiffness matrix would look like this:

$$K_{ij}^e = \begin{bmatrix} t_{11}^e + b_{11}^e + d_u & t_{12}^e + b_{12}^e & t_{13}^e + b_{12}^e & t_{14}^e + b_{12}^e \\ t_{21}^e + b_{21}^e & t_{22}^e + b_{22}^e + d_\theta^e & t_{23}^e + b_{23}^e & t_{24}^e + b_{23}^e \\ t_{31}^e + b_{31}^e & t_{32}^e + b_{32}^e & t_{33}^e + b_{33}^e & t_{34}^e + b_{34}^e \\ t_{41}^e + b_{41}^e & t_{42}^e + b_{42}^e & t_{43}^e + b_{43}^e & t_{44}^e + b_{44}^e \end{bmatrix} \tag{4.7}$$

4.4.3. Assembling the full structure model

The last step is to compose the full model mass matrix M and stiffness matrix K. The matrix is too big to fully describe and the exact matrix will change for different CFS configurations and the model grid size. In Figure 4.1 part of the system is visualised, mentioning the DOF's per element at the bottom. For example, the DOF's at node $x = x_{n+2}$ being $u(x_{n+2})$ and $\theta(x_{n+2})$ can be described. Considering the two bordering elements, it is easy to understand that the right boundary of the element on the left is the same node as the left boundary of the right element. In other words, one node is neighbouring two structure elements and the DOF's of this node are dependent on the cable input parameters of both elements. In case of a node with a floater, the floater input parameters are added as well. This dependency of a node on two elements explains the overlapping character in the global mass matrix and the stiffness matrix, which are included as respectively Equation C.1 and C.2 in Appendix C. The principle of superposition of the motions of both elements is used which means that the input characteristics are added up. In Equations C.1 and C.2, part of the matrices are shown for node $x = x_n$, $x = x_{n+1}$, $x = x_{n+2}$ and $x = x_{n+3}$. In the stiffness matrix tb_{ij}^e indicates the summation of the tension term and the bending stiffness term:

$$tb_{ij}^e = t_{ij}^e + b_{ij}^e$$

One can repeat this procedure going from left to right throughout the whole model. One can see that the elemental mass matrix and stiffness matrix are repeating themselves with a step size of two since there are two DOF's per node. The locations of the floater (added) mass and stiffness in matrix M and K depend on the chosen number of elements E_{ff} between two floaters. This determines the amount of nodes between two nodes with floaters and therefore the amount of rows and columns in the global stiffness matrix and mass matrix. Some other effects on the chosen number of nodes between floaters:

- When more elements are added to the system, also the amount of nodes and the DOF's increases. Therefore the mass matrix and stiffness matrix both grow in size (to the same extent for both matrices and both dimensions).
- As the number of elements between two floaters increases and the floater spacing remains constant, the element size h becomes smaller. This changes the outcome of the shape function's integrals and the structural mass and added mass of the cable for one element.
- The number of natural frequencies and modal shapes increases when the spatial domain is discretised in a more detailed way. More information on natural frequencies and modal shapes in the next Chapter 5.

4.5. Including the boundary conditions

The last step in assembling the full structure model is to include the system's boundary conditions (BC's). In Section 4.5.1 the boundaries of the CFS are studied in more detail and the two types of BC's are distinguished. Afterwards, in Section 4.5.2 there is accounted for the BC's in the FEM model set-up.

4.5.1. Definition of the boundary conditions

In reality, during a cable float out installation the cable is connected to a vessel at both ends. The offshore end of the cable is most likely connected to a cable-laying vessel (CLV). The nearshore end of the cable is connected to a smaller vessel, for instance a barge. However, the connection between vessel and cable is similar for both cable ends. The cable, coming out of the water, first touches the vessel on the chute. This is an arc shaped structure which is preventing the cable from bending with a radius smaller than the minimum bending radius. See an example of the chute of the CLV Nexus in the left image in Figure 4.2. After this connection, the cable is held by an tensioner system which is preventing the cable from moving in any translational direction or rotational direction. See right image in Figure 4.2. Besides that, it should be mentioned that the vessel itself, and therefore the cable connection point, does move in waves and currents. Looking at the aim of the model it is not necessary to include these vessel motions in the model. Namely, the goal is to compute natural frequencies which are fully determined by the structure and its connections and not by any external forces / motions. If one would study the precise motion and forces of the structure in certain hydraulic conditions, then it could be necessary to include the motions of the vessel.

Figure 4.2: Images of a chute system (left) and tensioner system (right) (Driessen, 2015) (4C Offshore, n.d.)

Whereas in the continuous model (Section 2.2.1 and Chapter 3) only simply supported BC's were applied, in this FEM model the difference between the two BC's is researched and therefore two types of BC's are applied: (1) a clamped beam and (2) a simply-supported beam.

- In a clamped beam model: the two beam ends are supported in a way that all translational and rotational motions are restricted. For these two locations the displacements, velocities and accelerations of the beam are equal to zero for all directions and each moment in time. For the FEM model this means:

$$u(x_0) = 0 \qquad \wedge \qquad \theta(x_0) = 0 \qquad \wedge \qquad u(x_N) = 0 \qquad \wedge \qquad \theta(x_N) = 0 \qquad \text{for all } t$$

- In a simply-supported beam model, the two beam ends are supported in a way that the translational motions are restricted, but the rotational motions are free. For the translational motions at the boundary nodes this means zero displacement, velocity and acceleration for each moment in time. The rotational displacement, velocity and acceleration at the boundary nodes have yet unknown values that can vary in time. For the FEM model this means:

$$u(x_0) = 0 \qquad \wedge \qquad \theta(x_0) \neq 0 \qquad \wedge \qquad u(x_N) = 0 \qquad \wedge \qquad \theta(x_N) \neq 0 \qquad \text{for all } t$$

4.5.2. Including the boundary conditions in the mass - and stiffness matrices

Up to this point the boundaries have been approached as regular nodes with a floater attached to it. However, a major difference between these two boundary nodes and the intermediate nodes is that (part of) the DOF's are already known. That's why the rows and columns belonging to these known DOF's can be removed from the global mass matrix M and global stiffness matrix K and the set-up of the FEM model changes. In case the simply supported beam BC's are applied, two rows and columns from matrix M and K are removed, corresponding to the vertical DOF's of the left - and right boundary node (in case of the mass matrix $\ddot{u}_0$ and $\ddot{u}_N$). In case the clamped beam BC's are applied, four rows and columns from matrix M and K are removed, corresponding to the vertical and rotational DOF's of the left - and right boundary node (in case of the mass matrix$\ddot{u}_0$, $\ddot{u}_N$, $\ddot{\theta}_0$ and $\ddot{\theta}_N$). In the matrices below, the implications for the global mass matrix procedure have been visualised for respectively simply supported - and clamped BC's. The same procedure holds for the stiffness matrix.

$$\begin{bmatrix} m^0_{11}+m_{u,f} & m^0_{12} & m^0_{13} & m^0_{14} & \rightarrow & \dots & 0 & 0 & 0 & 0 \\ m^0_{21} & m^0_{22}+m_{\theta,f} & m^0_{23} & m^0_{24} & \rightarrow & \dots & 0 & 0 & 0 & 0 \\ m^0_{31} & m^0_{32} & m^0_{33}+m^1_{11} & m^0_{34}+m^1_{12} & \rightarrow & \dots & 0 & 0 & 0 & 0 \\ m^0_{41} & m^0_{42} & m^0_{43}+m^1_{21} & m^0_{44}+m^1_{22} & \rightarrow & \dots & 0 & 0 & 0 & 0 \\ \downarrow & \downarrow & \downarrow & \downarrow & \searrow & \dots & \downarrow & \downarrow & \downarrow & \downarrow \\ \dots & \dots & \dots & \dots & \dots & \dots & \dots & \dots & \dots & \dots \\ 0 & 0 & 0 & 0 & \rightarrow & \dots & m^{E-1}_{33}+m^E_{11} & m^{E-1}_{34}+m^E_{12} & m^E_{13} & m^E_{14} \\ 0 & 0 & 0 & 0 & \rightarrow & \dots & m^{E-1}_{43}+m^E_{21} & m^{E-1}_{44}+m^E_{22} & m^E_{23} & m^E_{24} \\ 0 & 0 & 0 & 0 & \rightarrow & \dots & m^E_{31} & m^E_{32} & m^E_{33}+m_{u,f} & m^E_{34} \\ 0 & 0 & 0 & 0 & \rightarrow & \dots & m^E_{41} & m^E_{42} & m^E_{43} & m^e_{44}E+m_{\theta,f} \end{bmatrix} \begin{bmatrix} \ddot{u}_0 \\ \ddot{\theta}_0 \\ \ddot{u}_1 \\ \ddot{\theta}_1 \\ \downarrow \\ \dots \\ \ddot{u}_{N-1} \\ \ddot{\theta}_{N-1} \\ \ddot{u}_N \\ \ddot{\theta}_N \end{bmatrix}$$

$$\begin{bmatrix} m^0_{11}+m_{u,f} & m^0_{12} & m^0_{13} & m^0_{14} & \rightarrow & \dots & 0 & 0 & 0 & 0 \\ m^0_{21} & m^0_{22}+m_{\theta,f} & m^0_{23} & m^0_{24} & \rightarrow & \dots & 0 & 0 & 0 & 0 \\ m^0_{31} & m^0_{32} & m^0_{33}+m^1_{11} & m^0_{34}+m^1_{12} & \rightarrow & \dots & 0 & 0 & 0 & 0 \\ m^0_{41} & m^0_{42} & m^0_{43}+m^1_{21} & m^0_{44}+m^1_{22} & \rightarrow & \dots & 0 & 0 & 0 & 0 \\ \downarrow & \downarrow & \downarrow & \downarrow & \searrow & \dots & \downarrow & \downarrow & \downarrow & \downarrow \\ \dots & \dots & \dots & \dots & \dots & \dots & \dots & \dots & \dots & \dots \\ 0 & 0 & 0 & 0 & \rightarrow & \dots & m^{E-1}_{33}+m^E_{11} & m^{E-1}_{34}+m^E_{12} & m^E_{13} & m^E_{14} \\ 0 & 0 & 0 & 0 & \rightarrow & \dots & m^{E-1}_{43}+m^E_{21} & m^{E-1}_{44}+m^E_{22} & m^E_{23} & m^E_{24} \\ 0 & 0 & 0 & 0 & \rightarrow & \dots & m^E_{31} & m^E_{32} & m^E_{33}+m_{u,f} & m^E_{34} \\ 0 & 0 & 0 & 0 & \rightarrow & \dots & m^E_{41} & m^E_{42} & m^E_{43} & m^e_{44}E+m_{\theta,f} \end{bmatrix} \begin{bmatrix} \ddot{u}_0 \\ \ddot{\theta}_0 \\ \ddot{u}_1 \\ \ddot{\theta}_1 \\ \downarrow \\ \dots \\ \ddot{u}_{N-1} \\ \ddot{\theta}_{N-1} \\ \ddot{u}_N \\ \ddot{\theta}_N \end{bmatrix}$$

4.6. Adaptations to the model for horizontal direction

In the set-up of the FEM model explained above, the starting point was vertical DOF's of the CFS. However, in Chapter 7 it will appear to be that the modal behaviour of the CFS in horizontal direction is also relevant to study. Therefore a different version of the FEM model needs to be made that can perform a modal analysis in horizontal direction instead of the vertical direction. In this section, the hydrodynamic differences between the vertical and horizontal model will be explained briefly next to the required adaptations to the script of creating a FEM model.

In order to compare the two models, the model characteristics mentioned in Table 4.2 are recalled. First of all, considering the input characteristics for the mass matrix M nothing changes with respect to the structural mass of cable and floater. However, the added mass in translational and rotational direction of the floater (Equations 2.17 and 2.18) does change because the floater being partially submerged. Assuming a partially submerged spheroid shape, the equations for respectively horizontal and rotational added mass are (Newman, 2017):

$$m_{a,u,f} = \rho_w \cdot D_f \cdot L_f \tag{4.8}$$

$$m_{a,\theta,f} = \frac{1}{8}\pi\rho_w \cdot (\frac{L_f}{2})^4 \cdot D_f \tag{4.9}$$

Secondly, the input characteristics of the stiffness matrix are studied again. Due to the symmetric shape of the cable and based on documents of the cable supplier, it was concluded that the cable bending stiffness is the same for all bending directions. Therefore the contribution of bending stiffness to the stiffness matrix remains unchanged. Similarly, the contribution of the cable axial tension remains the same. The most important difference with the vertical direction is that for a horizontal direction the floater's buoyancy stiffness is not present. During a horizontal motion the draft of the floaters remains constant, so there is no change in upward buoyant force and therefore no spring force that needs to be modelled. Concluding, for the horizontal direction the stiffness matrix K consists only of a contribution from bending stiffness B and axial tension T. The absence of the floater's buoyancy stiffness simplifies the FEM model to a great extent and actually makes it a continuous model again.

Finally, to derive the global matrices the BC's need to be accounted for. This procedure to model simply supported BC's or clamped BC's, as was explained in Section 4.5, is the same. The simply supported BC restrict horizontal motion and the clamped BC restrict both horizontal motion and rotations.

4.7. Overview of simulated cases with finite-element-method model

In Table 4.3 below, an overview is given on the cases that were modelled with the FEM model. These cases were modelled for both the vertical direction and the horizontal direction.

Table 4.3: Overview of the simulated cases with the finite-element-method model including the changing input parameters

	Case A	**Case B**	**Case C**	**Case D**
Current velocity u [m/s]	0	0.35	0	0.35
Boundary conditions	simply supported	simply supported	clamped	clamped

5

Results and analysis of the Finite Element Model

In the previous chapter the set-up of the Finite Element Method (FEM) model was explained. The cable-floater-system (CFS) was modelled as a structure and all different structural parameters were determined. In this chapter the model is used and results are derived, presented and analysed. First, in Section 5.1 the natural frequencies of the CFS are treated. Secondly, in Section 5.2 the modal shapes of the CFS are studied. Next, using a modified version of the model, the results for the CFS in horizontal direction are shown in Section 5.3. Lastly, a parametric study is performed on the floater spacing in Section 5.4.

5.1. Natural frequencies of the cable-floater system

5.1.1. Derivation of the natural frequencies

The natural frequency of a structure is the frequency at which the structure oscillates in absence of any external force. This frequency is therefore only dependent on the structural characteristics of 1) the mass and 2) the stiffness and is independent from e.g. damping. The equation of motion (EQM) valid for this situation without external forcing can be distilled from Equation 4.6:

$$M_{ij}\ddot{u}_j + K_{ij}u_j = 0 \tag{5.1}$$

The general solution for this free vibration problem is the sum of a harmonic function $H(t)$ multiplied by each modal shape (*modal superposition*):

$$u(t) = \sum_i^E H_i(t) \cdot \phi_i = \sum_i^E (A_i cos(\omega_i t) + B_i sin(\omega_i t)) \cdot \phi_i = \Phi \cdot \sum_i^E (A_i cos(\omega_i t) + B_i sin(\omega_i t)) \tag{5.2}$$

By substituting the general solution, Equation 5.2, into the EQM, 5.1, this free vibration problem can be rewritten into Equation 5.3.

$$K \cdot \phi_i = \omega_i^2 \cdot M \cdot \phi_i \tag{5.3}$$

This equation is known as the *General Eigenvalue Problem*. The eigenvalues ω_i and eigenvectors ϕ_i of this problem can be solved using linear algebra principles and two input variables being the mass matrix M, Equation C.1, and stiffness matrix K, Equation C.2. The relation between eigenvalue λ, the angular frequency ω and natural frequency f is formulated in Equation 5.4. Using Equation 5.4 and the eigenvalues as output of Equation 5.3, the natural frequencies and natural periods ($T = 1/f$) are computed.

$$\lambda_i \equiv \omega_i^2 = (2\pi f_i)^2 = 4\pi^2 f_i^2 \tag{5.4}$$

Apart from structural parameters and hydraulic parameters, also the element size of the FEM model has influence on the natural frequencies of the model. To study this an sensitivity study was done on the element size. Several simulations of the model have been ran in which the element size was gradually decreased. The element size has been expressed as the number of elements between two floaters E_{ff}. For different number of elements between two adjacent floaters (x-axis) the outcome of the first mode natural frequency (y-axis) is shown below in Figure 5.1a. For an increasing amount of elements between two floaters and a constant distance between two floaters, the segment size is decreasing. This results in a more detailed grid of nodes and segments. In Figure 5.1b a plot with *log*-scale on both axes and on the y-axis the error in natural frequency value defined as the difference between the natural frequency of a certain number of elements between floaters and the natural frequency value with $E_{ff} = 14$. Through these points a linear line can be fitted. The slope of this line, $\Delta f_{nat} = -1.77$, is the order of accuracy of the model.

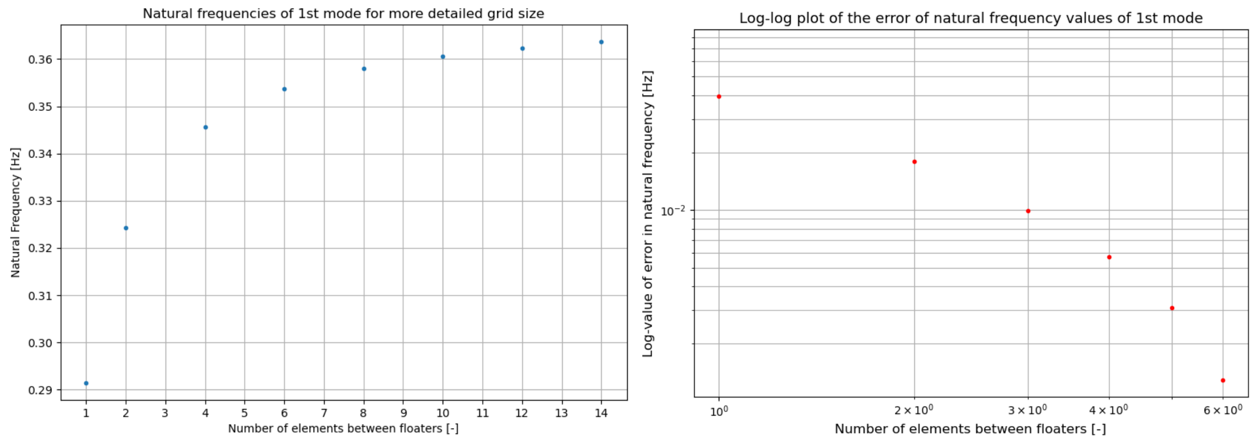

(a) **(b)**

Figure 5.1: Natural frequency values (left) and error (right) for first mode for different number of elements between floaters E_{ff}

One can see that for an increasing number of elements, the natural frequency of the first mode is also increasing. This increasing trend is a parabolic trend that is flattening up to a point where increasing the number of elements is no longer affecting the natural frequencies, the modal shapes and probably the dynamic behaviour of the CFS in general. Although, the results are more accurate for a bigger number of elements, the model is also computationally more demanding. A trade-off has to be made between these two aspects and the results in Figure 5.1a were studied. The change in natural frequency from six to eight elements between two elements is 1.20% and the change in natural frequency from eight to ten elements is for the first time below 1 %, namely 0.73 %. From ten to twelve elements the percentual change is 0.50%. Considering these results, the number of elements between two elements has been set to 10. Since the distance between two floaters Δ_f is = 2.05 m, the element size h is 0.205 m.

5.1.2. Presentation of the natural frequencies

With an element size set to 10 elements between floaters, there were simulated four base cases deviating in current velocity and type of boundary conditions (BC's). See Table 4.3. The numeric values for all input parameters of the CFS model can be found in Appendix A. The results on natural frequencies and natural periods, using these values, are presented in Table 5.1 and visualised in Figure 5.2.

Table 5.1: Natural frequency and natural period values for first 10 modes for 4 base cases

	Case A		**Case B**		**Case C**		**Case D**	
Mode	f_{nat} [Hz]	T_{nat} [s]	f_{nat} [Hz]	T_{nat} [s]	f_{nat} [Hz]	T_{nat} [s]	f_{nat} [Hz]	T_{nat} [s]
1	3.63E-01	2.75	3.63E-01	2.75	3.63E-01	2.75	3.63E-01	2.75
2	3.63E-01	2.75	3.63E-01	2.75	3.63E-01	2.75	3.63E-01	2.75
3	3.63E-01	2.75	3.63E-01	2.75	3.63E-01	2.75	3.63E-01	2.75
4	3.63E-01	2.75	3.63E-01	2.75	3.63E-01	2.75	3.63E-01	2.75
5	3.63E-01	2.75	3.63E-01	2.75	3.63E-01	2.75	3.63E-01	2.75
6	3.63E-01	2.75	3.63E-01	2.75	3.63E-01	2.75	3.64E-01	2.75
7	3.63E-01	2.75	3.64E-01	2.75	3.63E-01	2.75	3.64E-01	2.75
8	3.63E-01	2.75	3.64E-01	2.75	3.63E-01	2.75	3.64E-01	2.75
9	3.63E-01	2.75	3.64E-01	2.75	3.63E-01	2.75	3.64E-01	2.75
10	3.63E-01	2.75	3.64E-01	2.75	3.63E-01	2.75	3.64E-01	2.75

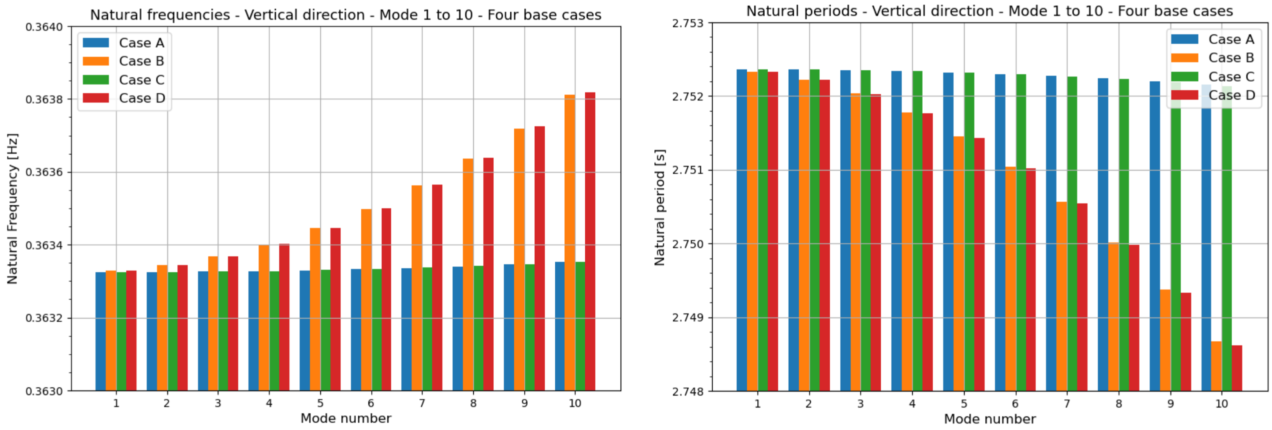

Figure 5.2: Natural frequencies and natural periods in vertical direction for eigenmode n =1-10 for four base cases A, B, C and D

5.1.3. Analysis of the results

While one studies the results of the natural frequencies and natural periods in Table 5.1 and Figure 5.2, there are several points that are remarkable. First of all, the natural frequency values are in the same range as an usual wave frequency spectrum, see Figure 3.2. The same conclusion was drawn in Chapter 3 using the EBB model on a continuous elastic foundation. This makes the hypothesis that the hydrodynamic behaviour of the CFS is influenced by resonance phenomena more relevant.

Secondly, for the first ten eigenmodes of the system, the differences in natural frequency values for different cases are tiny. It can therefore quickly be concluded that the influences of BC's and a current u_c on the natural frequency are small. Besides that, the differences between frequency values for different eigenmodes are tiny. Certainly for the first few eigenmodes, the natural frequencies are almost equal. As the eigenmode number increases also the difference between natural frequencies is growing in a parabolic way. However, also for these higher order eigenmodes, the differences between natural frequencies remain small. The small differences between natural frequencies are similar to results of hand calculations the EBB model on a continuous elastic foundation. See Chapter 3. These can partially be explained by taking into account again Equation 2.8. Although it is meant for an EBB on elastic foundation, it can help to explain the trends in the results of the FEM model as well. This equation consists of three elements that contribute to the natural frequency definition, respectively the bending stiffness, the axial tension stiffness and the discrete floater buoyancy stiffness.

Two parameters, the order of eigenmode *n* and the total length of the CFS L_{cfs}, are of more importance. These terms are present in the first two terms of the hand formula. In the first term, *n* to the fourth order is divided by L_{cfs} to the fourth order. In the second term, *n* to the second order is divided by L_{cfs} to the second order. The modelled CFS has a remarkably big length. If the magnitude of the length ($L_{cfs} \sim 10^3$) is compared to the number that has to be filled in for *n* ($n \sim 10^0$), it can be concluded that the influence of the order of eigenmode *n* is really small compared to the system length. Considering the fact that these numbers are in the first and second term respectively with a power four ($\sim L_{cfs}^4$) and a power two ($\sim L_{cfs}^2$), the difference in magnitude becomes extremely big. Furthermore, the power in the term n explains the fact that the natural frequency is changing less fast for the first few modes and is increasing more quickly for higher order modes. Finally, the equation above also explains that the third term will be relatively large for long dynamic systems. Therefore, for the situation of the CFS, one can conclude that the biggest contribution is originating from the spring coefficient K.

5.1.4. Conclusion on natural frequency results

The results regarding the natural frequencies of the CFS in vertical direction, confirm the conclusions that were made already in Section 3.3. The natural frequencies are relatively high within the wave frequency spectrum and are being dominated by the floater buoyancy stiffness. This dominance is caused by the large CFS length, which reduces the influence of the bending stiffness and tensional stiffness on the natural frequency. This dominance causes the natural frequency values for subsequent eigenmodes n to be almost equal.

5.2. Modal shapes of the cable-floater-system

5.2.1. Derivation of the modal shapes

From the *General Eigenvalue Problem*, Equation 5.3, not only the eigenvalues λ_i but also the eigenvectors ϕ_i can be extracted. The eigenvector matrix has a 2D shape, see Equation 5.5. Each eigenvalue has one eigenvector, which is organized in a vertical way in the eigenvector matrix. For example, the eigenvector belonging to the first eigenvalue and the first eigenmode is on the most left column of the eigenvector matrix. Therefore, the amount of eigenvectors and the amount of columns in the eigenvector matrix is equal to the amount of eigenvalues. This again is equal to the amount of degrees of freedom (DOF's), indicated below with Q. For every DOF there is one element in a certain eigenvector, so the length of one eigenvector and the amount of rows in the eigenvector matrix are also equal to Q. Q is equal to two times the amount of nodes. Summarizing, the eigenvector matrix has a 2D, square shape with a size of Q or two times the amount of nodes in both directions.

$$\Phi = \begin{bmatrix} \phi_{1,1} & \phi_{1,2} & \phi_{1,3} & \cdots & \phi_{1,Q} \\ \phi_{2,1} & \phi_{2,2} & \phi_{2,3} & \cdots & \phi_{2,Q} \\ \phi_{3,1} & \phi_{3,2} & \phi_{3,3} & \cdots & \phi_{3,Q} \\ \vdots & \vdots & \vdots & \vdots & \vdots \\ \phi_{Q,1} & \phi_{Q,2} & \phi_{Q,3} & \cdots & \phi_{Q,Q} \end{bmatrix} \tag{5.5}$$

There is a vertical DOF and a rotational DOF in our system. In order to visualise the modal shapes of the CFS, the elements in the eigenvector belonging to these two DOF's need to be separated. Odd numbered matrix elements $[1, 3, 5, ...(Q-3), (Q-1)]$ belong to the vertical DOF's of the nodes. Even elements $[2, 4, 6, ...(Q-2), Q]$ belong to the rotational DOF's of the nodes. Splitting the eigenvectors in this way, the result is two eigenvectors per eigenvalue. After the eigenvalues are transformed into natural frequencies the end result is:

1. An array of natural frequencies Ω:

$$\Omega = \begin{bmatrix} \omega_1 & \omega_2 & \omega_3 & \ldots & \omega_Q \end{bmatrix}$$

2. Q modal shape arrays describing vertical motion V:

$$\begin{aligned} V_1 &= \begin{bmatrix} \phi_{1,1} & \phi_{3,1} & \phi_{5,1} & \ldots & \phi_{Q-3,1} & \phi_{Q-1,1} \end{bmatrix}^T \\ V_2 &= \begin{bmatrix} \phi_{1,2} & \phi_{3,2} & \phi_{5,2} & \ldots & \phi_{Q-3,2} & \phi_{Q-1,2} \end{bmatrix}^T \\ V_3 &= \begin{bmatrix} \phi_{1,3} & \phi_{3,3} & \phi_{5,3} & \ldots & \phi_{Q-3,3} & \phi_{Q-1,3} \end{bmatrix}^T \\ \vdots &= \vdots \\ V_Q &= \begin{bmatrix} \phi_{1,Q} & \phi_{3,Q} & \phi_{5,Q} & \ldots & \phi_{Q-3,Q} & \phi_{Q-1,Q} \end{bmatrix}^T \end{aligned}$$

3. Q modal shape arrays describing rotational motion R:

$$\begin{aligned} R_1 &= \begin{bmatrix} \phi_{0,1} & \phi_{2,1} & \phi_{4,1} & \ldots & \phi_{Q-2,1} & \phi_{Q,1} \end{bmatrix}^T \\ R_2 &= \begin{bmatrix} \phi_{0,2} & \phi_{2,2} & \phi_{4,2} & \ldots & \phi_{Q-2,2} & \phi_{Q,2} \end{bmatrix}^T \\ R_3 &= \begin{bmatrix} \phi_{0,3} & \phi_{2,3} & \phi_{4,3} & \ldots & \phi_{Q-2,3} & \phi_{Q,3} \end{bmatrix}^T \\ \vdots &= \vdots \\ R_Q &= \begin{bmatrix} \phi_{0,Q} & \phi_{2,Q} & \phi_{4,Q} & \ldots & \phi_{Q-2,Q} & \phi_{Q,Q} \end{bmatrix}^T \end{aligned}$$

5.2.2. Presentation of the modal shapes

The vertical - and rotational modal shapes of the first five natural frequencies are presented in Figure 5.4 for four cases. First of all, these cases are varying in the presence or absence of a current, see Section 2.4.4. Secondly these cases are varying in the type of boundary conditions (BC's), namely *clamped* and *simply supported*. See Section 4.5.1. In Figure 5.4 from top to bottom respectively cases A, B, C and D are presented. Both the vertical modal shapes (left) and the rotational modal shapes (right) are shown. According to Equation B.1, the rotational modal shape is the derivative of the vertical modal shape. On the vertical axis is the node deflection which values are taken from the eigenvector. These values are dimensionless since they depend on the magnitude of the forcing and the amount of damping on the structure when it is moving in time domain. The dimensionless value expresses the deflection at a certain node relative to the other nodes in the system. On the horizontal axis is the coordinate belonging to the node.

5.2.3. Analysis of the results

Although the modal shapes do have a number of irregularities, in general the modal shapes are as one would expect. For example, for simply supported BC's the vertical modal shapes reach their boundary point under an angle since the CFS is free to rotate. Correspondingly, the left and right end of the rotational modal shapes suddenly stop at their maximum deflection. For the clamped BC's the boundary points are not allowed to rotate. This leads to a vertical modal shape that goes from a sharp arc shape into a horizontal orientated beam at the left and right end. Similarly, the rotational modal shape goes to zero gradually. However, overall and excluding the boundaries of the modal shapes, the modal shapes are, just like the natural frequencies, almost equal for all modelled cases.

These phenomena as just explained hold for both the base cases without current (case A and C) and the base cases with a current $u = 0.35$ m/s (case B and D). Comparing cases with equal BC's but different current (case A vs. B and case C vs. D), it can quickly be noted that the modal shapes are approximately equal, just like the natural frequencies were. Tests have been done with a higher current velocity of $u = 1.0$ m/s after which could be concluded that the results do not significantly change. The explanation of this is most likely the dominance of the floater buoyancy stiffness in the computations of modal behaviour.

Apart from the global oscillations in the modal shapes, in both the vertical and rotational modal shapes there are also local oscillations. These local oscillations are not visible in the vertical modal shapes on the left and hardly visible on the rotational modal shapes on the right. Therefore, a detailed plot is shown in Figure 5.3 below. Studying these local oscillations in more detail, it was found out that the wave length of one local oscillation is equal to the floater spacing. The nodes of these local oscillations are located at the positions of the floaters with one whole oscillation in between two floaters. Tests with an increased floater spacing show an equal increase in local wave length. See Section 5.4. For tests without the floater buoyancy stiffness, the local oscillations were absent for any floater spacing, current velocity and BC's and are similar to the results in horizontal direction (Section 5.3).

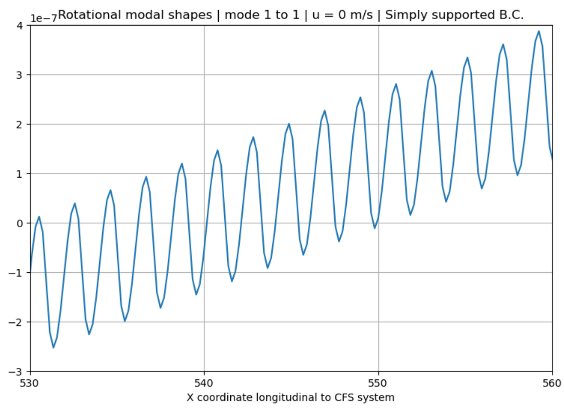

Figure 5.3: Local oscillations in rotational modal shape of 1st mode of base case 1

5.2.4. Conclusion on the modal shapes results

In conclusion, not only the natural frequency values but also the modal shapes are influenced significantly by the floater buoyancy. The dominance of the floater buoyancy stiffness translates into local oscillations in the modal shapes of which the wave length is equal to the floater spacing. In Section 5.4, the influence of the floater buoyancy will be studied in more detail.

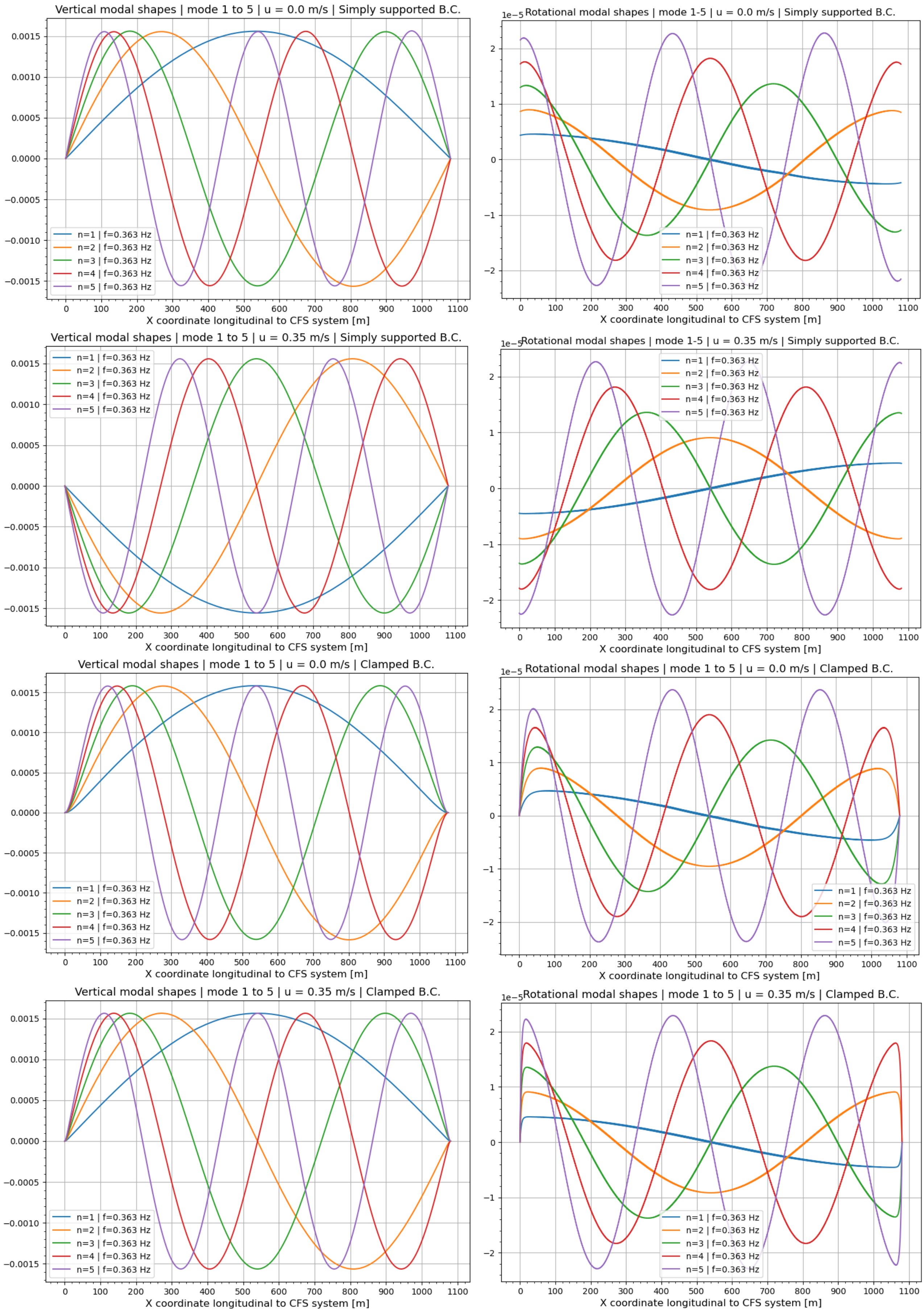

Figure 5.4: Vertical and rotational modal shapes of the cable-floater-system for four cases in vertical direction

5.3. Results for the model in horizontal direction

In Section 5.1 and 5.2 the results of the FEM model for vibrations in vertical direction were presented and interpreted in terms of respectively natural frequencies and modal shapes. However, as will turn out in the analysis of the OrcaFlex model simulation results, the modal behaviour of the CFS in horizontal direction is also relevant. In the same way as the vertical direction, the natural frequencies and modal shapes for the FEM model in horizontal direction can be derived. In Section 4.6 it was explained how a FEM model changes for the horizontal direction. In summary, there are some changes in the added masses values, but the biggest change is the absence of the floater's buoyancy stiffness.

5.3.1. Natural frequencies in horizontal direction

For the same cases as in the FEM model in vertical direction, the results concerning natural frequencies and natural periods are shown in Table 5.2 and Figure 5.5. It can quickly be noticed that the results in horizontal direction are in a different order of magnitude compared to the natural frequencies in vertical direction. Furthermore, cases B and D have a far lower natural period than cases A and C. This can simply be explained by the fact that cases B and D include a current that induces a axial tension in the cable. This tension acts as a spring, increases the stiffness of the dynamic system and therefore reduces the natural period. In the natural frequencies in the vertical direction, the effect of the current on the modal behaviour was negligible due to the dominance of the floater's buoyancy stiffness. In the horizontal direction, the floater's buoyancy stiffness is absent and the effect of the current can be seen more clearly in the results. Besides that, case B and D that include a current, are steadily increasing in approximately a linear way. However, in case A and C the frequencies are increasing less quickly and seem to increase in a parabolic way.

Table 5.2: Natural frequency and natural period values for 4 base cases in horizontal direction

	Case A		**Case B**		**Case C**		**Case D**	
Mode	f_{nat} [Hz]	T_{nat} [s]	f_{nat} [Hz]	T_{nat} [s]	f_{nat} [Hz]	T_{nat} [s]	f_{nat} [Hz]	T_{nat} [s]
1	2.50E-04	4.00E+03	8.67E-03	1.15E+02	3.20E-04	3.12E+03	8.73E-03	1.15E+02
2	3.50E-04	2.85E+03	1.73E-02	5.77E+01	5.71E-04	1.75E+03	1.75E-02	5.73E+01
3	8.65E-04	1.16E+03	2.60E-02	3.84E+01	1.17E-03	8.53E+02	2.62E-02	3.82E+01
4	1.53E-03	6.54E+02	3.47E-02	2.88E+01	1.93E-03	5.18E+02	3.50E-02	2.86E+01
5	2.38E-03	4.19E+02	4.34E-02	2.30E+01	2.88E-03	3.47E+02	4.37E-02	2.29E+01
6	3.43E-03	2.91E+02	5.21E-02	1.92E+01	4.02E-03	2.48E+02	5.25E-02	1.91E+01
7	4.67E-03	2.14E+02	6.08E-02	1.64E+01	5.36E-03	1.87E+02	6.13E-02	1.63E+01
8	6.10E-03	1.64E+02	6.96E-02	1.44E+01	6.88E-03	1.45E+02	7.01E-02	1.43E+01
9	7.71E-03	1.30E+02	7.84E-02	1.28E+01	8.60E-03	1.16E+02	7.89E-02	1.27E+01
10	9.52E-03	1.05E+02	8.72E-02	1.15E+01	1.05E-02	9.52E+01	8.78E-02	1.14E+01

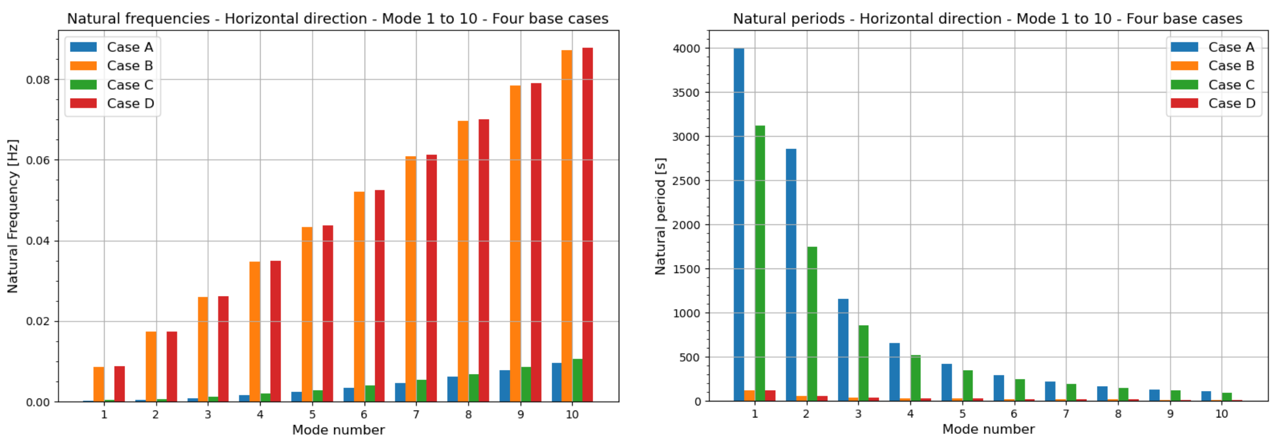

Figure 5.5: Natural frequencies and natural periods in horizontal direction of eigenmode 1-10 for 4 base cases

5.3.2. Modal shapes in horizontal direction

In a similar way as for the vertical direction, the modal shapes for the horizontal direction are presented below in Figure 5.6. In general, these modal shape look similar to the modal shapes for the vertical direction. The differences in shape and magnitude between the different model cases are small, apart from the expected differences at the boundaries for the different boundary conditions. However, three remarks need to made:

- First of all, when the figures in Section 5.2 are compared with the modal shapes in Figure 5.6, one can see that the local oscillations are not present for the horizontal direction. The reason for this is the absence of the discrete buoyancy stiffness in the model for horizontal direction.
- The amplitude of the horizontal modal shapes ($\hat{\phi} \approx 0.008$) are significantly larger than the amplitudes for the vertical modal shapes ($\hat{\phi} \approx 0.0015$). This is caused by the smaller stiffness of the CFS in the horizontal direction.
- Finally, the horizontal and rotational modal shape for the first mode for cases A and C have an odd shape at the left boundary. What would be expected is a shape that is symmetric along a vertical line in the middle. It is unclear what causes this asymmetry. It could be the correct shape, but it is also likely that this is a numerical error made in the process of setting up the models for these two cases. This shape can not be explained yet in this research.

5.3.3. Conclusions based on the results in horizontal direction

In terms of the modelling approach, the differences between the FEM model in horizontal direction and vertical direction were explained already (see Section 4.6. However, comparing the results of the vertical model (Section 5.2) with the results of the horizontal model there can be made a few remarks:

- First of all, the deflections are larger for the horizontal modal shapes than for the vertical modal shapes. This would mean bigger bending moments in the horizontal direction than in the vertical direction and could also have implications for the axial tension/compression force in the cable. However, there are more parameters that determine the magnitude of this force and for that dynamic analyses are needed.
- Secondly, in the horizontal direction there are no local oscillations occurring in the modal shapes in between individual floaters, which do occur in the vertical direction. A conclusion that could be drawn from this is that a detailed discrete EBB model has less additional value compared to the vertical direction. A simple continuous EBB model, as studied in Chapter 2.3, should be detailed enough for satisfying, accurate results.
- The natural frequencies in horizontal direction are from a different order than the vertical natural frequencies. In the horizontal direction the natural frequencies are not close to the wave frequencies that give the workability issues for Van Oord. This makes it, in the scope of this research, not interesting to further research the dynamic behaviour of the CFS in horizontal direction.

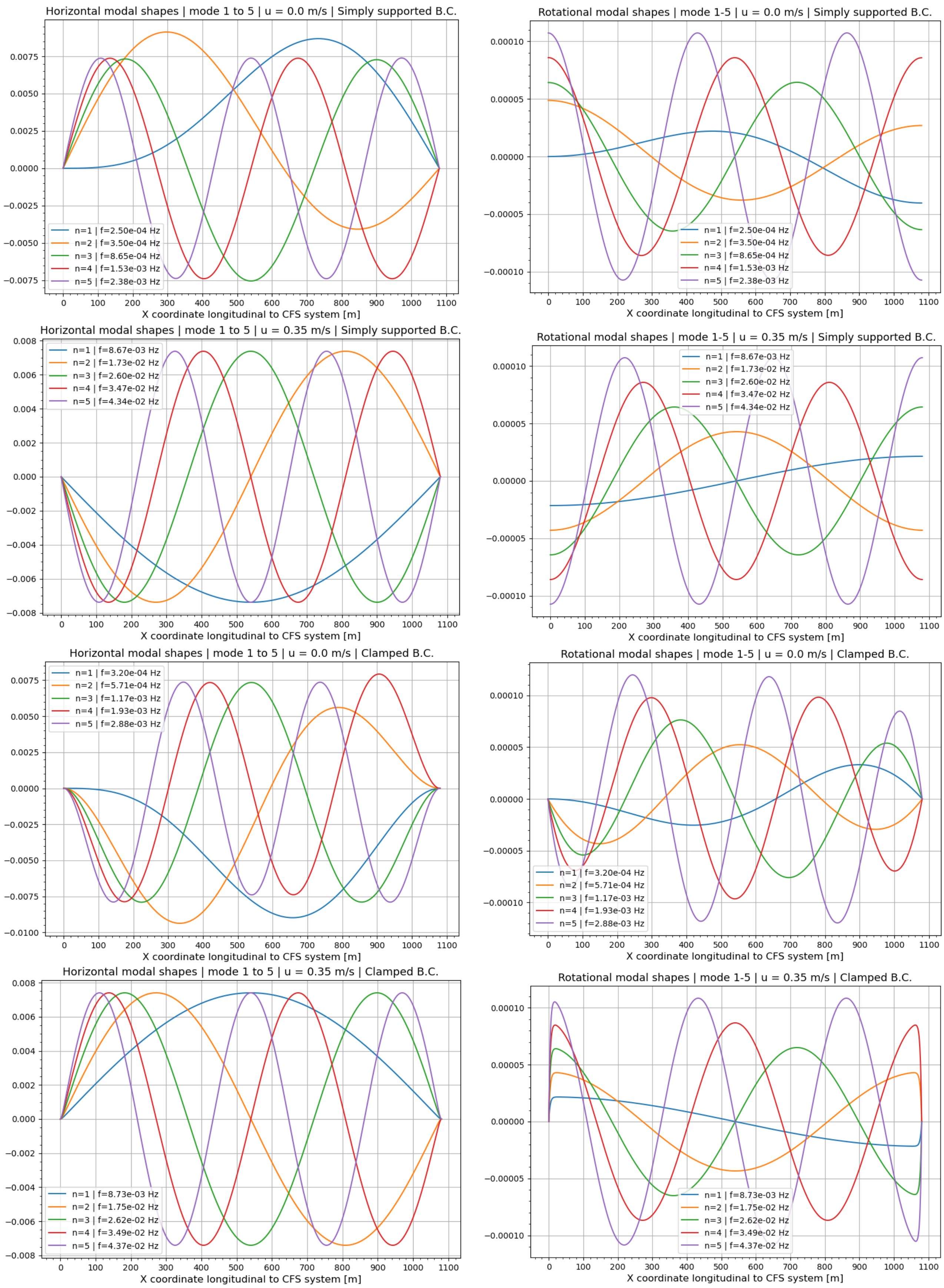

Figure 5.6: Horizontal and rotational modal shapes of the CFS for four cases in horizontal direction

5.4. Parametric study on the floater spacing in the cable-floater-system

5.4.1. Relevance of a parametric study

As was concluded already multiple times in Section 5.1, 5.2 and 5.3, the modal response of the CFS in vertical direction is dominated by the floater buoyancy stiffness. Therefore, it is interesting to discover the changes in the modal response when the configuration of the floater in the CFS is adapted. The spacing determines the positions of the buoyancy stiffness contributions in the mass matrix and stiffness matrix. So, this parametric study is relevant because the modal response of this type of system can better be understood and its sensitivity for the floater buoyancy stiffness can be quantified. This concerns the first part of the research objective (see Section 1.5.1).

The second part of the research objective addresses improvements on the CFS design. To come up with these improvement and to defend them, certain input parameters in the FEM model, that characterise the CFS design need to be changed. Only then good recommendations can be made on the design of the CFS. This improvements on the CFS design are not included in this section, but are mentioned in Section 8.5. However, the parametric study in this section has been used to come up with recommendations on the design.

5.4.2. Presentation of the results

In order to check the modal response of the CFS with a different floater spacing, the spatial grid along the x-axis has to be redefined compared to the grid used in Section 5.1, 5.2 and 5.3. See Figure 4.1. Based on the CFS length L_{cfs} and the chosen spacing Δ_f, a number of CFS segments from floater to floater (L_{cfs}/Δ_f) is determined. Next, the number of elements from floater to floater E_{ff} is defined. This number was chosen so that the longitudinal length of one element h remains about constant for all modelled configurations. Finally, the model can be defined and modal calculations can be done. For increasing floater spacing values, a selection of the results of the vertical modal shapes are shown in Figure 5.7. Worth to mention is that in this parametric study, the static equilibrium is not respected. In other words, the spacing has increased continuously beyond the value that the collection of floaters can keep the cable afloat.

The dominance of the floater buoyancy stiffness in the modal behaviour of the CFS is changing with an increasing floater spacing. In order to analyse the results better, it is useful to quantify this dominance as was done in Chapter 3 as well. The FEM model models an EBB on a discrete elastic foundation whereas in formulas used in Chapter 3 are valid for an EBB on a continuous elastic foundation. However, these are also useful for comparing the contributions of the different elements of the CFS and study the relative values instead of the absolute values. Recalling the analysis done in Section 3.3.1 on the different parameters of the CFS contributing to the natural frequency, it is interesting to study how the dominance of the floater buoyancy has changed. In Table 5.3 the values for the buoyancy stiffness different term of Equation 2.8 are presented for different floater spacing values.

Table 5.3: Change in magnitude of the buoyancy stiffness term in the natural frequency formula

Δ_f [m]	2.05	10.0	15.0	20.5	100	540	none
K [N/m]	7493	1536	1024	749.3	153.6	28.45	0
$\frac{K}{4\pi^2 M}$	1.212	2.485E-01	1.657E-01	1.212E-01	2.485E-02	4.602E-03	0

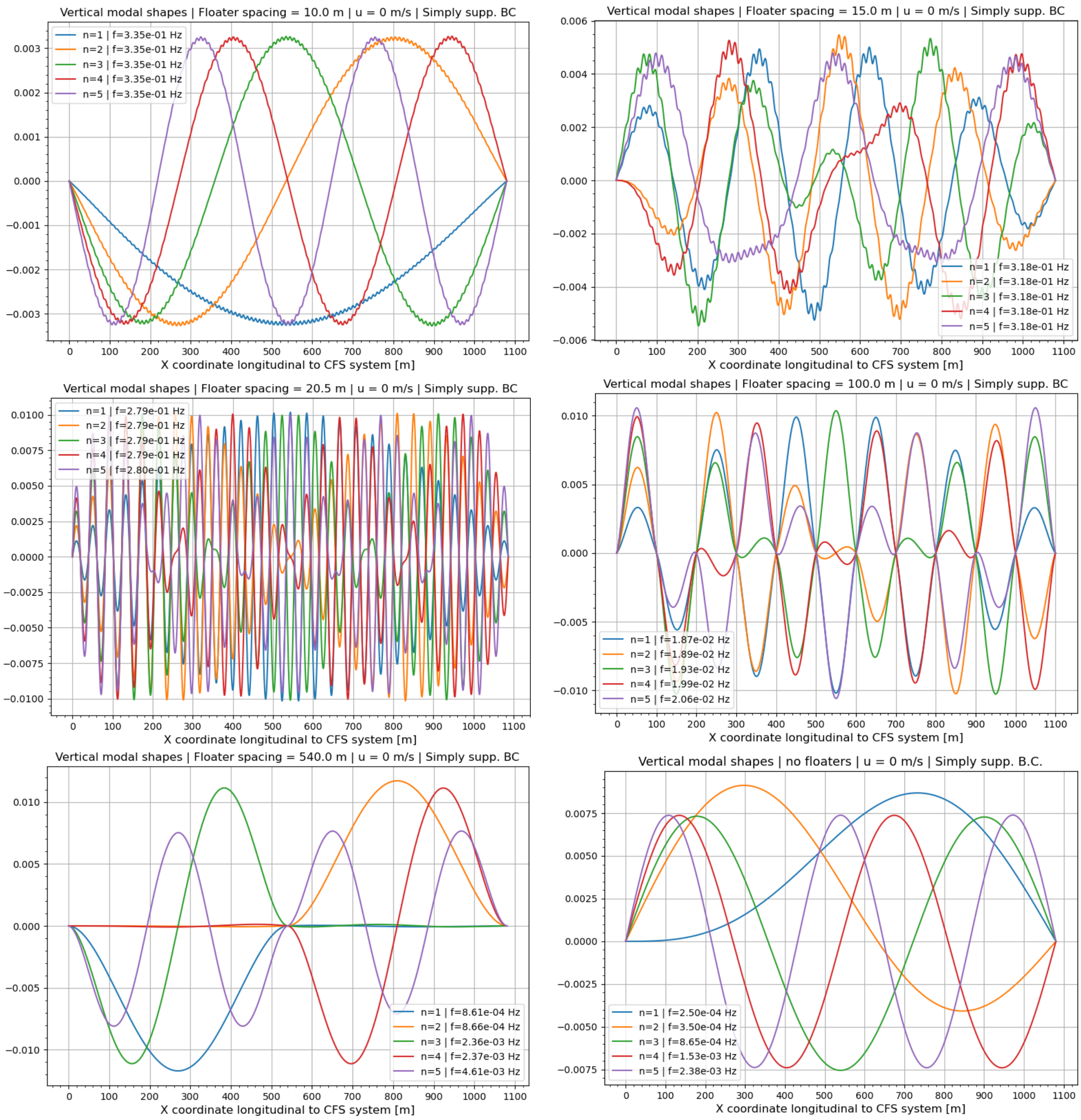

Figure 5.7: Vertical modal shapes for case A for an increasing floater spacing Δ_f

5.4.3. Analysis of the results

Regarding the modal shapes results, two aspects of the modal shapes can be separated. These are:

- The local oscillations caused by the presence of the floaters and determined by the floater characteristics.
- The global scale conventional modal shapes, which are determined by both the floater characteristics and the cable characteristics like mass, bending stiffness and axial tension.

First of all, what is noted quickly is that a bigger floater spacing causes bigger local oscillations in length and amplitude, also visualised in Figure 5.8 with only the first modes plotted. This remark corresponds with the observations made in Section 5.2.3. However, what can be concluded from these parametric study results is that the modal shapes are getting so dominant that the floater oscillations cancel out the global conventional modal shapes. Besides this change in character of the modal shapes, also the magnitudes of the modal shapes are increasing. This is easy to imagine as a less stiff system with less floaters is allowed to move more freely and has a bigger deflection than a more stiff system with a big number of floaters.

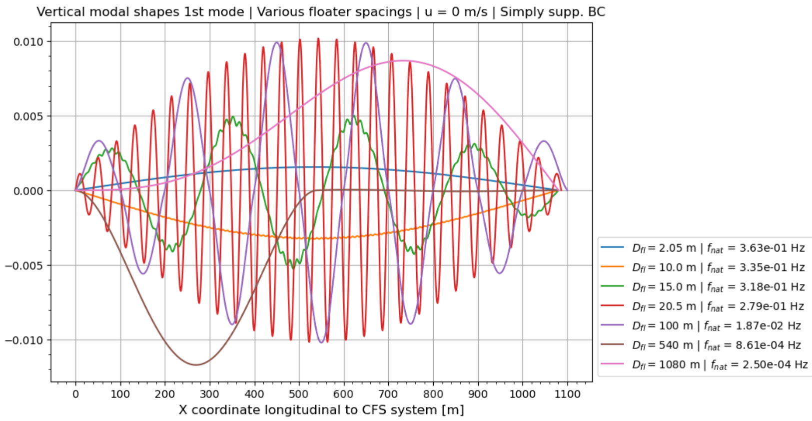

Figure 5.8: Vertical modal shapes of first eigenmode for case A for an increasing floater spacing Δ_f

In the legend of each graph in Figure 5.7 the natural frequencies are mentioned for the first five eigenmodes. It can quickly be concluded how much these values depend on the floater characteristics. When other parameters like the CFS mass or the current velocity u_c causing axial tension were modified, the natural frequency values barely changed. However, the natural frequency values does change for different floater spacing. Besides that, the difference between natural frequency values for successive modes is increasing for an increasing floater spacing. Although it should be stressed this occurs to a really small extent and in particular for the case with one one floater (bottom left in Figure 5.7). As the wave length is really small with a small floater spacing, there is not much change in the modal shape from the 1st mode to the 2nd mode, to the 3rd mode etc. However, for a big floater spacing and a big wave length the modal shapes do change for successive modes and therefore also the natural frequency values increase in bigger steps.

Regarding the change in the buoyancy stiffness term in the natural frequency formula, study Table 5.3. It can be noticed that with a bigger floater spacing, the term decreases in magnitude. However, even for a CFS with one floater ($\Delta_f = 540$ m), the buoyancy stiffness term remains bigger than the bending stiffness term (=1.969E-09) and the tensional stiffness term (=1.630E-05) (both not influenced by the floater spacing). The influence of the floater buoyancy stiffness for bigger spacing is visible in the modal shapes and frequency values as well. E.g. in the bottom left graph of Figure 5.7, the modal shapes all have zero oscillation at the floater location in the middle. The consequence is that the modal shapes of $n = 1$ (blue) and $n = 2$ (red) are equal but mirrored vertically and horizontally around the floater location. The result is that the frequency values are almost equal as well. The same holds for $n = 3$ and $n = 4$.

To sum up, in this parametric study on the floater spacing, the modal shapes and natural frequency values illustrate why the natural frequency values of successive modes are so close to each other for the small floater spacing in the original CFS design. A smaller floater spacing causes local oscillations with a smaller wave length. As a consequence, this smaller wave length causes a small change in natural frequency from one eigenmode to the next eigenmode. A bigger floater spacing causes the modal shapes to grow as well and natural frequencies to decrease. However, the rate of change of frequencies for subsequent eigenmodes does not change due to dominance of the floater buoyancy stiffness.

5.4.4. Conclusions on the parametric study

Concluding, the buoyancy of the floaters continues to dominate the modal behaviour of the CFS also for a bigger floater spacing up to point of only one floater. Changes in bending stiffness, mass or axial tension are hardly visible in the modal shapes and frequencies. Therefore, it would be interesting to see how the buoyancy stiffness term and tensional stiffness term (of Equation 2.8) become more dominant with a large floater spacing, by changing the bending stiffness and the axial tension via the current velocity. Besides that, FEM models with a smaller length could be computed, since the bending stiffness term and tensional stiffness term will then increase as well. These parametric analyses could be done in future research.

Part III

OrcaFlex models

6
Set-up of the Orcaflex computer model

In Chapter 4 and 5 the Finite Element Method (FEM) model was elaborately discussed and results were presented of the modal analysis of the structure. Unfortunately the model can not compute the stresses in the cable. The software package Orcaflex will be used to compare results with the FEM model and to extend the research with dynamic analysis and to study internal forces in the cable-floater system (CFS). In this chapter, first of all the set-up of the Orcaflex model is described in Section 6.1. Next, in Section 6.2 the input for the cases that were simulated is summed up and their differences are explained. Finally, in Section 6.3 an overview is given of all cases, modelled in OrcaFlex.

6.1. Theoretical explanation of the Orcaflex model

6.1.1. Modelling method of the cable

In order to model the cable, Orcaflex uses a FEM model of a line. The model consists of non-dimensional (lumped) nodes and straight segments. See Figure 6.1a. The segments connect the nodes via axial springs and dampers, torsion springs and dampers and bending springs and dampers. These model the characteristics of axial, torsional and bending stiffness. In the nodes all the other cable's properties are modelled, like structural mass, added mass, buoyancy and drag. These nodes have 6 degrees of freedom (DOF's). Three translational DOF's, being X, Y, Z, and three rotational DOF's, being azimuth α, declination δ and gamma γ. The approach is slightly different compared to the FEM model in chapter 4 where the cable is modelled as an Euler Bernoulli Beam (EBB) and all cable characteristics are modelled in this beam element in the model (and not in the node). The approach is slightly different but the method is the same.

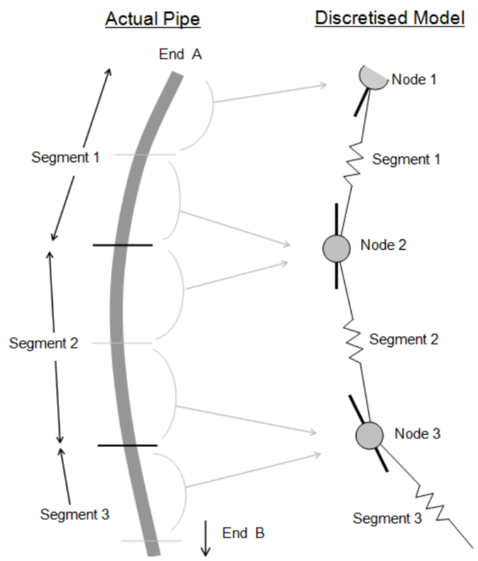

(a) An overview

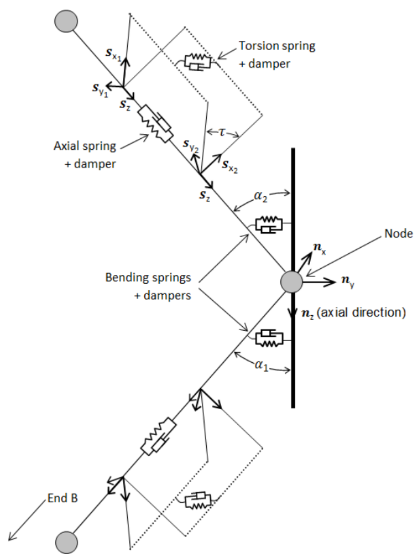

(b) Including spring-dampers

Figure 6.1: Orcaflex finite element line model (Orcina, 2021)

6.1.2. Modelling the floaters

In Orcaflex, the floaters are modelled as so-called 'attachments' to the line. The type of attachment that is used for the floaters are 'clumps'. The main assumption in modelling these attachments is that their properties are concentrated and connected to a (dimensionless) node on a line. The floater's properties that the clump takes into account are structural mass, added mass, volume, buoyancy forces and hydrodynamic drag forces. These properties are connected to the line via the node that it is attached to. Clumps have the three DOF's X, Y and Z and these positions are determined by the positions of the node to which the clump is attached. (Orcina, 2021). Important to mention is that, just as in the new made FEM model script, the change in buoyancy force is linearised in OrcaFlex as well. (Orcina, 2022a)

6.1.3. Modelling the environment

In the model that has been made for this research there are two important conditions, which are 1) waves and 2) current. It is assumed that the depth is so big that deep water wave conditions can be assumed. This means that the wave characteristics are not influenced by the sea bed. Lastly, the influence of wind is not taken into account in this research. For this model, the most simple waves have been set. This means that there has been set up one wave train consisting of an Airy wave. An Airy wave is a regular, linear wave with a certain amplitude and frequency that is constant in space and time. The Airy wave theory assumes that the fluid layer has a uniform mean depth, and that the fluid flow is inviscid, incompressible and irrational. The theory is only applicable in conditions with a small wave amplitude compared to the water depth and the wave length. In other words:

$$H_{wave} \ll d_{water} \qquad\qquad H_{wave} \ll L_{wave}$$

The Airy wave theory assumes that in deep water conditions water particles move in closed circles. At the surface these orbits have a radius equal to the wave amplitude and this radius decreases deeper into the water column. "The orbit's diameter is reduced to 4% of its free-surface value at a depth of half a wavelength." (Orcina, 2021) By assuming this wave pattern, the motion of water particles can be described in a linear way. See the Airy wave theory explained in Figure 6.2 below. Similar to the wave configuration also for the current the simplest set up has been applied. This entails that a horizontal current (in XY plane) was modelled being equal in magnitude and direction for every (X, Y, Z) position and constant in time.

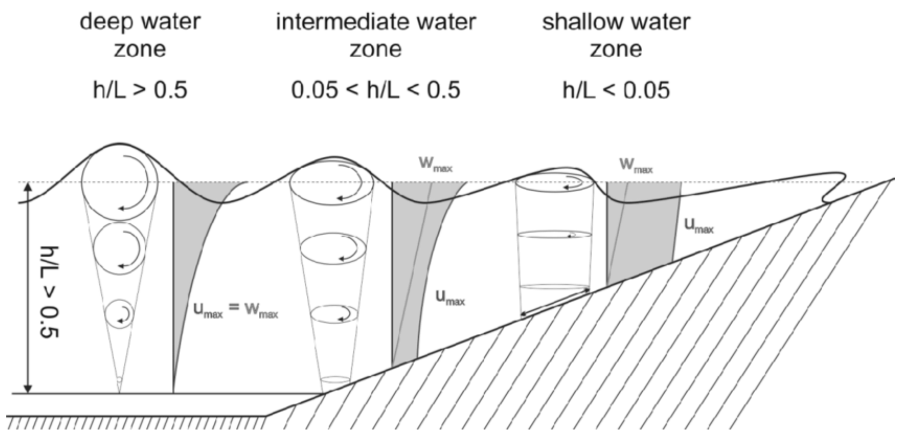

Figure 6.2: Principle of the Airy wave theory (Karow et al., 2020)

6.1.4. Different types of model analysis

Orcaflex can perform two main types of analyses: a static analysis and a dynamic analysis. In a static analysis the structure is loaded under its time-constant loads of gravity, buoyancy and currents. In x, y and z dimension an equilibrium in forces is found. In the static analysis the time dimension is absent. In the dynamic analysis, the coordinates of the modelled structure in static equilibrium are used as a starting point to perform an analysis in time. (So, if there is conducted a dynamic analysis, there will always also be conducted a static analysis.) The wave forcing is now also present which causes the structure to be no longer in a static equilibrium and therefore movement of the structure. These forces on the structure, resulting internal forces and stresses and motions of the structure are computed in the dynamic analysis. These computations are done for a given simulation period T_{sim} and for a given time step. This dynamic analysis can be done with multiple solution methods being frequency domain integration, explicit time domain integration and implicit time domain integration. (Orcina, 2021)

In both time domain analysis and frequency domain analysis, the response of the structure is computed and is expressed in various response parameters like accelerations and internal stresses. The main difference between analyses in the time domain and frequency domain is the fact that in time domain the dynamics of the CFS is computed at a collection of points in time, over a certain period with a certain time step. In a frequency domain analysis the CFS dynamics are also computed in time, but also for a range of input frequencies, in this case the wave frequencies. The variable of interest and over which the response parameters are expressed, are different. In a frequency domain simulation the response parameters (accelerations, internal stresses etc.) are computed for certain frequencies or a domain of frequencies. The result of a frequency domain simulation is insight in how much of the variation of a response parameter is occurring for which frequencies. In a time domain simulation the response parameters are computed every time step over a certain time period. Besides that, simulations in time domain are possible with explicit integration and implicit integration. The difference between explicit and implicit integration is which input is used to compute the system's response at a certain time step. An explicit time domain integration computes the future status of a system based on its current status. An implicit time domain integration computes the futures status of a system by using its current status and its future status as input.

In the model analyses of this research the *implicit time domain* method has been used, because this method was also used in earlier simulations by Van Oord which gave the unsatisfying results regarding peaks in effective tension forces in the cable. By using this same method, the same type of peaks in effective tension could be created and studied. Van Oord uses this method as it is the most quick and reliable method not often giving errors.

6.2. The input parameters of the Orcaflex model

In Section 6.1 the set-up of the OrcaFlex model was explained from a theoretical perspective. The actual input values that are used in the simulated cases of the different OrcaFlex models are explained here. This entails input parameters regarding the modelled waves, the modelled currents and the modelled CFS.

6.2.1. Input parameters concerning the hydraulic waves

The most crucial input parameters are the wave characteristics, which are the wave height, the wave frequency and the wave direction. As the aim of this study is to research the relation between wave frequencies and the structure's response, the most important wave input parameter is the wave frequency. In order to test the hypothesis formulated in Section 1.5.2 and explained in Section 3.3.2, the wave frequencies that are used as input are chosen above, equal to and below the natural frequency that was computed with the FEM model in vertical direction. See chapter 4 and 5. The chosen wave frequencies a relatively far apart and not all close to the computed natural frequency, because analysis on first simulation results with wave frequencies really close to each other showed almost the same dynamic behaviour in the CFS. Based on these experiences, the self computed natural frequencies and the wave frequency spectrum used by Van Oord in their simulations, a set of wave frequencies are designated and modelled in Orcaflex, see Table 6.1 below.

Regarding the wave height it was chosen to keep this input parameter constant in order to eliminate potential effects of changing the height on the behaviour. Remember that the input parameter of interest is the wave frequency. To come up with a reasonable wave height, the maximum wave height was computed. As was explained in Section 6.1, in this model the Airy wave theory has been chosen and is therefore also chosen to describe the relation between wave frequency and the maximum wave height. According to the theory of gravity waves, the dispersion relation is:

$$\omega^2 = gk \cdot tanh(kd)$$

Besides the assumptions of using this particular wave theory, it is also assumed that the water depth is at least twice as big as the wave length. This means that '*deep water wave conditions*' are assumed. Considering this assumption, it can be stated:

$$\frac{h}{L} > \frac{1}{2} \qquad \rightarrow \qquad kd \gg 1 \qquad \rightarrow \qquad tanh(kd) \approx 1 \qquad \rightarrow \qquad \omega^2 = (gk)^{1/2}$$

This simplification and the expressions for angular frequency ω and wave number k can be combined to rewrite the dispersion relation. In order to find the relation with the wave height, the gravity wave breaking condition (*the Miche criterium*) is used. See these expressions on the left in Equation 6.1. With Equation 6.1 the maximum wave height for all wave frequencies was computed. With the wave period that are mentioned in Table 6.1, a wave height of 0.4 m was chosen for all simulations.

$$\left.\begin{aligned} \omega^2 &= (gk)^{1/2} \\ k &= 2\pi/\lambda \\ \omega &= 2\pi f \\ \frac{H}{\lambda} &= \frac{1}{7} \end{aligned}\right\} H = \frac{0.2217}{f^2} \tag{6.1}$$

Regarding the wave direction, only the wave direction parallel to the CFS was chosen. The aim with this wave direction is to create an OrcaFlex model that resembles the situation in the FEM model as good as possible. In the FEM model the vertical direction was most interesting, regarding the wave frequency range matching the wave frequency spectrum. Therefore, in an effort to eliminate the horizontal motions of the CFS due to horizontal wave forcing as much as possible, the wave direction was chosen parallel to the CFS.

Conclusion

Summarizing the range of input parameters for wave frequency, wave height and wave direction, there are a set of configurations to be modelled, see Table 6.1 and Table 6.2 in the next sections.

6.2.2. Input parameters concerning the tidal current

Another external hydraulic load which is of importance in computing the structural response of the CFS, is the (tidal) current that is present in the hydraulic environment. The two characteristics of the current are (1) its velocity and (2) its direction. The current direction was modelled perpendicular to the CFS, because this is the dominating current direction of the tidal currents. This is 90 degrees. The velocity is chosen to be either 0 or 0.35 m/s. The velocity is assumed to be constant over the water depth. The value of 0.35 m/s was copied from the OrcaFlex analyses that were done by Van Oord already before the start of this research project. In order to be able to assume deep water wave conditions and regular waves, the water depth is chosen to be 100 meter. See all characteristics summarised below in Table 6.1 and a top-view of the modelled situation in Figure 6.3.

Table 6.1: Environmental input parameters

Wave characteristics	**Unity**	**Magnitude**
Wave origin (x-coordinate)	m	-100
Wave type	-	Airy
Wave direction	deg	0
Wave period	s	1.5 - 6.0
Wave height (2x amplitude)	m	0.4
Current characteristics	**Unity**	**Magnitude**
Current velocity	m/s	0 - 0.35
Current direction	deg	90
Other environmental characteristics	**Unity**	**Magnitude**
Water depth	m	100

6.2.3. Input parameters concerning the cable-floater-system

In the analyses done in OrcaFlex the parameters in the CFS remained constant. In Section 5.4 a parametric study with the FEM model was described, in which the structural parameters were adapted. A parametric study like this has not been done in OrcaFlex due to a limited amount of time. The structural parameters that were used in this first analysis are summarised in Table A.1 in Appendix A.

Most structural parameters do not need an extra explanation, however the difference between the total CFS length ($= 1080$ m) and the distance between the two end connections in x-direction ($= 1030$ m) does. See also Figure 6.3 for clarification. The distance between the two end connections is shorter than the CFS length, which means that there is an over length. This over length is required in OrcaFlex to model the CFS in a realistic way. If these two input parameter are modelled equal to each other, OrcaFlex gives a huge tension force as a computation result. Only when this over length is added to the OrcaFlex model, the CFS is able to move in its environment of waves and current. It is this interaction between the hydraulic environment and the CFS, that is the topic of interest in this part of the research. Therefore, it was chosen to use the same over length in this research as was used in earlier OrcaFlex models created by Van Oord.

Conclusion

Concluding, the inclusion of this over length is required from a computational perspective. It causes a difference with the FEM model, that can not and does not include this over length.

6.3. Overview of the simulated cases with OrcaFlex

In Table 6.2 an overview can be found of the cases that were modelled in Orcaflex and the variation in input parameters for the different cases. These input parameters partially match with the (variation in) input parameters of the FEM model which were the presence/absence of a current and the variation in boundary conditions (BC's). Since it was concluded that the BC's hardly influence the results of modal analysis, the BC's are not varied with in the OrcaFlex simulations. In total eight simulations were done, varying mostly in wave period but also in presence/absence of a current. In case A2 and B2, the natural period that was computed with the FEM model is used as wave period. See Section 5.1. In the next chapter the results of all these simulated cases are presented, analysed and discussed. In this chapter one will notice that also other OrcaFlex input parameters are modified. However, these parameters concern the modelling settings such as simulation time step, grid size and simulation period and not the physical parameters involving the structure or the hydraulic environment. Therefore, the variation in these parameters are not treated as new modelled cases and are not included in Table 6.2.

Table 6.2: Overview of all cases, modelled in OrcaFlex, and their variation in input parameters

Case name:	**A1**	**A2**	**A3**	**A4**	**A5**	**B1**	**B2**	**B3**	**B4**	**B5**
current velocity: u [m/s]	0.0	0.0	0.0	0.0	0.0	0.35	0.35	0.35	0.35	0.35
Wave period: T [s]	1.5	2.75	4.0	5.0	6.0	1.5	2.75	4.0	5.0	6.0

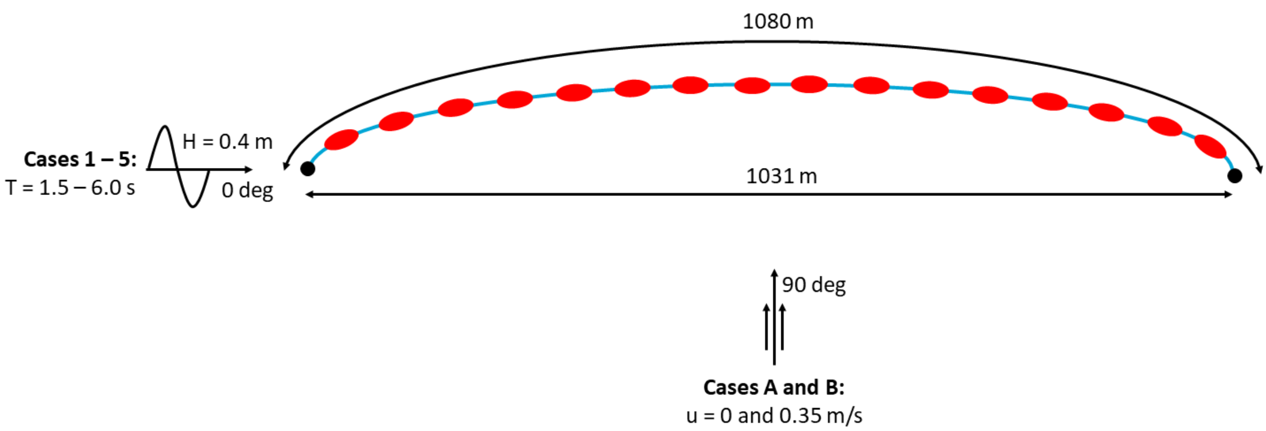

Figure 6.3: Overview of the OrcaFlex model with environmental input parameters and different model cases (topview)

7 Results and analysis of the OrcaFlex simulations

In the previous chapter all the necessary preparative steps for the simulations in the OrcaFlex software were explained. In this chapter the process of doing the simulations and the simulation results are presented and analysed. First, the results for cases with current are presented and analysed in Section 7.1. Next, the results for the cases without current are presented and analysed in Section 7.2. Afterwards, the results for the cases without current are studied more in depth in the frequency domain in Section 7.3 and studied on a smaller scale in Section 7.4.1.

The simulation results are shown using different types of graphs:

- Time history graphs: show the magnitude of a variable of interest (y-axis) in time (x-axis) at a specific arc length position of the cable.
- Range graphs: present the maximum, minimum and mean values of a certain variable throughout the complete or part of the time domain (y-axis) over the positions along the arc length of the cable (x-axis).
- Extreme value plots: show the maximum, minimum and mean values of a specific variable throughout the complete/part of the simulated time domain and the complete cable arc length (y-axis) over the varied input parameter (x-axis). In other words, these plots show the extreme values of the range graphs of various simulations.
- Spectral density plots: these graphs show the spectral density / energy of a certain variable throughout (part of) the time domain (y-axis) over the frequency (y-axis). The graph studies the signal of a certain variable in the same simulation as for the time history but shows it in a different way compared to the time history graph.

7.1. Results including current

First, the cases with a current, case B1 until B5 (Table 6.2), were simulated in OrcaFlex. The reason to start with these cases is that it appeared to be more easy to do a static and dynamic analysis of the CFS in a constant current. The current ensures that there is an horizontal equilibrium in forces between the current drag force and the forces at the CFS boundaries leading to a tension stress throughout the cable. Only when this static equilibrium is derived a dynamic analysis can be done.

The most interesting results to show are the range graphs and the extreme value plots of the axial force in the cable, in OrcaFlex referred to as the effective tension. For all simulated wave periods T_w (in OrcaFlex referred to with T_p) for the complete simulated time domain T_{sim} and for the entire spatial domain (cable arc length L_{arc}), the tension is not exceeding its maximum and minimum values. See the range graphs in Figure 7.2. Furthermore, comparing the extreme values for different wave periods in Figure 7.1 there is no peak in axial cable force in the simulation with a wave period equal to the natural period.

Conclusion

Concluding, the cases B1 to B5 are of little interest in finding an answers to the research question what explains peak axial cable forces and are therefore not further studied.

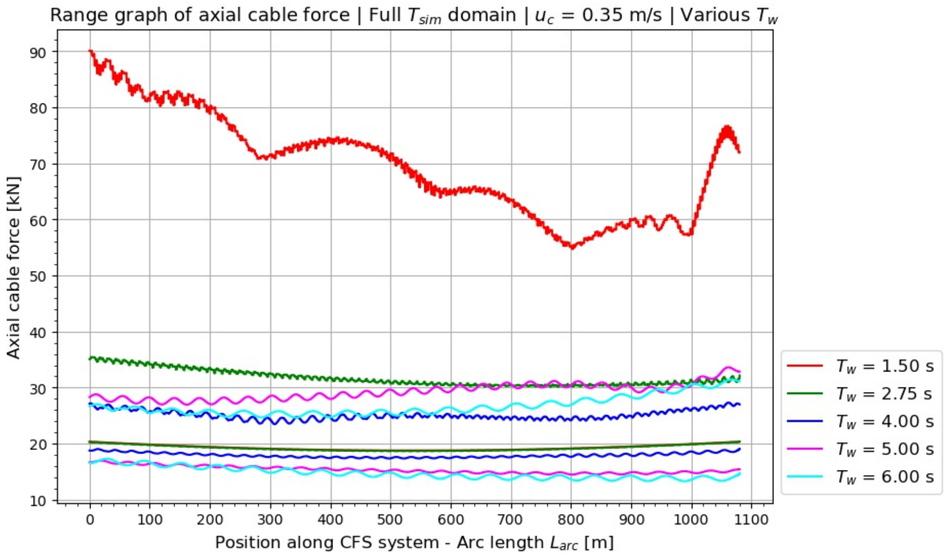

Figure 7.1: Range graph of axial cable force for various wave periods T_w with current

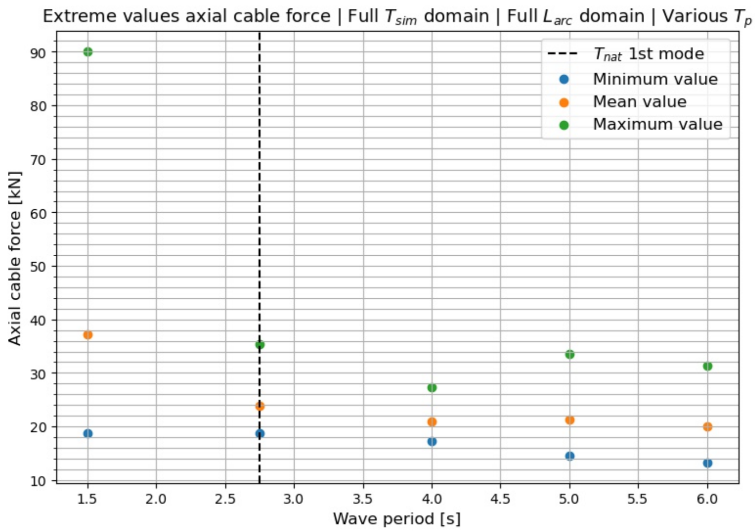

Figure 7.2: Extreme values of axial cable force for various wave periods T_w with current

7.2. Results excluding current

7.2.1. Moving cable-floater-system in Stokes drift

In the analysis of the CFS behaviour in an environment without current, the results from simulations of cases A1 until A5 are studied (Table 6.2). Whereas the two versions of the model only slightly differ when applying the FEM model for a modal analysis, these simulations are really different when the OrcaFlex model is applied for a dynamic analysis. For the case excluding current, the CFS is not stable in its global shape and node positions. In particular in the x-direction the position of the CFS is unstable. See the results for a modelled wave with a period $T_w = 2.75$ s in Figure 7.3. On the left, the x positions of multiple nodes are plotted. On the right a detail of the node at an arc length of 1000 meter is plotted. Secondly, in Figure 7.4 a top view is shown of the end position of the CFS after the simulation time of 6000 seconds. One can see that the structure has been moved in the direction of the waves, going from left to right in the figure. This phenomenon can be explained by *'second order wave drift'* or *'Stokes' drift'*. According to (Journée et al., 2015), the second order wave forces originate from wave load components which have frequencies both higher and lower than the wave frequencies. These forces are proportional to the square of the wave amplitudes. These forces contain a non-zero mean component in the wave direction and this is causing structures in waves to move in the direction of the waves (Journée et al., 2015). This could also be the cause of irregular axial force throughout the cable. Certainly in the first half of the simulation there is a large variation in maximum and minimum axial cable force values. See Figure 7.5.

Conclusion

Considering this unstable behaviour in most of the simulation, it was concluded to focus on the last 1000 seconds on the simulation period: $5000 \leq T_{sim} \leq 6000$ s.

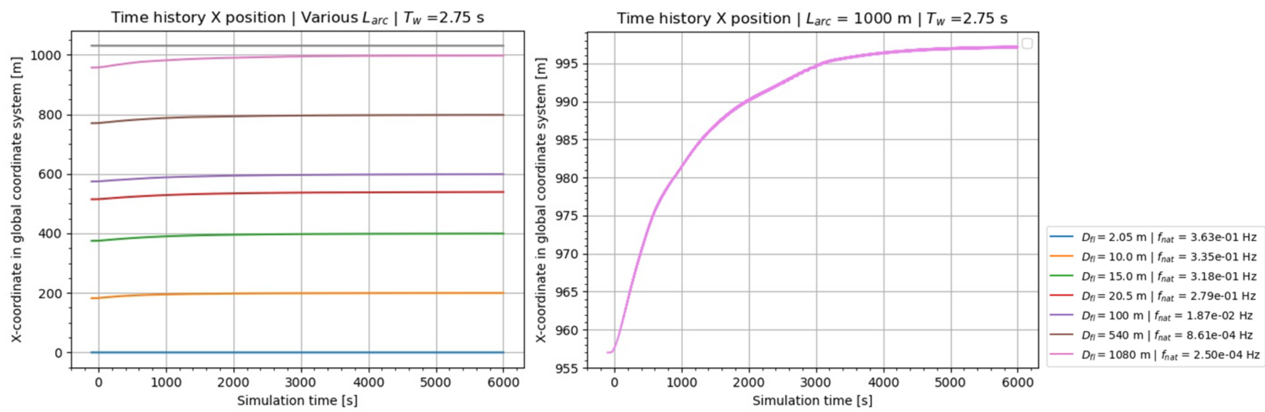

Figure 7.3: Time history of the X coordinate for several arc lengths ($L_{arc} = 1000$ m detailed) with $T_w = 2.75$ s and no current

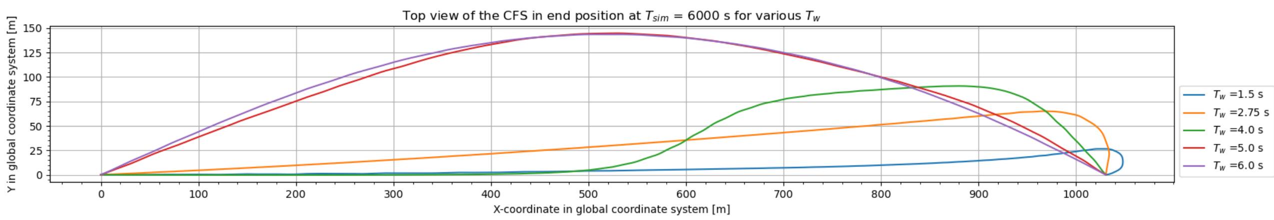

Figure 7.4: Top view of the cable-floater-system in its end position at T_{sim} for various T_w

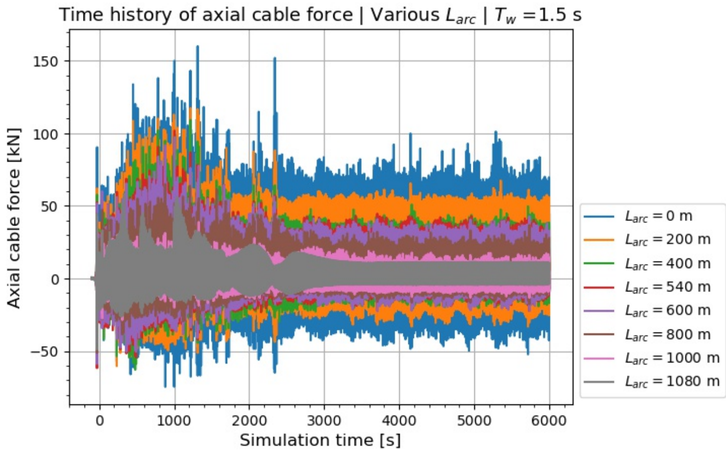

Figure 7.5: Time history of the axial cable force with $T_w = 1.5$ s for various arc lengths and no current

7.2.2. The axial cable force throughout the cable

For the selected time domain range graphs were made for all simulated wave periods. See Figure 7.6. First of all, when comparing these graphs big differences can be noticed in magnitude of axial cable force between wave periods. In case of longer wave periods the wave lengths are longer as well and therefore one might expect higher tension forces. However, the tension forces are highest for the shortest wave periods and it can be noticed that for $T_w = 1.5$ s (top left graph in Figure 7.6), the axial cable force is indeed exceeding the compression limit value of -15 kN. More explanation on these frequencies in Section 7.3.

There are differences in tension force in the cable between different wave periods. However, throughout the cable for one wave period simulation there are also big differences in tension forces. This is in particular the case for the simulations with $T_w = 1.5$ s (case A1) and $T_w = 2.773$ s (case A2). In case A1 the maximum and minimum value are at the left end of the cable ($L_{arc} = 0$ m) whereas in case A2 the maximum and minimum value are at the right end of the cable ($L_{arc} = 1080$ m). See Figure 7.6. Apart from the maximum and minimum force, the mean axial cable force (orange line) is decreasing from left end to right end for case A1, A2 and A3 (biggest decrease for A1) and for case A4 and A5 the mean tension value is zero in the whole cable arc length. This effect can be explained by taking a closer look at the phenomenon of Stokes drift. The Stokes drift velocity for deep water waves is described with Equation 7.1 (Phillips, 1978). Using this equation and the expression for propagation speed $c = L/T = \omega/k$, the expression can be rewritten into Equation 7.2

$$\bar{u}_s \approx \omega k a^2 e^{2kz} \tag{7.1}$$

$$\bar{u}_s \approx (\omega k) \cdot a^2 \cdot e^{2kz} = (ck^2)a^2 e^{2kz} = c \cdot s^2 \cdot e^{2kz} \tag{7.2}$$

In this expression s is the wave steepness and is defined by multiplying the wave number and the wave amplitude: $s = ka$. In simulating cases A1 until A5, the wave period is gradually increased, whereas the wave amplitude remains the same. As a result, the wave steepness is decreasing for an increasing wave period. Since the wave steepness is related to the Stokes drift velocity in a quadratic way, the Stokes drift velocity quickly diminishes from steep waves to more gentle waves (from case A1 to A5). This Stokes drift velocity does influence the drag on the cable significantly. The drag force due to Stokes drift is constant along the cable since the Stokes drift velocity is also constant along the cable. This constant drag force causes a tension force in the cable that is biggest at the left where waves and current are coming from and slowly decreases to zero at the right end. This cable tension force is visible in the results of the axial cable force in Figure 7.6. For cases A1, A2 and A3 (top row), having a small wave period, the mean tension (orange line) is slowly decreasing from left to right. Studying case A4 and A5 (bottom row), it can be concluded that the influence of Stokes drift on the CFS has disappeared for a wave period T_w of 5 seconds and 6 seconds in combination with the chosen wave height of 0.4 m.

Conclusion

Concluding, the Stokes drift current causes a mean axial tension force in the cable (orange line in Figure 7.6) that is decreasing in wave direction throughout the cable, occurring to the most extent for the smallest wave period.

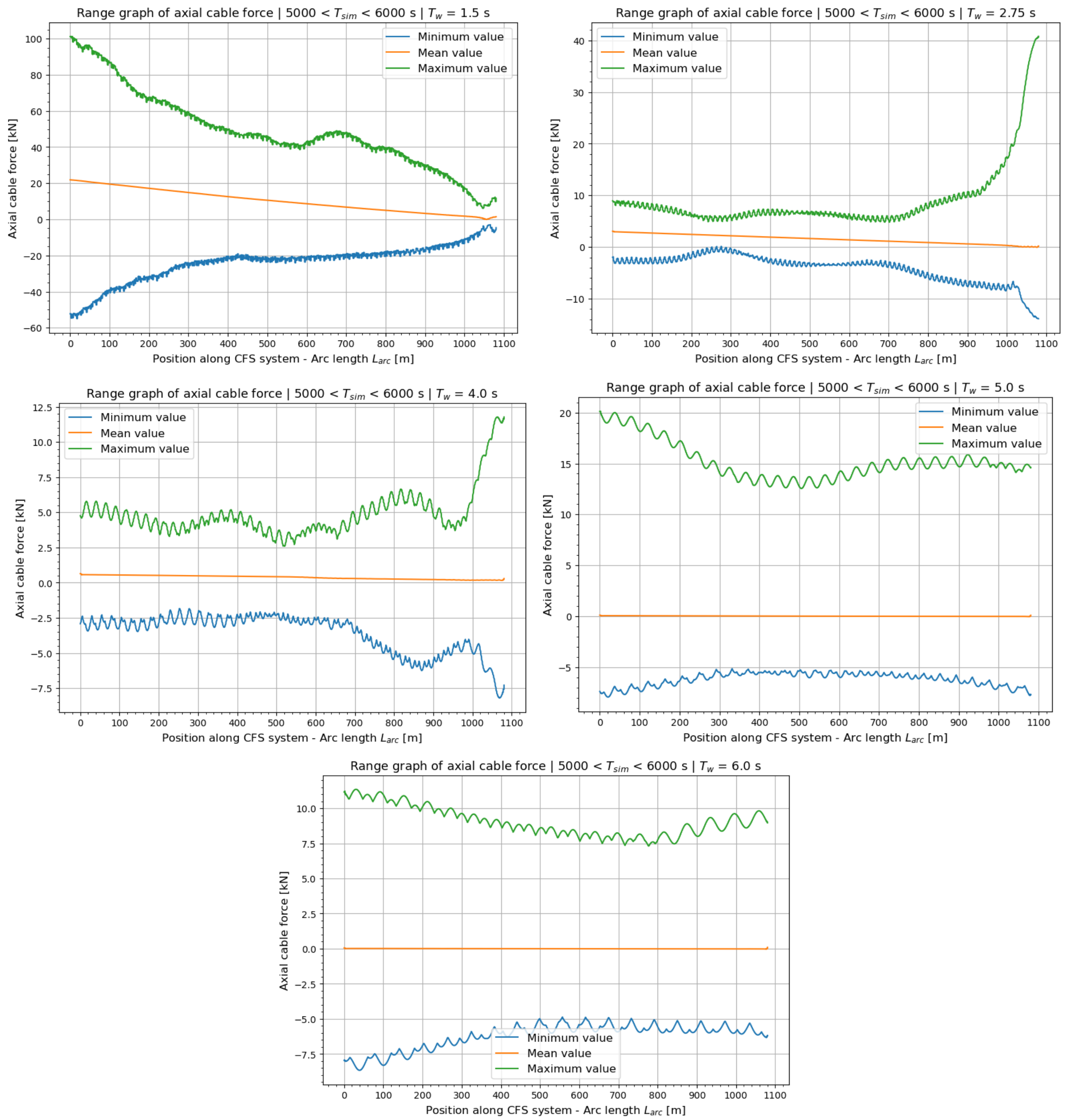

Figure 7.6: Range graphs of axial cable force along cable for various T_w and $5000 \leq T_{sim} \leq 6000$ s

In the range graphs in Figure 7.6 the effect of Stokes drift on the cable axial force was visible. However, also in the end position of the CFS at the end of the dynamic simulation ($T_{sim} = 6000$ s) differences are visible between the simulated wave periods. See Figure 7.4. In this figure, the waves come from the left and propagate in positive x direction. For the smallest wave period $T_w = 1.5$ s (blue), the largest Stokes drift velocity is largest and therefore the CFS is in this case has moved most to the right during the simulation period. One can notice that for $T_w = 5.0$ s and $T_w = 6.0$ s the CFS is barely moving due to Stokes drift. It should be noted that this phenomenon is only taking place for model cases A1-A5 and not for cases B1-B5 that includes a constant current perpendicular to the CFS. This constant (tidal) current dominates the Stokes drift current induced by the waves.

Conclusion

Concluding, Figure 7.6 shows that Stokes drift has a big effect on the dynamics of the CFS at a global system scale. This is an other important conclusion.

7.2.3. The extreme values in axial cable force at the two cable ends

Taking into account the effects of Stokes drift and the mean Stokes induced tension force one could argue that the left end of the CFS ($L_{arc} = 0$ m) and the right end of the CFS ($L_{arc} = 1080$ m) are different situations that should be studied independently from each other. In Figure 7.7 the extreme value plots of the axial cable force are given for $L_{arc} = 0$ m and $L_{arc} = 1080$ m. From the right graph it can be concluded that at the right end the biggest axial cable forces are indeed as expected for the case A2 with a wave period equal to the natural period ($T_w = T_{nat} = 2.75$ s). If one would consider only these OrcaFlex results at the right end of the CFS, one could confirm the hypothesis that resonance could be the cause of peak forces in the cable of a CFS. However, for the left end this hypothesis is not satisfied, because at this location (left graph) the biggest axial cable forces occur for the smallest simulated wave period, not equal to the natural period ($T_w = 1.5$ s $\neq T_{nat}$). A probable cause is the 'extra' mean axial tension cable force due to Stokes drift, which is influencing the motion of the cable. At the left end, the cable is under tension and can not move freely in the applied regular waves. At the right end there is an excess length of the cable due to the cable's over length applied in the model and the Stokes drift which over time moves this excess length to the right downstream end.

Conclusion

Concluding, the most extreme values in axial cable forces occur for different locations in the cable for different wave periods due to different hydrodynamic behaviour of the cable. In order to find out the differences in cable behaviour at the left and right end, the simulation results are studied at a smaller scale in Section 7.4.1.

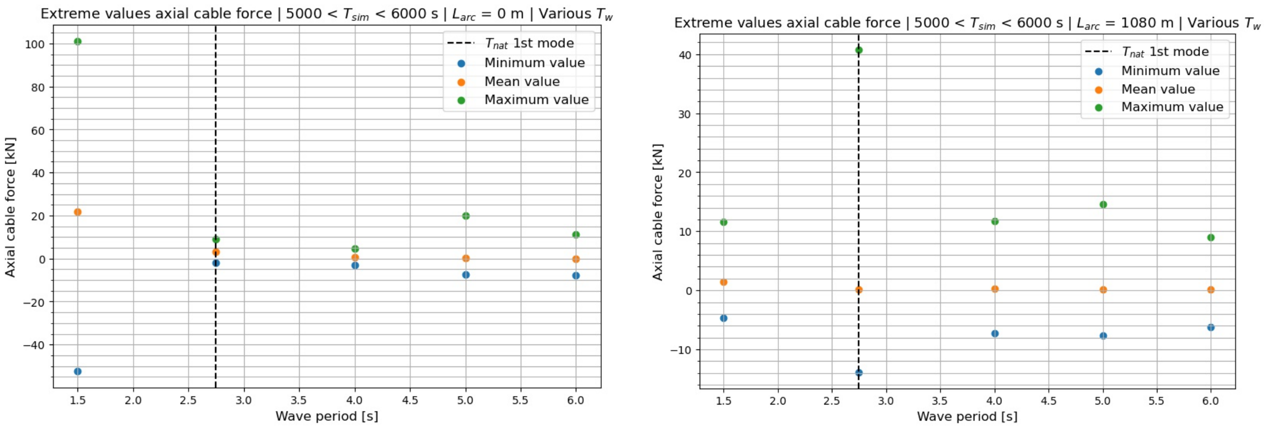

Figure 7.7: Extreme value plots of the axial cable force at the left - and right cable end for various T_w and $5000 \leq T_{sim} \leq 6000$ s

7.3. In frequency domain

In this section the time domain results are transformed to frequency domain results and analysed in a different way. However, first the concept of frequency domain vs time domain will be clarified and the mathematical transformation from results in time domain to frequency domain is briefly explained. With this background knowledge it is easier to interpret the spectral density plots, also computed using OrcaFlex software.

7.3.1. From time domain to frequency domain

The difference between time domain and frequency domain were explained already in Section 6.1.4. Although the OrcaFlex simulations in this research were all done using the implicit time domain method, these results can also be used to study the hydrodynamic behaviour in frequency domain. OrcaFlex can transform the data series of a certain variable (e.g. acceleration of a floater or axial cable force) in time domain to a data series of the same variable in frequency domain. The key point is that an irregular time series of the variable can be reproduced as the sum of a large number of harmonic components (a '*Fourier*' series). See Figure 7.8. Each of these harmonic components is characterised by one frequency value, one amplitude value and one phase value. Using the amplitudes of each harmonic component, the spectral density can be computed for this harmonic component. The spectral density values for all harmonic components (vertical axis) and their frequency (x axis) combined result in a spectral density spectrum plots (Holthuijsen, 2007). These graphs can be generated with OrcaFlex and are a valuable addition to the graphs in time domain (time history).

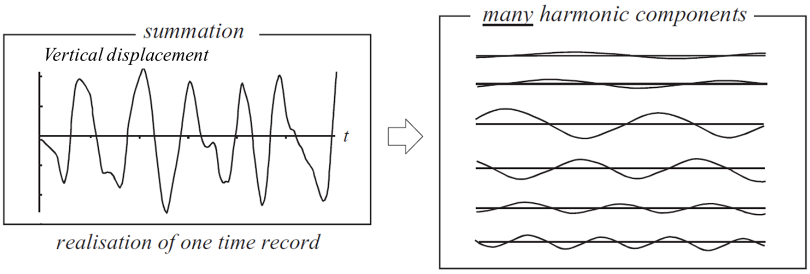

Figure 7.8: Visualisation of the build up of a time domain signal as the sum of harmonic components (Adapted from (Holthuijsen, 2007))

7.3.2. Comparing spectral density plots

Similar to the analysis done in Section 7.2 also in this section only the results the last part of the time history are analysed ($5000 < T_{sim} < 6000s$). Besides that, only the simulations without a current are analysed. In Figure 7.9 two graphs are shown for different arc lengths $L_{arc} = 20$ m and $L_{arc} = 1050$ m. These graphs show the spectral density of the total displacement in X, Y and Z direction for various wave periods. The dashed line shows the wave frequency in corresponding color with the spectral density. The total X, Y, Z displacement was derived before its spectral density was computed by using Pythagoras on the displacements in all three directions:

$$XYZ\ [m]\ = \sqrt{X^2 + Y^2 + Z^2}$$

As could be expected the peak in spectral density of displacement is for the same frequency as the wave frequency of that same OrcaFlex simulation. Surprisingly, this does not hold for the spectral density with $T_w = 1.5$ s at $L_{arc} = 20$ m. An other important learning point from this is that at different locations in the cable L_{arc} the cable does not respond to the same wave frequencies. At different locations the cable interacts with waves with a different wave periods. For example, the spectral density graph at $L_{arc} = 20$ m shows that the cable is mostly responding to waves with $T_w = 1.5$ s. However, for the same simulation period at location $L_{arc} = 1050$ m, the cable is mostly responding to waves with $T_w = 2.75$ s and 4.0 s. This means that the physical situation at both locations in the cable is significantly different. Therefore, in Section 7.4.1 the results will be studied at a smaller scale. In Appendix F all the results can be found of the spectral analysis at twenty locations throughout the cable.

Conclusion

From these graphs and Figure 7.9 it can be concluded that the interaction of the CFS and waves with different periods is changing along the CFS length.

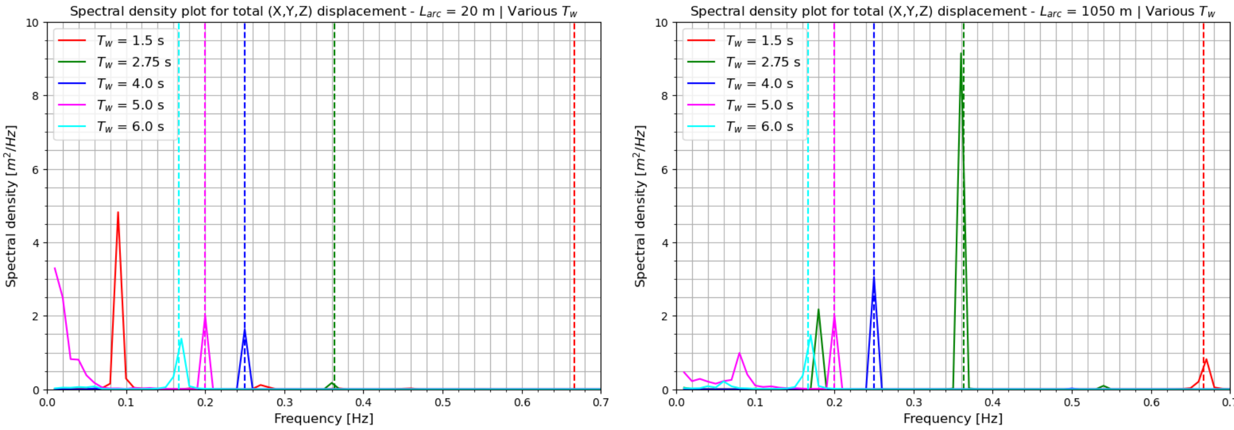

Figure 7.9: Spectral density total displacement ($\sqrt{X^2+Y^2+Z^2}$) at $L_{arc} = 20$ m and $L_{arc} = 1050$ m for various T_w

7.3.3. Study on the energy of the floater's buoyancy

In Chapter 5 it was concluded multiple times that the CFS is dominated by the floater buoyancy stiffness. As was concluded in the previous sections, the response of the CFS to certain waves is different along the cable length. Therefore, it is interesting to see what the influence is of the floater buoyancy along the CFS and to quantify this influence. The elastic potential energy, originating from the floater buoyancy force, can be computed using the spectral density results for the displacement in Z-direction. As the floater is modelled as a spring, the elastic potential energy can be computed with the formula for spring energy. See Equation 7.3 for formula for the vertical spring energy in which the same symbols are used as Chapter 4:

$$E_{D,u} = \frac{1}{2} k_{D,u} u^2 \tag{7.3}$$

Using this equation and the spectral density for the displacement in Z-direction, which is equal to the displacement u in Equation 7.3, the spring energy can be computed for every location in the CFS. For this computation the same selection of the total simulation period was used as earlier ($5000 < T_{sim} < 6000$ s). This computation was done for all simulated wave periods which give the result presented in Figure 7.10. What immediately can be noticed is the peak in spring energy close to the right end ($L_{arc} = 1080$ m) for the wave period equal to the natural period $T_{nat} = 2.75$ s. This peak confirms the explanation that resonance phenomena are taking place at this location. The peak for $T_w = 4.0$ s around $L_{arc} = 600$ m can not be explained quickly and should be studied in further research. It should be stressed that this graph does not a complete overview of the energy in the CFS. In addition to the spring energy there is kinetic energy and other forms of potential energy. These include the gravitational potential energy due to the weight of the CFS and elastic potential energy due to the cable's bending stiffness, the tensional stiffness and rotational stiffness of the floater. Besides that, this graph shows the energy for only the last 1000 seconds of the simulation period. If resonance is taking place in the OrcaFlex model with $T_w = 2.75$ s, the modal shapes derived with the FEM model, should be visible in the vertical displacement results from OrcaFlex as well. This is studied in Section 7.4.2.

Conclusion

Concluding, the peak in spring buoyancy energy close to the right end in the CFS ($L_{arc} = 1080$ m) for $T_w = T_{nat} = 2.75$ s confirms the hypothesis that the peak in axial cable force at these locations are caused by resonance phenomena.

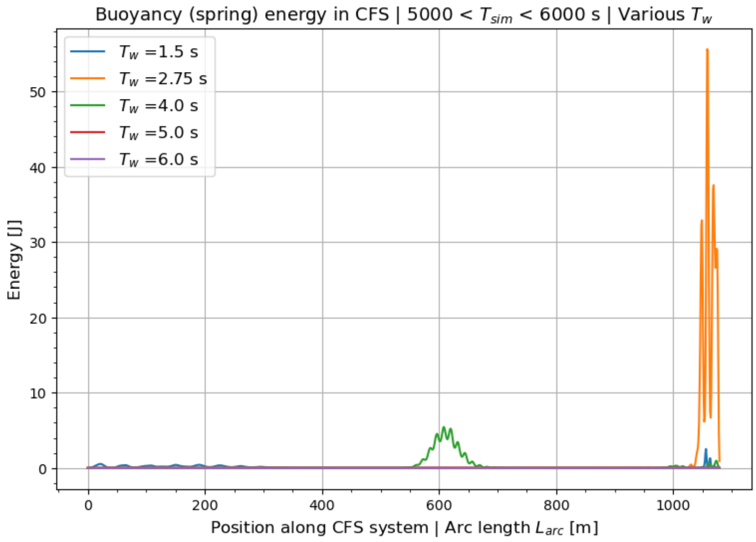

Figure 7.10: Spring energy of the floater's buoyancy throughout the cable-floater-system for various T_w

7.4. On a smaller node scale

7.4.1. Comparing displacements and forces of a single node

In Figure 7.9 the spectral density was plotted of the total displacement *XYZ*. In order to learn more on the peaks in spectral density around $L_{arc} = 20$m and $x_{cfs} = 1050$m, the individual time history graphs of X, Y, Z were studied at these specific locations for respectively $T_w = 1.5$ s and $T_w = 2.75$ s. See Figure 7.11 and 7.12. It is difficult to precisely explain the different spectral density graphs for different CFS positions using these time history plots. However, the plots are useful to study the hydrodynamic behaviour in vertical direction Z because the occurrence of resonance is studied in this direction. One can see that the vibrations at an arc length $L_{arc} = 20$ m are really small compared to the hydraulic wave amplitude (= 0.2 m) shown in black in the plot. However, the vibrations at $L_{arc} = 1050$ m have about the same amplitude as the hydraulic wave. Translating this difference to reality, it could be concluded that the CFS at $L_{arc} = 20$ m is not able to move in vertical direction with the waves passing by, while the CFS is free to move vertically at $L_{arc} = 1050$ m. Regarding the motions of these CFS nodes in X and Y direction, one has to understand that the values in X, Y and Z direction are based on a global coordinate system. Therefore, for $L_{arc} = 20$ m the motion in Y direction is the horizontal motion perpendicular to the cable. For $L_{arc} = 1050$ m, the motion in X direction is better representing the horizontal motion perpendicular to the cable. The reason for this discrepancy between the left end and right end is that the orientation of the CFS is different at both ends (see Figure 7.4). When the horizontal motions of the CFS would like to be further studied, one should transform these values from a global coordinate system to a local coordinate system using the method of rotation matrices and using the azimuth / yaw angles, also computed in the OrcaFlex simulations. This is considered outside the scope of this research since the main interest is vertical motions.

Conclusion

It could be concluded that the CFS at $L_{arc} = 20$ m is not able to move in vertical direction with the waves passing by, while the CFS is free to move vertically at $L_{arc} = 1050$ m.

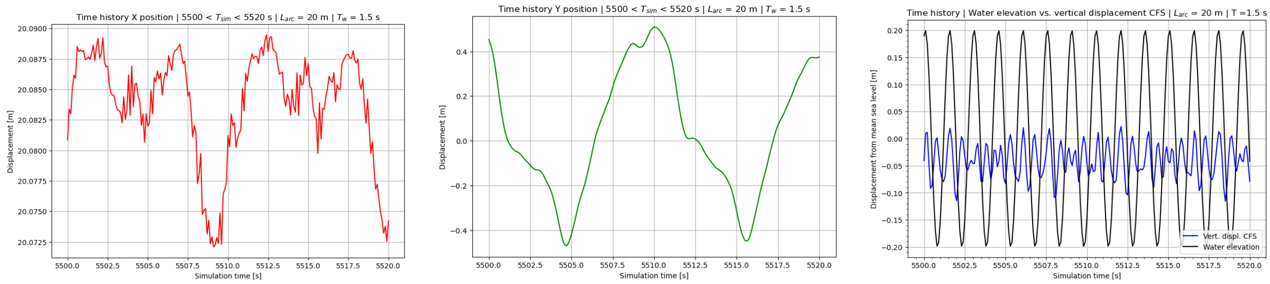

Figure 7.11: Time history graphs of displacements X, Y and Z (resp.) at $L_{arc} = 20$ m for $T_w = 1.5$ s

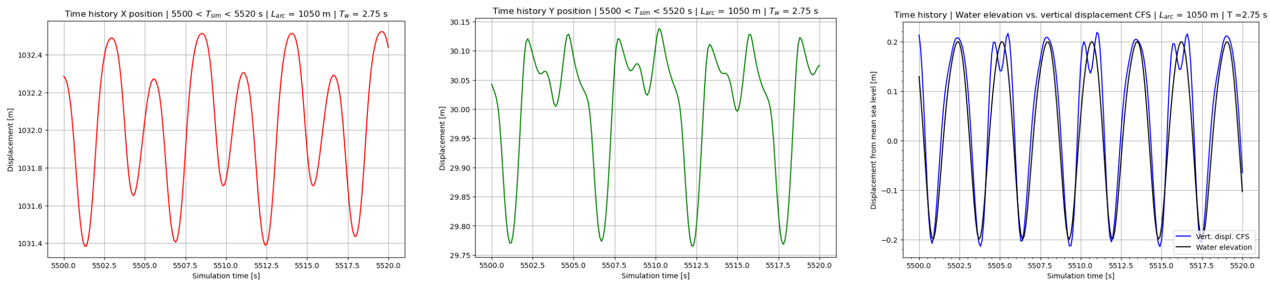

Figure 7.12: Time history graphs of displacements X, Y and Z (resp.) at $L_{arc} = 1050$ m for $T_w = 2.75$ s

7.4.2. Comparing OrcaFlex results with local oscillations in modal shapes of the finite-element-method model

In various previous analyses at has been explained that the peak axial cable forces at the right end of the CFS for $T_w = 2.75$ s could be caused by resonance phenomena. If resonance would occur, the modal shapes for a natural frequency of $T_{nat} = 2.75$ s, as computed in Chapter 5, should also be visible in the results for the OrcaFlex simulation with $T_w = 2.75$ s. The modal shapes have been computed in vertical direction and it is at the right end of the CFS that resonance might be taking place. Therefore, these vertical displacement results are studied in more detail in range graphs and compared with the modal shapes. In Figure 7.13a, 7.13b, 7.13c the maximum and minimum displacement in vertical Z direction is plotted for respectively the full arc length, around $L_{arc} = 400$ m and $L_{arc} = 1050$ m. Since the local oscillations in the modal shapes are really small, the range graphs are zoomed in.

In the modal shapes, the wave length of the one local oscillation is exactly equal to the floater spacing, $\Delta_f = 2.05$ m, (see Figure 5.3) and has its nodes at the floater locations and right in the middle between two floaters. In the range graphs in Figure 7.13 these nodes should be visible as points with a less extreme value (a relatively low value for maximal values and a relatively high value for minimal values) and the distance between these less extreme points should be half the floater spacing. Regarding Figure 7.13c, there are no local oscillations observed at all at the right end where resonance might occur. However, when a different location in the cable is studied ($L_{arc} \approx 400$ m was randomly chosen), there are local oscillations observed. See Figure 7.13b. Two remarks that should be made is that the position of nodes in the lines of maximal - and minimal displacement do not align in space (along the cable arc length) and that the distance between two nodes in the range graph is equal to the floater spacing D_f and not half of the floater spacing.

In particular the observation that local oscillations are absent at the right end of the CFS (Figure 7.13c) is important, because it is contradictory to the conclusions made earlier that the peak tension forces at the right end could be caused by resonance phenomena. Besides that, the wave length of the local oscillations in the OrcaFlex results does not match with the local oscillations in the modal shapes in the FEM model. On the contrary, when the OrcaFlex range graphs for other wave periods are studied in the same detailed way as well, it can be concluded that this standing wave behaviour (typical when resonance is taking place) of local oscillations with a wave length in same order as the floater spacing is only taking place for the OrcaFlex results with $T_w = T_{nat}$. This is an important indication that resonance could take place for $T_w = 2.75$ s, but should be further researched. Besides, it is useful to research further why this standing wave behaviour is occurring throughout the whole CFS but not at the cable's right end. Furthermore, it should be studied whether the local oscillations in the modal shapes of the FEM model results could be incorrect and should in fact have the same wave length as the local oscillations that were observed in the OrcaFlex model results, which is also more expected from a physical point of view.

Conclusion

Concluding, the local oscillations that are characterising the modal shapes generated with the FEM model, are also present in the OrcaFlex results of vertical displacement. However, their wave length and pattern is slightly different and the local oscillations are not present at the right cable end where they were expected.

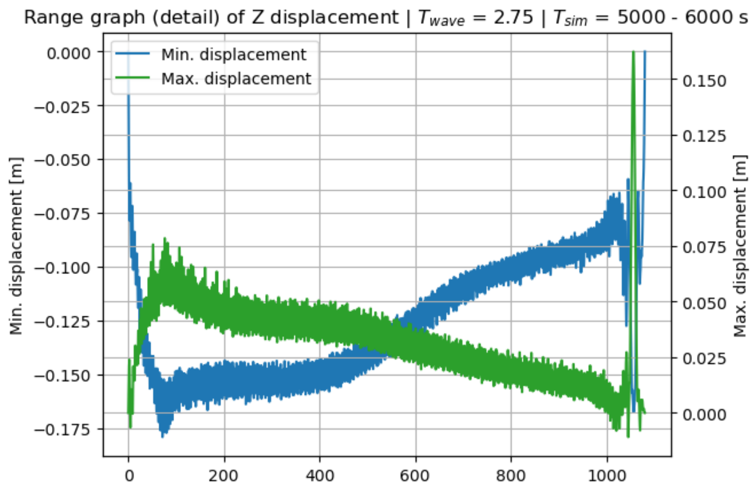

(a) Full arc length

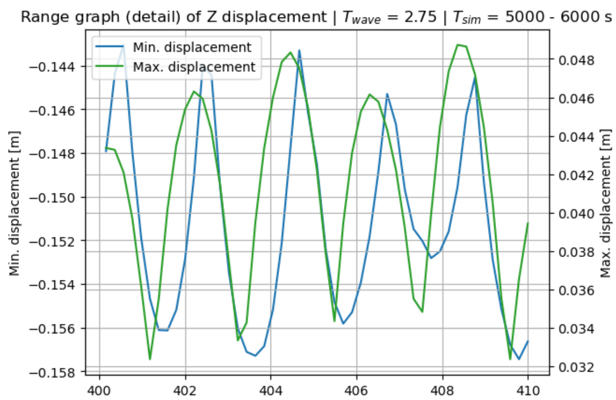

(b) $400 \leq L_{arc} \leq 410$ m

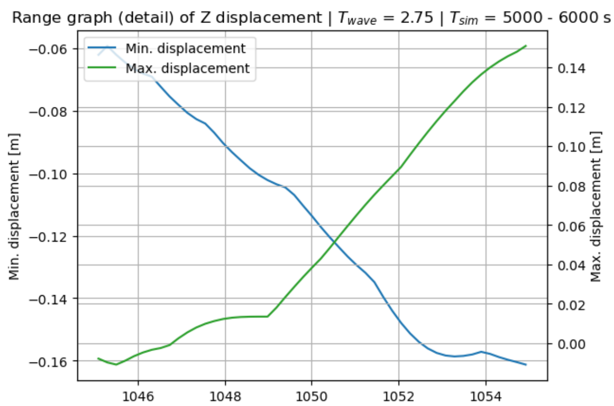

(c) $1045 \leq L_{arc} \leq 1055$ m

Figure 7.13: Detailed range graphs showing maxima and minima of vertical displacement for $T_w = 2.75$ s

Part IV

Reflections

8
Discussion

In Part B, a new finite element method (FEM) script was set up to model the cable-floater-system (CFS). Modal analyses were done and the results on natural frequencies and modal shapes were derived, presented and analysed. In Part C, OrcaFlex software was used to model the CFS. Dynamic analyses were done on the CFS and these results were analysed. In this chapter, the set-up of both models and the results of both models will be reflected upon. Also suggestions for improvement on the models are explained. Parallels between the two models and differences are explained. In order to maintain overview, in paragraph 8.1 the characteristics of both modelling methods are summarised. Afterwards, first the FEM model is discussed in paragraph 8.2 followed by a discussion on the OrcaFlex model in paragraph 8.3. Learning points regarding the research objective to gain understanding on the hydrodynamic behaviour of the CFS are formulated in paragraph 8.4. Finally, in paragraph 8.5 the second part of the research objective is addressed and ways to optimise the CFS design are discussed.

8.1. An overview on the characteristics of both modelling methods

It is important to stress that the two modelling methods are not aimed to be the same. The new FEM model was aimed to do modal analysis, whereas the OrcaFlex models were used for dynamic analysis. Both models use the FEM although the approach is slightly different. See the explanation in paragraph 6.1.1. In both approaches the elements are defined in the spatial domain with a 1D local coordinate system, that moves as the CFS moves. In the FEM model it is referred to with x. In the OrcaFlex model it is indicated with L_{arc}. A major difference is that the FEM model has 2 degrees of freedom (DOF's) per node, is a 1D model in spatial domain (u) and excludes torsional and axial stiffness and damping. OrcaFlex does include these, has 6 DOF's per node and is therefore a 3D model in spatial domain (X, Y, Z). In both modelling methods, the floaters are modelled as dimensionless, lumped masses. Moreover, a brief overview of these main similarities and differences between both model set-ups is given in Table 8.1. This table also includes a comparison in modelled environment and types of analyses that can be applied.

Table 8.1: A comparison of both model set-ups

Model aspect	FEM model	OrcaFlex model
Modelling method CFS	FEM	FEM
# DOF's per node	2 (u, θ)	6 ($X, Y, Z, \alpha, \delta, \gamma$)
Inclusion of damping	no	yes
Local coordinate system	1D (x)	1D (L_{arc})
Global coordinate system	1D (u)	3D (X, Y, Z)
Constant (tidal) current	yes	yes
Wave forcing	no	yes
Stokes drift	no	yes
Modal analysis	yes	no
Static analysis	yes	yes
Dynamic analysis	no	yes

8.2. Discussion on the finite-element-method models

In Chapter 4 the set-up of the FEM model was explained and the model itself was used in Chapter 5 to compute the natural frequencies and modal shapes of the CFS for different directions and configurations. In this paragraph the applicability and qualities of the model are discussed as well as the shortcomings and future improvements of the model.

8.2.1. Applicability and qualities of the finite-element-method models

The main goal of setting up an extra model parallel to the OrcaFlex model was first of all to compute the modal behaviour of the CFS. Secondly, the method of FEM modelling was chosen with the aim of being able to model each floater individually and nonetheless maintain small computation times. Reflecting on the FEM model set-up and results it could be stated that these two goals have been achieved. In a computation time of 25 minutes, the model is set up for a certain configuration and computes natural frequencies and detailed modal shapes, in which also local cable behaviour is visible. Besides that, at the start of the project, a version of the FEM model for the horizontal direction was considered as a 'nice-to-have'. Since it appeared to be relatively easy to rewrite the model for the horizontal direction, this was also done.

In particular, the FEM model is useful for first analyses on different CFS designs, that are being considered by Van Oord during projects. Depending on this design, for all specific cable characteristics, floater characteristics and different types of boundary conditions resembling best the situation of a chute, tensioner system and vessel, the system's modal behaviour can be visualised. Regarding the environment of the project, the current velocity can also be adapted in these computations. For the specifications of the Van Oord Greater Changhua project, in the vertical direction the chosen parameters resulted in a system dominated by the floater characteristics. Choosing other cable parameters, other types of boundary conditions or a different current velocity made hardly any difference. A discrete model, like the created FEM model in this research, is of additional value when the dynamics of the CFS in vertical direction are studied due to the occurrence of local oscillations. When the dynamics of the CFS in horizontal direction are studied, the discrete FEM model is not required necessarily, due to the absence of local oscillations due to the absence of discrete floater buoyancy stiffness. When the design of the CFS is changed significantly these preferences might change.

Nevertheless, the modal analysis results for the vertical direction and for the horizontal direction can be different for other CFS designs. Conclusions on the results for the CFS design that was used in this research, can not be assumed to be valid for other CFS designs for other Van Oord projects. However, the FEM model is a good tool to quickly assess and come up with conclusions regarding modal behaviour on other CFS designs.

8.2.2. Improvements and extensions of finite-element-method modelling approach

Although in paragraph 8.2.1 it was stated that the main goals of the model were achieved, the FEM model does also have several aspects on which the model could be improved or extended. Five possible improvements on the FEM model will be explained below. Number 1, 2 and 5 concern improvements of the current existing FEM model and will therefore increase the accuracy of the modal analysis results. Number 3 and 4 concern extensions on the current FEM model and will therefore not increase accuracy of modal analysis results but produce results in addition to the current modal analysis results. The five possible improvements/extensions, explained below, are:

1. Validation of the FEM model with measurement data;
2. A more detailed expression for the spring coefficient representing the floater's buoyancy;
3. Extension of the FEM model structure with more DOF's per node resulting in a 2D or 3D model;
4. Extension of the computations in the FEM model with a dynamic analysis in time;
5. Changing the FEM model structure so that an axial tension varying over the CFS length can be modelled;
6. Changing the FEM model structure to model the floater characteristics along the full floater length.

Validation of the finite-element-method models

First of all, the FEM model has not yet been validated with a different model or with data from field measurements or scale model tests. Measuring the motions of a structure is relatively easy compared to measuring forces. It could be performed by attaching Inertial Measurement Unit (IMU) sensors to the structure at certain locations. This could be a real scale CFS and measurements being during Van Oord projects, but it could also be a scale model of the CFS that is being tested in a research flume. Besides that, the FEM model would then have to be extended so that it is possible to compute the motions of the CFS in time for certain environments (see the fourth improvement explained below). Afterwards, the environmental input parameters in the FEM model should be matched with environmental conditions of the field measurements or model tests. Similarly, the CFS input parameters should be equal to the CFS design used in the tests. When the tests and model calculations are done with corresponding input parameters, finally the measurement data can be compared with the data that was computed by the FEM model. Based on the conclusions drawn from this comparison, the FEM model can be further improved.

A more accurate spring coefficient

Secondly, the definition of the spring coefficient representing the floater's buoyancy could be improved. In the analysis of the results in Chapter 5, it was concluded multiple times that the buoyancy stiffness is dominating the outcome of the modal analysis in vertical direction. The buoyancy stiffness is expressed by the spring coefficient that was determined in a relatively straight forward way in paragraph 2.4.2 whereas in hindsight the impact of the spring coefficient value is huge. Therefore, when the model is improved big improvements can be made with a more accurate definition of the spring coefficient, in particular the coefficient in the vertical direction. The shape and all dimensions of the floater with a cable inside have to be defined in more detail. In particular the cross sectional area at the water line and above and below the water line should be defined in detail. Preferably the spring coefficient is determined in a non-linear way, which means the value is a function in the vertical direction. A disadvantage is that this is more difficult to process in the FEM model and the non-linear spring coefficient can be difficult to determine accurately. First of all, the definition of the spring coefficient can be improved by more accurately studying the geometry of the floater over the height of the floater and include this in the definition of the spring coefficient. However, the floater is a flexible structure and under the weight of the cable and the hydrostatic pressure of water, the exact geometry of the floater is deforming in the real situation in water. What should be considered is to do model tests specifically on determining the floater spring coefficient. One would have to push a floater underwater (with piece of cable in it to maintain the correct shape) while recording both the deflection/distance, that the floater is being pushed downwards or pulled upwards, as well as the force that is needed to move the floater downwards or upwards. From these two parameters the spring coefficient values over the vertical direction can be computed using the spring force formula.

Extension to 2D or 3D models

Thirdly, the FEM model can be extended with more DOF's per node. In the FEM model only 2 DOF's are included per node: a vertical translational DOF and a rotational DOF. However, considering each node in the CFS model as rigid body, there are six DOF's that could be included for every node in the FEM model. See Figure 8.1. In the FEM model the *heave* motion (ξ_2) and the *pitch* motion (ξ_6) are included. In Chapter 4 these motions were referred to by respectively u and θ. With the assumption that vertical motion of the CFS is the biggest and the main interest and assuming that the wave direction is parallel to the CFS at all locations, these simplifications are comprehensible. However, in Chapter 7 it was shown that the CFS is a really mobile structure in waves and to understand the CFS behaviour better, it is inevitable to include more dimensions in one FEM model. Up to now, there have been made separate models for the modal behaviour of CFS in vertical direction and horizontal direction at the same time. However, there has not been made a script yet that can create a FEM model that includes both the vertical and horizontal direction. Therefore the FEM model could be extended first of all by including the DOF's *sway* (ξ_3) and *yaw* (ξ_5). When these motions are included, the FEM model has become a 2D model in which the horizontal motion perpendicular to the cable is also included. Lastly, also the *surge* motion (ξ_1) of cable segments could be included. Since we can assume that the diameter of the cable (or in the Euler Bernoulli Beam (EBB) model the width of the beam) is really small compared to the length of the cable, it is not necessary to take into account the rotational DOF *roll* (ξ_4).

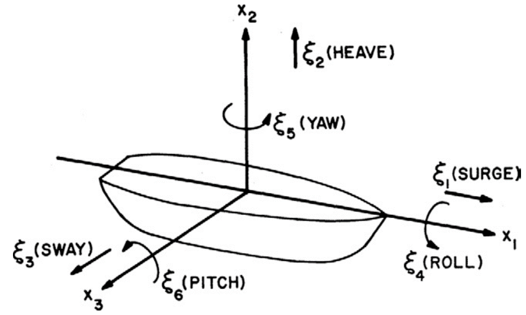

Figure 8.1: Definition sketch of body motions in six degrees of freedom (Newman, 2017)

Extension with dynamic analysis

Fourth, the FEM model can be extended with dynamic computations in addition to the modal computations. At the moment the computations that are done with the FEM model include only a modal analysis giving the natural frequencies and modal shapes as a result. However, Van Oord is most interested in the behaviour of the cable in terms of CFS motions, the bending radius of the cable and internal forces and moments in the cable. In order to do so, simulations in time would have to be done with the model. The model has to be expanded by introducing the relevant external forces on the model and by using the principle of modal superposition, see Equation 5.2. The external forces, mentioned in paragraph 4.2.2, have to be included on the right side of the equation of motion (EQM) of each element. See the strong form of the EQM in Equation 4.2 and the weak form in 4.5. Afterwards, the eigenvectors, already computed with the modal analysis, are used in the modal superposition calculations that give displacements, velocities and accelerations of each node in time.

A variable axial tension

Fifth, the FEM model can be adapted so that it can include an axial tension that is varying throughout the CFS length caused by the Stokes drift current. In theory, in each elemental stiffness matrix, as part of the EQM's of one element, a different value of the axial tension stiffness could be substituted. See paragraph 4.4.2. With a different value for the axial tension T in a specific element, the input values t_{ij}^e of the elemental stiffness matrix K_{ij}^e will also be different. Therefore also the elemental stiffness matrix K_{ij}^e and the global stiffness matrix K of the CFS will be different. However, this only makes it possible to include the variable axial tension in the modal analysis but does not solve the problem that was described in paragraph 8.3.2. This problem is that due to higher axial tension forces the CFS is not able to move and interact with the waves. As a consequence resonance phenomena would, if they occur, not be visible in the results. Considering the dominance of the floater buoyancy stiffness in the modal behaviour of the CFS, this variable axial tension is not expected to have a big effect on the natural frequency and modal shapes results and changing the FEM model structure may not be useful. However, it could be really useful when the FEM model is also extended and made suitable for dynamic analysis in time or in the FEM model in horizontal direction. In the results of OrcaFlex simulations it was remarked that the mean axial tension have big effects on the local hydrodynamic behaviour of the CFS. Therefore, it seems that it is crucial that this varying mean axial tension is included in the FEM model if it is extended to do dynamic analyses.

Modelling the floater characteristics along the floater length

Lastly, the FEM model structure could be adapted in order to model the floater characteristics along the full floater length. In this research the floaters have been considered as 'lumped masses' and floater characteristics have been assigned to certain nodes in contrary to cable that have a continuous character. This approach was chosen because the OrcaFlex software is modelling the CFS in this way. However, in reality the floater has a length and its mass and stiffness characteristics are distributed along this length. To model the floater as a continuous structure, in future research it could be chosen to model the floater with the section of the cable in it, as an EBB on a continuous elastic foundation. The mass of the cable and floater is combined and expressed as mass per unit length. Also the buoyancy stiffness in vertical direction and rotational direction are expressed as a parameter over unit length. The unsupported cable section in between two floaters is modelled in the same way as in this research (Chapter 4). Depending on the desired accuracy, these sections with and without floater characteristics can be split in more elements. It should be remarked that per definition the FEM model discretises all CFS characteristics. So, also with this adapted modelling approach of the floater as continuous model element, the model splits it into separate elements in the same way as it does for the cable. Besides that, if comparisons want to be made with the current OrcaFlex models this recommendation is invalid, because it deviates more from the OrcaFlex modelling method. An alternative could be to also change the OrcaFlex modelling method in order that the floater length is respected and included.

A summary of suggested improvements and extensions

In Figure 8.2 the input and output of the FEM model is summarised and the possible extensions on the FEM model are highlighted. The current input consists if cable properties, floater properties, CFS properties, environmental properties and model settings. The current output are the natural frequencies and the modal shapes. In red the possible extensions on input and output are mentioned. The initial conditions, the wave characteristics as external forcing and the time interval on the input are necessary in order to perform dynamic computations. The output are matrices of displacements, velocities and accelerations for every node and for the chosen time intervals. Together this describes the steady-state-response of the structure. The choice of a spatial domain in 1D, 2D or 3D refers to the extension of the model with more DOF's per node. This does not lead to other type of output but it does give more output regarding natural frequencies and modal shapes in more directions.

In Appendix D the two described extensions of the FEM model are discussed in more detail. The required mathematical adaptations to the FEM model are briefly explained and this can be seen as a starting point for further research on the FEM model.

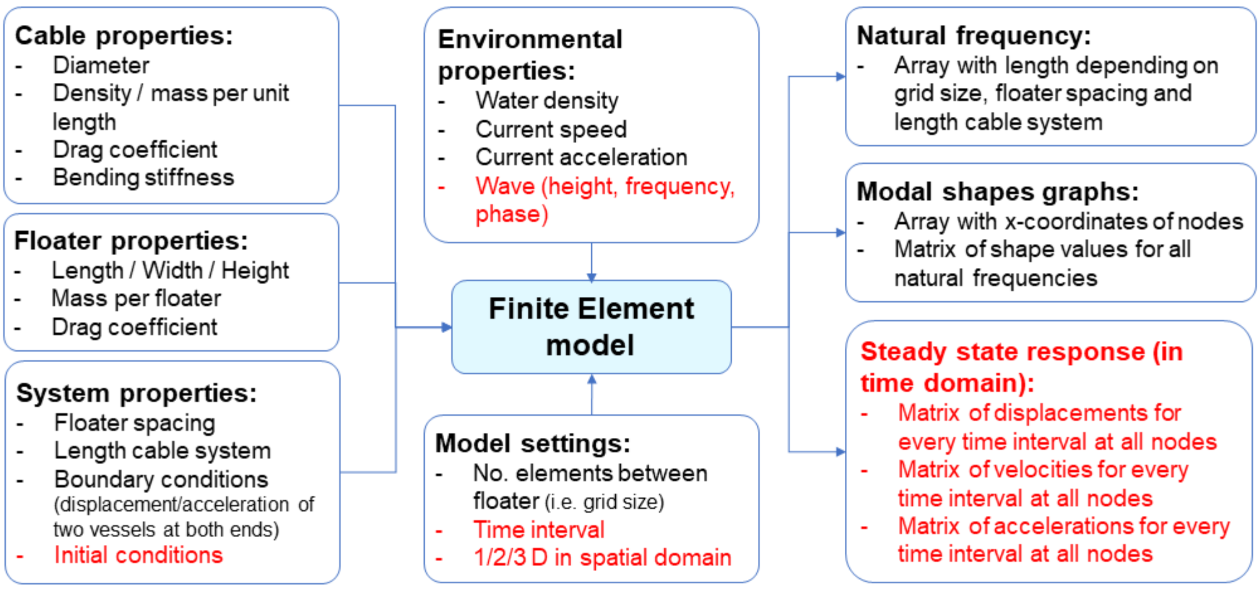

Figure 8.2: Scheme of the finite-element-method model with the input, output and possible extensions (red)

8.3. Discussion on the OrcaFlex models

In Chapter 6 the theory behind the modelling software of OrcaFlex was briefly explained and the modelling set-up and modelling cases were presented. Afterwards, the results of the OrcaFlex simulations were presented in various ways and analysed in Chapter 7. In this paragraph, a reflection is given on the modelling method, the most important results are further interpreted, potential improvements are explained and in particular an extension of the structural analysis with stresses.

8.3.1. Reflection on the modelling process

The aim of the OrcaFlex model was that it should be able to replicate the dynamic behaviour results that Van Oord has been experiencing during projects. At the same time, the goal was also to be able to make comparisons between the OrcaFlex model and the FEM model. Therefore, the set-up of the model has been kept really simple. The most important simplifications compared to the models used by Van Oord are the boundary conditions (BC's) that were modelled as fixed points rather than moving vessels. Besides that, less cases were modelled. For example, the wave direction and the current direction has not been varied with. On the one hand, its can be concluded that the model succeeded in replicating the behaviour of the models that were made by Van Oord. The peaks in tension forces in the cable and compression stresses exceeding the maximum value were also observed in the results of this model and could be studied and compared for multiple environments. On the other hand, the dynamic model in OrcaFlex was still extensive and complex compared to the FEM model.

Effects of horizontal wave forces on the simulation results

Most importantly, the OrcaFlex model was allowed to move in all directions in the global XYZ coordinate system. This 3D coordinate system in combination with the needed over length in the cable, caused that the cable had an arc shape (in the horizontal plane). See Figure 7.4. If the cable would be a straight line and waves come in in parallel direction to the cable, this would have caused less horizontal forces and motions. But in this arc shape the waves hit the CFS under all different angles in the horizontal plane along the CFS length. Besides the structure, also the modelled waves are quite complex. Next to the intended vertical oscillation of the modelled regular Airy wave, the wave also has two horizontal components. First, there is the horizontal oscillation as part of the circular pattern of the Airy wave (see Figure 6.2). Besides that, there is the second-order (Stokes) drift. Especially the last phenomenon has had a significant influence on the model results and has distorted the hydrodynamic interaction between the wave frequency as input and the axial cable forces as output.

Impact of Stokes drift on the required simulation period

Furthermore, Stokes drift has forced the simulation periods T_{sim} to be increased several times in order to study the hydrodynamic behaviour in a stable situation, because the Stokes drift causes the whole CFS to move in wave direction and change in global shape. In paragraph 7.2.1 simulation period has finally been set to $T_{sim} = 6000$ s, considering mostly the OrcaFlex simulation with $T_w = 2.75$ s. For this wave period and smaller, the positioning of the CFS is almost stable after 6000 seconds due to the relatively high Stokes drift current velocity. However, Stokes drift is also occurring for the higher, modelled wave periods. Due to the smaller steepness of these waves, Stokes drift current velocity smaller and that's why it will take more time for the CFS to find a stable position. Considering this research in retrospect, this means that the OrcaFlex simulations require a variable simulation period depending on the chosen wave frequency. This also means that the performed simulations with $T_w = 4.0, 5.0$ and 6.0 s require a larger simulation period than was chosen in this research, before the hydrodynamic behaviour can be studied properly. How to deal with this larger simulation periods in OrcaFlex is explained in paragraph 8.3.4.

Influence of damping on the simulation results

Finally, damping of the CFS is an important difference between the two models and the fact that damping is included in the OrcaFlex most likely has had influence on the results in OrcaFlex. The damping causes deflections and tension forces to be smaller and as a consequence it is more difficult to test the hypothesis. Damping could be defined as the resistance that a structure experiences when it is moving in fluid. This resistance influences the velocities of the structure and is included in the dynamic analyses in OrcaFlex. Damping is proportional to the drag force that a moving object in fluid experiences. The drag is defined as the friction between object and surrounding fluid. This makes it attractive to vary with the drag coefficients in

OrcaFlex in order to research the impact of damping on the hydrodynamic behaviour of the CFS. However, the magnitude of the drag coefficient does not only determine the resisting force from a fluid on a moving structure, but it also influences the force of moving fluid on a structure (so vice versa). For example, simulations were done with a drag coefficient equal to zero and these results showed a really small interaction between the structure and the hydraulic environment (waves and currents). Therefore, including damping in OrcaFlex simulations in a satisfying way is difficult and could be studied in future research.

8.3.2. Interpretation of the results

The overall conclusion that could be made after analysing the results is that the hydrodynamic responses of the CFS to different wave frequencies and current presence or absence are ambiguous. The response is different for each wave frequency and is different throughout the cable length. Of all the results that were discussed in Chapter 7, this was most clearly visible in the spectral density graphs.

The sections with the most extreme effective tension values are located at the system's boundaries ($L_{arc} =$ 0 m and $L_{arc} =$ 1080 m). The fact that these high tension forces occur close to the boundaries raises the question what the influence of the boundary conditions (BC's) is on the computed tension values. The cables are fixed in translational DOF's and free in rotational DOF's, so the forces are not caused by bending moments but normal stresses / axial tension in the cable. A quick test with only one fixed BC and one free BC (in translational and rotational DOF's), learns that the boundaries have a big effect on the magnitude of the effective tension forces. An important point to make is that in the real situation the boundaries are not fixed points but vessels that are also moving on the waves like the CFS. Although the hydrodynamic behaviour of the vessel will be different from the behaviour of the CFS, modelling the BC's as moving points instead of fixed points could already reduce (or increase) the tension forces in the cables and better resemble the real situation. See also paragraph 8.5.4.

Although both the left end ($L_{arc} = 20$ m) and right end ($L_{arc} = 1050$ m) are influenced by the same type of BC's, the hydrodynamic behaviour at these locations, causing peak effective tension forces, were really different. In paragraph 7.4.1 the vertical motion close to the two cable ends, each for the wave period with their highest value, were compared. It was concluded that the vertical motion at the left end is really small compared to the right end . These peak values occur for both the left end and the right end at small wave periods. For these small wave periods, there is a bigger wave steepness, resulting in Stokes drift and thus a mean axial tension that is high at the left end and very small/zero at the right end. At the left end, the CFS is barely moving in vertical direction and the amplitudes are significantly smaller than the wave amplitude (see Figure 7.11). I.e. in the vertical direction the CFS is not interacting much with the waves, because the mean axial tension is restricting the CFS to do so. At the right end, the CFS is moving vertically with the same amplitude as the waves (see Figure 7.12). I.e. at these locations the CFS is interacting better with the waves, because it is less restricted by the axial tension.

This interaction can transfer the hydraulic forces of the waves into tension forces on the CFS with a certain pace, that can or can not match with the natural frequency in which the CFS prefers to move. This interaction between wave and CFS is required in order to observe resonance. This phenomenon as described above could be part of the answer in explaining that at the right end the highest tension values are occurring for the wave frequency equal to natural frequency and that this is not the case at the left end (see Figure 7.7). This answer is reinforced by the distribution of floater buoyancy energy along the CFS. In this way it would partially explain why the hypothesis is not confirmed with most of the OrcaFlex results. On the contrary, when the modal shapes of the FEM model were compared to the vertical displacements of the CFS for the OrcaFlex simulation with $f_{nat} = 2.75$, this did not show good resemblances. This observation has to be taken into account as well when concluding on the hypothesis about resonance as the cause of peak tension forces in the cable. See Chapter 9.

It remains difficult to explain the high axial cable forces at the left end. Since the CFS does not move up and down while waves are passing by, the structure will appear above the water line in the wave troughs. The FEM model set-up and OrcaFlex model set-up are not accounting for this situation since the FEM model assumes that the cable will be below the water surface at all times and both model set-ups are use linearised spring coefficients to define the relation between vertical displacement and buoyancy force. Therefore, a well-founded answer regarding the peaks in axial cable force at the left end can not be given in this research.

8.3.3. Extension of the structural analysis with stresses

While researching internal forces in the CFS under a certain hydraulic, external forcing, the focus in this research has been on the axial cable force, or effective tension as defined in OrcaFlex. This force is the tensile force (positive) or compression force (negative), occurring in the cable, pointing in axial direction (so parallel to cable length). The reason to study this force is that it is this force that is exceeding its allowable values, in particular its negative, minimum value for compression. However, strictly speaking, when a structure is failing, it is the material that is failing and to study this failing mechanism the stress *in* in a structure should be studied instead of a force acting *on* a structure. The forces on a beam, a normal force, a lateral force and a bending moment, can be transformed to respectively axial stress, shear stress and a bending stress. In this study the stresses in cable parallel (axial) direction would be most interesting to study. However, an export cable is a complex structure consisting of multiple (copper) cores, several protective layers around it and steel reinforcement in the outside layer (see sketch on the left in Figure 8.3) and several cable elements are often able to move separately from each other. The export cable is therefore not a homogeneous material and has non-linear structural characteristics. This makes it hard to compute the stresses in the cable from the forces acting on the cable.

In order to make these computations more simple, the cable could again be simplified to a homogeneous beam that is one solid structure and has the same material properties throughout the cross-section. With this assumption the bending stress and axial stress can be computed. The sum of these two stresses is the compound stress which has its minimum and maximum at the outer surface, most far from the (bending moment) rotation centre. See the equations and summation of stresses illustrated in Figure 8.3. Including this method in an extended version of the FEM model is useful when stresses would like to be studied in addition to forces. OrcaFlex can also computes stresses in the cable, also for the simulations done in this research. Studying these could improve understanding of the true material behaviour and failure mechanisms.

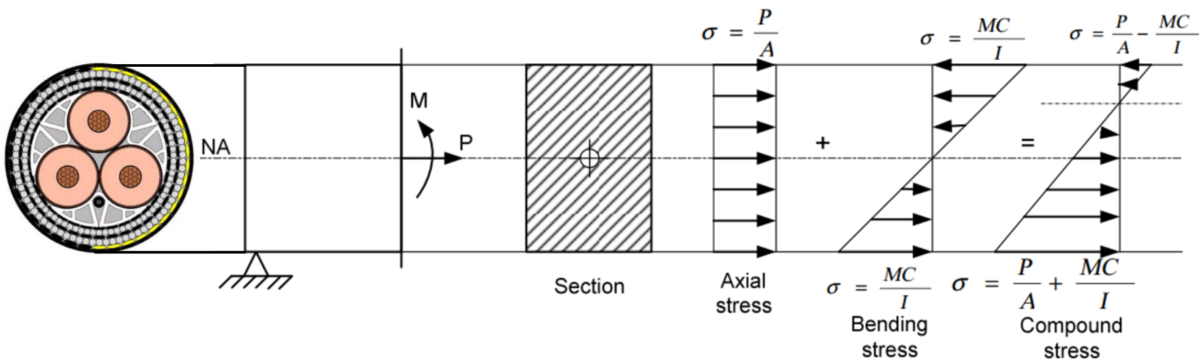

Figure 8.3: Simplified method to compute compound stress in cable (Adapted from (KOWL, 2018) and (Alfeehan, 2018)

8.3.4. Improvements on the OrcaFlex modelling method

In order to get more certainty on the interpretation of the results and to get a better understanding of the CFS behaviour in general, the OrcaFlex models could be improved in multiple ways. This discussion started with the two goals of the model to replicate the behaviour observed at other Van Oord projects and the aim to have two similar models in the OrcaFlex model vs. the FEM model. Since the first goal was achieved and the second goal not, the recommended improvements address the second goal. The most important potential improvements are:

1. Do simulations with OrcaFlex models of the CFS in frequency domain instead of the implicit time domain method.
2. To exclude Stokes drift effects, set the drag coefficients in horizontal direction equal to zero in the OrcaFlex model set-up.
3. To research Stokes drift further, increase the simulation periods or apply an extra current, imitating Stokes drift, in the static analysis.
4. Include a more detailed (non-linear) spring coefficient, defining the floater buoyancy, in the OrcaFlex model set-up.

Simulate in frequency domain

The OrcaFlex model could be made more similar to the FEM model by adapting the wave forcing in the horizontal direction. First of all, the oscillating horizontal forcing by the Airy wave is really hard to remove from the dynamic system as the OrcaFlex software is designed for the response on hydraulic forces. The option of modelling only the vertical component of a wave does not exist in OrcaFlex. Besides that, in order to focus on the waves, the Stokes drift should be excluded. Unfortunately this is not possible according to Orcina, the developer of OrcaFlex (Orcina, 2022b). A solution for this would be to simulate the model in frequency domain instead of time domain. (Please notice that the frequency domain results in paragraph 7.3 were derived with results from simulation in time domain.) The frequency domain solver in OrcaFlex for the dynamic response of the system at wave frequency ”is defined to be that of the system subject to *first order* dynamic loading associated with the wave elevation stochastic process.” (Orcina, n.d.) Since the Stokes drift is a second order wave loading the Stokes drift will not be included in the computations which is due to the different approach of a computation in frequency domain. ”As in the time domain, the wave elevation process is described by user-specified wave elevation spectra. Unlike the time domain, the wave elevation spectra are not used to synthesise a particular realisation of the sea state. Instead, frequency domain analysis solves for the wave frequency response process of the system by applying a series of linear mappings to the wave elevation process.” (Orcina, n.d.). As the computation method is different, the results will also be different and these results could be more useful in studying the relation between the wave frequency and hydrodynamic motions and forces.

Zero drag coefficients in horizontal direction

If simulations in frequency domain would not give satisfying results or are not possible for a different reason, it could be attempted to exclude the horizontal direction as much as possible regarding the forcing in the OrcaFlex model. If possible in OrcaFlex, the drag coefficient in the horizontal direction of the cable and floaters could be set to zero while maintaining the drag coefficient in vertical direction. This would eliminate the effect of Stokes drift on the CFS by setting the drag force equal to zero. Also the horizontal drag force caused by the waves is set to zero. Since the vertical drag coefficient is still included, the hydrodynamic behaviour of the CFS can be simulated exclusively in the vertical direction.

Increased simulation periods or Stokes drift imitating current

Instead of excluding the effects of Stokes drift, its could also be valuable to research the impact of Stokes drift on the hydrodynamic behaviour of the CFS in more detail. In this case, the simulation periods need to be increased until the CFS reaches a stable end position in the spatial domain that it will also reach in reality. Since the effects of Stokes drift are smaller on bigger wave periods, the necessary simulation period has to be increased significantly for bigger wave periods in particular. Since the Stokes drift is only included in dynamic analyses, the computation times are high. It could be researched whether the Stokes drift current can be imitated with a constant current included in the static analysis. To do this, this constant current should first be computed manually taking into account the applied wave environment. The CFS end position, resulting from the static analysis, can than be taken as starting position for a dynamic analysis, in which the imitating current is removed again.

Including a more detailed expression for the floater's buoyancy

In paragraph 8.2.2 it was already discussed how the expression of the spring coefficient in the FEM model can be defined more accurately. After having a more accurate definition it is important that the same spring coefficient values are also implemented in the same way in the OrcaFlex model. Preferably the spring coefficient is expressed as a function over vertical deflection (so non-linear), but it is unknown whether OrcaFlex can deal with this non-linear spring coefficients or spring coefficient functions in any certain way. OrcaFlex defines the (change in) buoyancy force of the floater using the described shape of the ’clump’, representing the floater in OrcaFlex. Therefore, a more complex shape should be used in OrcaFlex in order to describe the spring coefficient more accurately. Besides these recommendations for a better definition of the spring coefficient, a backup plan could be to do a lot more simulations in OrcaFlex using a range of wave frequencies equal to the uncertainty range of the natural frequency value. However, this is really time consuming method as modelling the long CFS’s in OrcaFlex costs a lot of computation time.

8.4. Understanding of the cable-floater-system

In the discussions on the FEM models and OrcaFlex models in respectively paragraph 8.2 and 8.3 much attention has given on the differences in the used modelling methods, recommendations on these methods for future research and explanation of certain results. From a more zoomed out perspective, in this paragraph a reflection is given on the lessons that were learned in this research. The three most important characteristics of the hydrodynamic behaviour of the CFS that were found out in this research are explained below:

1. The CFS is a very stiff dynamic system in the vertical direction that is dominated by the dimensions of the floaters and the spacing between floaters;
2. The CFS shows hydrodynamic behaviour on a small scale that is different throughout the whole length of the CFS;
3. The CFS is very sensitive to Stokes drift due to its large length and position at or close to the water surface.

First of all, in the vertical direction the CFS is a very stiff dynamic system that is dominated by the dimensions of the floaters and the spacing between floaters. This is the first important characteristic of the CFS. On a global, system scale, the structural dynamic behaviour of the CFS is dominated by the floater buoyancy stiffness and is hardly influenced by the current induced axial tension, the cable's bending stiffness and the structural and added mass of the cable and the floater. The relatively high buoyancy of the floaters cause local, tiny oscillations in the modal shapes of the CFS and these oscillations cause the natural frequencies of the CFS to be relatively high, compared to the large system. These high frequencies are in the same range as hydraulic wave frequencies and induce resonance phenomena. The modelling results from this research show that these resonance phenomena are taking place on a smaller local scale and in certain conditions. On the contrary, the dynamic system of the CFS in horizontal direction is less stiff, which results in significantly lower natural frequencies, far outside the range of hydraulic wave frequencies.

There are differences in hydrodynamic behaviour on a smaller scale throughout the length of the CFS. This can be seen as the second important characteristic of the CFS. The differences in hydrodynamic behaviour throughout the CFS are most likely caused by Stokes drift. The CFS has appeared to be very prone to Stokes drift, which can be explained by the fact that the CFS is a large structure, fully situated close to the water surface. This sensitivity to Stokes drift can be seen as a third characteristic of the CFS. The Stokes drift current causes a drag force acting on the CFS. The CFS is a flexible structure that will align with the wave direction as far as possible respecting fixed boundaries and other (tidal) currents. This Stokes drift causes a mean axial tension force that is decreasing throughout the cable length from the upstream point to the downstream point. Besides that, if there is an over length in the CFS, the CFS moves in the wave direction and the global shape of the CFS changes. Firstly, this changing CFS shape induces local differences in the hydrodynamic behaviour of the CFS.

Secondly, the variance in the mean axial tension in the cable also has as a consequence that the CFS responds to the hydraulic waves in a very different way throughout the cable length. At locations with a high mean axial tension, the CFS is not free to move up and down with the waves. The interaction between the wave and the structure, that is necessary for resonance to occur, is distorted. At these locations with a high mean axial tension, resonance is therefore not taking place. At location with a low or zero mean axial tension, the CFS can move more freely and interaction between the waves and structure is taking place to a bigger extent. At these locations resonance could take place and most of the results in this research, although not all, confirm this.

Conclusion

In essence, the three CFS characteristics described above are the most important findings from this research regarding the hydrodynamic behaviour of the CFS during the float-out-installations.

8.5. Optimisation of the design of the cable-floater-system

During the research new insights were gained on the hydrodynamic behaviour of the CFS. These insights have lead to recommendations for optimising the design of the CFS. These will be explained in this paragraph. The CFS consists of two main elements being the cable and the floaters. From the perspective of Van Oord, adaptations to the cable to optimize the CFS design are not preferred. The cable is designed based on requirements for its function of transporting electricity and based on environmental requirements at its final location on / below the sea bottom. In addition, in so-called *transportation & installation (TI) projects* the cable is bought and supplied by the client and Van Oord has no voice at all in the cable specifications. Besides that, the focus will be on design suggestions that follow from the new understanding gained in this research on the hydrodynamic behaviour of the CFS. Therefore, in this paragraph the most recommendations will be made concerning the floater design.

8.5.1. Increasing the floater spacing

In paragraph 3.3.2 is was concluded that the CFS natural frequency is interfering with a common wave frequency spectrum. This interference is not desirable considering the potential occurrence of resonance phenomena. Considering the JONSWAP spectrum visualised in Figure 3.2 it could be stated that wave frequencies smaller than 0.15 Hz are almost non-existent. Since the modal behaviour of the CFS is dominated by the floater, changing the floater design is the most convenient in order to change the natural frequency of the CFS apart from the practical reasons explained in the introduction of this paragraph. In paragraph 5.4 a parametric study was done regarding modal shapes and frequencies for a variable floater spacing. Extending this parametric study and using the FEM model it has been computed that with a floater spacing of Δ_f = 29.0 m, the natural frequencies of the CFS of the first five modes are below $f = 0.15$ Hz. See the modal shapes and exact frequency values in Figure 8.4.

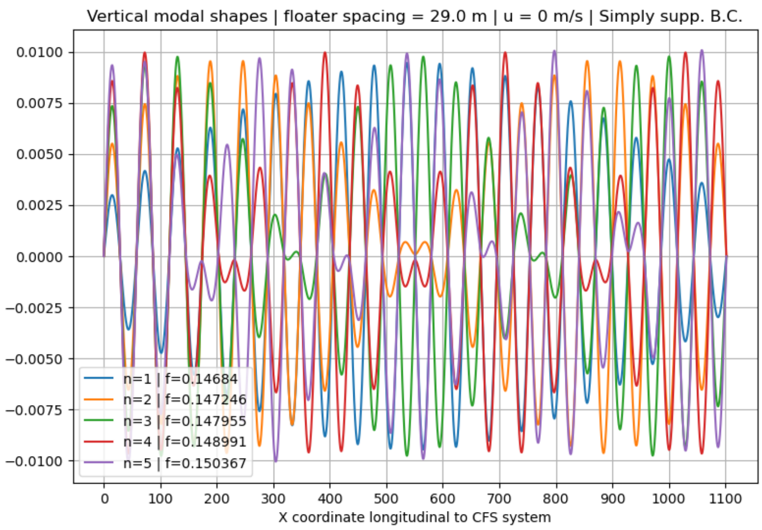

Figure 8.4: Vertical modal shapes for case A with a floater spacing Δ_f of 29.0 m

From the perspective of reducing the chance of resonance phenomena, changing this floater distance could be a useful recommendation. However, with this floater spacing the CFS is not in a vertical static equilibrium, i.e. the system will sink. This problem may be solved by increasing the buoyancy of a floater. However, increasing the buoyancy may also increase the discrete spring coefficient in the model, as a consequence increase the stiffness of the model and finally the CFS natural frequency. Namely, the horizontal length L_f and width of the floater W_f are increasing the buoyancy but also the natural frequency. See Equation 2.19. If the buoyancy should be increased without increasing the vertical spring coefficient, a solution could be to increase the height of the floater H_f. Computing a new static equilibrium with a floater spacing $D_{fl} = 29.0$ m, the minimum height of the floater would have to be $H_f = 1.71$ m. In order to have a safe structure it could be considered to design buoys of $H_f = 2.0$ m.

With these adaptations in floater spacing and floater height, there is much less chance that local waves and the CFS will interact causing resonance and the CFS stays floating for the cable parameters of the Greater Changhua project. However, there are also disadvantages and other considerations than resonance and buoyancy to keep in mind. Other aspects that should be kept in mind are the additional added mass on the bigger floaters, the bigger bending moments that will occur in the cable at the float locations and the bending radius of the cable that has a limiting value as well. Besides that, the environment has a limited depth since the installation method of *float-outs* is intended for shallow waters. The necessary depth for the CFS would be the sum of the draft of the floater ($H_f = 1.7$ m), the vertical deflection of the cables and a certain safety clearance underneath. Further calculations and design iterations could be done. However, most likely the advantage of a lower natural frequency outside the wave frequency spectrum does not outweigh the disadvantages regarding i.a. the CFS draft and the induced bending moments.

8.5.2. Change the damping of the floater

In Chapter 5 its was shown that only the natural frequencies for vertical oscillations are within the wave frequency spectrum and could potentially cause resonance. If one wants to reduce these effects, the drag coefficient should be increased in this direction. The drag coefficient depends on the shape, size and surface roughness of the structure on one side and the Reynolds number of the fluid on the other side. From an engineering perspective, the fluid characteristics can not be adjusted and at the start of this paragraph it was already explained that the cable design can not be changed. Therefore it is the vertical shape and size of the floater or its surface roughness that should be adapted. Changing the surface roughness will probably be difficult and not have a large effect. Furthermore, it is unattractive to increase the floater's water piercing area (horizontal cross sectional area at its water line) from the perspective of the floater's spring coefficient and its influence on the natural frequency value. Furthermore, the (underwater) drag area of the floater in the horizontal direction should be kept small in order to not further increase forces induced by (tidal) currents.

8.5.3. Summary of the researched design adaptations

These design preferences could be summarised in five proposals for the adapted floater design. The first and fourth proposal originate from the goal to prevent resonance to take place. The fifth proposal has the goal to reduce the impact if resonance would occur.

- The floater spacing should be increased in order to lower the natural frequencies of the system until outside the wave frequency spectrum.
- The floater should have a big underwater volume in order to create a larger buoyancy force that can counteract the larger floater spacing.
- Since the water depths are small at the locations where float-out-installation procedures take place, the draft of of the floater should, also with a bigger underwater volume, be as small as possible.
- The floater should have a relatively small water piercing area (horizontal cross sectional area at its water line) and to certain range above and below the water line. This range should be chosen based on the expected wave height and the preferred range of application for different cable weights and floater spacing.
- The floater should have a big underwater drag area in vertical direction. At the same time, the horizontal drag area should remain small. The result is that there would be needed an underwater, horizontal plane-like shape to add damping in the vertical direction.

8.5.4. Other potential design optimisations

These proposals should be seen as a starting point of a further optimisation of the CFS design, because they are still conflicting and there are can be made many more considerations. In the paragraphs above, the experiences from the parametric study on the floater spacing were used to adapt the CFS design. However, it would be useful to do a parametric study on the floater's dimensions as well. With a smaller water piercing area of the floater, the spring coefficient, representing the change in buoyancy force, will also be smaller and therefore the stiffness of the CFS as well. As a result, the natural frequencies will decrease as well. Regarding the bending moments in the cable and the minimum allowed bending radius of the cable, it may also be preferred to have smaller floaters with a smaller spacing instead of bigger floaters with a bigger spacing.

Besides that, it could be studied how the suspension on the working vessels can be made more flexible since it was found that it is beneficial for the cable axial tension when the CFS can move along with the waves. The tensioner system on board of the vessels can regulate the cable's mean axial tension and tension forces are most extreme close to the boundaries. If the model is further developed and properly validated, it could be that results recommend that a different tension value at the boundaries is desired for different wave frequencies. The tensioner system could then be designed so that the tension value in the cable is varied depending on the dominant wave frequency in the environment. However, more research on the relation between wave frequency and axial tension at these boundary locations and the applicability in practice should be done. Besides that, design parameters at the interface between floater and cable could be changed: e.g. lowering the cable deeper below the sea level. Lastly, it can be researched whether it is beneficial to add more suspension (boundary) points to the CFS. Certainly when the lengths of the CFS are increasing in future projects this may become inevitable.

8.5.5. Conclusion on the optimisation of the cable-floater-system

In conclusion, it can be recommended to focus on the design of the floaters when the CFS design should be optimised. It is difficult to successfully combine all these proposed design adaptations and it is inevitable that a trade-off between different aspects needs to be made. More detailed research, including parametric studies on other design parameters than the floater spacing, needs to be done on this trade off and other options for optimisation of the CFS design.

9 Conclusions

In this chapter the conclusions that can be drawn from this research are explained. First, the research objective is evaluated and discussed to and in which extent it is completed. Afterwards, the research question is answered.

9.1. Conclusions regarding the research objective

As was formulated in Chapter 1, the first part of the research objective was *to gain understanding on the hydrodynamic behaviour, structural behaviour and modelling methods of floating export cables during float out cable installations*. To obtain this objective, first literature research was done on how the structure of a cable-floater-system (CFS) can be modelled as a dynamic system and how the CFS can be modelled in its hydraulic environment. Next, a new finite-element-method (FEM) model was created which models the CFS structure in the vertical or horizontal direction. It was able to do a modal analysis on the structure in its hydraulic environment giving the natural frequencies and modal shapes as results. Besides that, existing models in OrcaFlex were edited, new OrcaFlex models were made and simulations were done with different hydraulic environments. With these models dynamic analyses in time domain were done and the hydrodynamic behaviour of the CFS was studied. Combining the two models, it was managed to assess the hypothesis that resonance is (part of) the cause of peak tension forces in a CFS. In conclusion, by doing these different analyses and assessing the hypothesis on resonance certainly new understanding has been gained on the behaviour and modelling methods of a CFS during float out cable installations.

Concerning the second part of the research objective, *potential optimisation of the design of the cable-floater-system*, the conclusions from the different result analyses have been used to come up with recommendations. Furthermore, with the aim of optimisation of the CFS design a parametric study was done using the self made FEM model. With in mind the discovered dominance of the floater's buoyancy stiffness in the modal behaviour of the CFS and the different design goal for the export cable, the study on optimising the CFS design was focused on the design of the floater. Less attention has been given to the cable design, the CFS suspension at the vessels and the installation procedures. In conclusion, using the new understanding on CFS behaviour well-founded suggestions have been made to optimise the design of the CFS.

9.2. Answers to the main research question

The main research question was defined in Chapter 1 in the following way: *"Which explanation can be given for extreme internal stresses in the cable-floater-system under wave and current loads using dynamic modelling methods and to which improvements of the design of the cable-floater-system does this explanation lead?"* The first part of the question, concerning the explanation, will be answered first and afterwards the second part of the question is answered.

Based on the modal analysis done with the FEM model, it could be concluded that the CFS is a really stiff structure from a dynamic perspective. It was computed and shown in different ways how the dynamics of the CFS are dominated by the buoyancy stiffness of the floaters. This high stiffness results in relatively high natural frequencies, compared to other structures of a similar scale. The natural frequency of the system was computed with different methods and was determined to be within the wave frequency spectrum of usual sea states. Since these frequencies are in the similar range, the hypothesis was stated that the peak axial cable forces are caused by resonance phenomena. After this research it can be concluded that this hypothesis can not be confirmed for the CFS in general. However, modelling results show that it is likely that for certain locations in the CFS resonance is indeed causing high axial cable forces.

An important conclusion that can be drawn is that one integral explanation on the occurrence of extreme axial cable forces can not be given, because the hydrodynamic behaviour is changing throughout the CFS length. The CFS is sensitive to wave induced Stokes drift currents which are causing a mean axial tension force, that is varying in magnitude along the CFS. This tension force significantly influences the motions and as a result the peak axial cable forces. This could lead to different responses of the CFS to the wave frequency in the same range as the natural frequency of the CFS. For example, at cable locations with a low mean axial tension force the highest axial cable forces are observed for a simulation with the wave frequency equal to the system's natural frequency. Therefore, at these locations there is more reason to state that it is resonance that causes peak tension forces. Stokes drift current velocity and the mean axial tension force as a consequence, depend on the wave steepness which in turn depends on the wave frequency. This mechanism explains why the peaks in tension forces are in particular occurring for high frequency waves.

Under the condition that the explanations given above and earlier in the report can be proven in a more convincing way by means of future research, there can be made several improvements to the design of the CFS. In order to eliminate possible resonance phenomena, the CFS's natural frequency can be decreased by creating a less stiff structure. This could be achieved by increasing the floater spacing. This simultaneously requires the floater to increase in buoyancy volume (underwater) while the horizontal cross sectional area above, at and below the water line remains constant. A different strategy could be to decrease the floater's dimensions, therefore reducing the floater's buoyancy spring coefficient, which results in a less stiff structure as well. However, for this option no parametric study has been done yet. Instead of eliminating the occurrence of resonance, a different strategy is to reduce the impact of the resonance. This can be achieved by increasing the vertical drag force of the structure. Most simply this can be accomplished by increasing the floater's drag area in the vertical direction.

10
Recommendations

In this chapter all the gained understanding and experience in modelling and studying the hydrodynamic and structural behaviour of a cable-floater-system (CFS) is used to formulate recommendations. These include recommendations for further modelling and analysis of the model results on respectively the finite-element-method (FEM) models and the OrcaFlex models. In Chapter 8.2 and 8.3, recommendations were given already regarding the performed research. In this chapter the already proposed recommendations regarding future modelling are briefly repeated and expanded with other modelling ideas. Lastly, more general recommendations for future research on hydrodynamic behaviour of the CFS are given.

10.1. Recommendations regarding the finite-element-method models

The FEM model was created newly for this research. It is therefore relatively basic and can be extended in many ways for future research goals regarding the research on CFS behaviour. The main recommendations regarding modelling with the FEM model are:

- Add the structural damping and external forces to the equations of motion (EQM's) and compute the response of the CFS to the forces with a time domain simulation using modal superposition.
- Extend the FEM model structure with extra degrees of freedom (DOF's) for each node. Start with including the sway motion and yaw motion, which make it possible to model the dynamic behaviour in horizontal direction perpendicular to the CFS length. If needed, also the surge motion could be included.
- In case the model is adapted for simulations in time domain and also horizontal DOF's are included: model a varying axial tension over the cable length in order to study what the effect is of this tension force caused by Stokes drift on the motion of the CFS.
- Change the FEM model structure from floaters as lumped mass (point characteristics) to floaters along the full floater length (continuous characteristics).
- Define the spring coefficient of the floater's buoyancy in a more accurate, preferably non-linear way. This can be done by studying the exact shape of the floater carrying a cable and/or by doing model tests.
- Do a parametric study on the floater dimensions, in addition to the study on floater spacing, for better understanding of the modal behaviour and CFS design optimisation.

10.2. Recommendations regarding the OrcaFlex models

In OrcaFlex there are already a lot of possibilities and the main goal for future adaptations should be to further simplify the dynamic situation to better understand the results and be able to compare with the FEM model. Besides that, other recommendations are:

- When in particular resonance and the relation between wave frequency and CFS tension forces is studied, it is recommended to do simulations in frequency domain instead of time domain. This eliminates the effect of Stokes drift and can be an alternative for doing more, time-consuming simulations in time domain.

- When the effects of Stokes drift are wished to be further studied, the simulation periods need to be increased significantly for bigger modelled wave periods or the Stokes drift current could be imitated with a constant current included in the static analysis.
- In deep water wave conditions, do a set of simulations for different wave frequencies and a wave height adapting so that the wave steepness remains constant. Insights can be gained on the influence of the wave steepness on CFS motions and forces and potentially model input for future simulations can be chosen in a more intelligent way.
- Model the exact shape of a cable carrying floater in a more detailed way in OrcaFlex and define the exact vertical position of the floater relative to the cable (in the software called *offset*). This effects the definition of the buoyancy spring coefficient of the CFS. For the exceeding modelling cases the cable comes out of the water which is contradictory to footage from installations.
- In case the horizontal motions would like to be further studied, these results should be rewritten from being defined in a global coordinate system into a local coordinate system using rotation matrices.
- To reduce the influence of horizontal wave forces, simulations could be done with the horizontal drag coefficients of the CFS equal to zero and the vertical drag coefficients unchanged.
- Modelling the boundary conditions in a more elastic, realistic way could have big impact on the CFS behaviour in the OrcaFlex models close to the boundaries, where extreme values currently occur.
- Do more simulations in time domain with wave frequencies in the range of the natural frequency. Certainly when the exact natural frequency remains difficult to compute this could be useful.

10.3. General recommendations for further research

Besides the recommendations specifically for both models, there are also formulated some general recommendations:

- In Section 8.4, three main elements are explained that characterise the hydrodynamic behaviour of the CFS. In future research these three characteristics and the mechanical theory behind it, should be studied more thoroughly by doing literature study, different numerical model simulations, scale model tests or other research methods. More in detail on the sensitivity of Stokes drift, it is interesting to research how the influence of Stokes drift on the CFS changes in a more realistic, coastal environment, that better resembles project sites. A decreasing water depth causes waves to flatten in their shape and their steepness to decrease. Consequently, Stokes drift velocity should decrease and could become less dominant in the hydrodynamic behaviour of the CFS as observed in the OrcaFlex simulations of this research.
- In this research the focus has been modal analysis and dynamic analysis in time and little attention is given to the structural aspects of an Euler Bernoulli beam, the structural model of the CFS. Future research could be done more from a structural perspective. For example, there should be focused on stresses in the cable rather than only the forces on the cable. Besides that, the physical origin and plausibility of the compression forces in the OrcaFlex results can be researched by studying structural beam theory and the computational set-up of OrcaFlex.
- To research questions like these, future research should also be focused more on a small spatial scale (floater) instead of a global scale (CFS). A main conclusion from this global scale analysis is that the CFS hydrodynamic response is completely different throughout the its length. So specific locations of interest, e.g. close to the boundaries, should be studied separately and more detailed, perhaps with the help of a different, new model including only a small section of the CFS.
- By comparing the models of the two modelling methods a lot of understanding has been gained. To a certain extent the results of one model could be verified with results of a model from the other modelling method. However, since the goals of both modelling methods are different, the overlap between the models is really small and the type of results is different. In order to be able to trust the output of both models, they need to be validated. Therefore, data need to be gathered from the offshore field or from model tests to be conducted. Only then, the insecurities and questions on the OrcaFlex model results can be fully taken away.

Part V

References & appendices

References

4C Offshore. (n.d.). *Image of an example of a cable tensioner system.* 4C Offshore.

Alfeehan, A. (2018). *Mechanics of materials - chaper two - compound (combined) stresses.* https://uomustansiriyah.edu.iq/media/lectures/5/5_2018_03_13!09_32_06_PM.pdf. Mustansiriyah University.

Blevins, R. D. (2016). *Formulas for dynamics, acoustics and vibration*. Wiley.

Brown, M., & Elliott, L. (1988). Two-dimensional dynamic analysis of a floating hose string. *Applied Ocean Research*, *10*(1), 20–34. https://doi.org/10.1016/s0141-1187(88)80021-x.

Chellapilla, K. R. (2016). Finite element analysis of free flexural vibrations of a rotor-bearing system with permanent magnetic bearings.

Colomes Gene, O. (2021). *Introduction to computational dynamics for offshore structures - lecture slides*. Delft University of Technology.

Det Norske Veritas. (2010). *Recommended practice dnv-rp-c205 - environmental conditions and environmental loads*. Det Norske Veritas.

Donoghue, T. O., & Halliwell, A. (1990). Vertical bending moments and axial forces in a floating marine hose-string. *Engineering Structures*, *12*(2), 124–133. https://doi.org/10.1016/0141-0296(90)90018-n.

Driessen, R. (2015). *Image of the chute system at the nexus van oord.* The Factory Files.

Fu, S., Xu, Y., Hu, K., & Zhang, Y. (2013). Experimental investigation on hydrodynamics of floating cylinder in oscillatory and steady flows by forced oscillation test. *Marine Structures*, *34*, 41–55. https://doi.org/10.1016/j.marstruc.2013.08.005.

Holthuijsen, L. H. (2007). *Waves in oceanic and coastal waters*. Cambridge University Press.

Journée, J. M. J., Massie, W. W., & Huijsmans, R. H. M. (2015). *Offshore hydromechanics*. Delft University of Technology.

Karow, N., Kandler, L., Brede, M., & Grundmann, S. (2020, 01). Turbulent transport of discharged ground water in oceanic bottom boundary layers in a water channel experiment. doi: 10.5194/os-2019-116

KOWL. (2018). *Cable plan kincardine offshore windfarm project.* https://marine.gov.scot/sites/default/files/00536352.pdf.

Li, Y., Gui, F., & Teng, B. (2007). Hydrodynamic behavior of a straight floating pipe under wave conditions. *Ocean Engineering*, *34*(3–4), 552–559. https://doi.org/10.1016/j.oceaneng.2006.01.012.

Lin, L. (n.d., n.d.). *Introduction to finite element modelling - university of california at berkeley.* https://lwlin.me.berkeley.edu/me128/FEMNotes.pdf. (Accessed on 15-02-2022)

LS Cable System Ltd. (2020). Internal document.

Metrikine, A. (2022). (Personal communication on 11-03-2022)

Morison, J., Johnson, J., & Schaaf, S. (1950). The force exerted by surface waves on piles. *Journal of Petroleum Technology*, *2*(05), 149–154. https://doi.org/10.2118/950149-g.

Newman, J. N. (2017). *Marine hydrodynamics*. Massachusetts Institute of Technology.

Orcina. (n.d.). *Orcaflex.* https://www.orcina.com/orcaflex/. (Accessed on 15-02-2022)

Orcina. (2021). *Orcaflex help 11.2d.* https://www.orcina.com/webhelp/OrcaFlex/. (Retrieved on 7 September 2022)

Orcina. (2022a). (Personal communication via email on 04-05-2022)

Orcina. (2022b). (Personal communication via email on 09-12-2022)

Papathanasiou, T. K., Karperaki, A., Theotokoglou, E. E., & Belibassakis, K. A. (2015). A higher order fem for time-domain hydroelastic analysis of large floating bodies in an inhomogeneous shallow water environment. *Proceedings of the Royal Society A: Mathematical, Physical and Engineering Sciences*, *471*(2173). https://doi.org/10.1098/rspa.2014.0643.

Phillips, O. M. (1978). The dynamics of the upper ocean. *Journal of Fluid Mechanics*, *88*(4), 793-794. https://doi.org/10.1002/zamm.19790590714.

Simone, A. (2011). *An introduction to the analysis of slender structures*. Delft University of Technology.

Simscale. (n.d., n.d.). *What is cfd | computational fluid dynamics?* https://www.simscale.com/docs/simwiki/cfd-computational-fluid-dynamics/what-is-cfd-computational-fluid-dynamics/. (Accessed on 15-02-2022)

Spijkers, J. M. J., Vrouwenvelder, A. W. C. M., & Klaver, E. C. (2006). *Dynamics of structures. part 1 vibration of structures*. Delft University of Technology.

Sundar, V., Sundaravadivelu, R., & Purushotham, S. (1988). Hydrodynamic characteristics of moored floating pipe breakwaters in random waves. proceedings of the institution of mechanical engineers. *Part M: Journal of Engineering for the Maritime Environment*, *217*(2), 95–110. https://doi.org/10.1243/147509003321921346.

Teng, B., & Li, Y. C. (1991). The wave-current force spectrum on inclined cylinders. *Ocean Engineering*, *18*(6), 535–553. https://doi.org/10.1016/0029-8018(91)90008-e.

Van Oord. (n.d.-a). *Internal footage.* Van Oord.

Van Oord. (n.d.-b). *Kabellegmateriaal van oord.* https://www.vanoord.com/nl/materieel/kabellegmaterieel/. (Accessed on 21-12-2022)

Van Oord. (2020a). Internal document. *Van Oord*.

Van Oord. (2020b). Internal document.

Van Oord. (2021). Internal document. *Van Oord*.

van der Mout, A. (2017). *Blowing in the wind: floating for maximum buoyancy - offshorewind.biz.* https://www.offshorewind.biz/2017/04/05/blowing-in-the-wind-floating-for-maximum-buoyancy/. (Accessed on 21-02-2022)

Xu, T., Dong, G., Zhao, Y., Ma, X., & Ma, Y. (2013). Hydrodynamic characteristics of floating pipes in random waves. proceedings of the international conference on offshore mechanics and arctic engineering. *OMAE*. https://doi.org/10.1115/OMAE2013-10164.

Zhang, S. F., Chen, C., Zhang, Q. X., Zhang, D. M., & Zhang, F. (2015). Wave loads computation for offshore floating hose based on partially immersed cylinder model of improved morison formula. *The Open Petroleum Engineering Journal*, *8*(1), 130–137. https://doi.org/10.2174/1874834101508010130.

A

Input parameters for OrcaFlex models and finite-element-method models

Table A.1: All input parameters of the cable-floater-system and the hydraulic environment applied in OrcaFlex (OF) models and/or finite-element-method (FEM) models or other, unused technical specifications (none)

Environmental parameters				
Parameter:	**Symbol:**	**Magnitude:**	**Unity:**	**OF and/or FEM:**
Density sea water	ρ_w	1025	kg/m^3	OF and FEM
Gravitational acceleration	g	9.81	m/s^2	OF and FEM
Current velocity	u	variable	m/s	OF and FEM
Wave height	H	0.4	m	OF
Wave period	T_p	variable	s	OF
Cable-floater-system parameters				
Parameter:	**Symbol:**	**Magnitude:**	**Unity:**	**OF and/or FEM:**
Total length	L_{cfs}	1080	m	OF and FEM
Distance between floaters	Δ_f	2.05	m	OF and FEM
Offset between mid point cable and floater	-	0	m	OF
Distance between the two line ends	-	1030.57	m	OF
Target segment - / element length (grid size)	Δx	0.205	m	OF and FEM
Boundary conditions OrcaFlex model	Simply supported			OF
Boundary conditions FEM model	Simply supported or clamped			FEM
Cable parameters (type: CU1600SQ)				
Parameter:	**Symbol:**	**Magnitude:**	**Unity:**	**OF and/or FEM:**
Overall diameter	D_c	0.2926	m	OF and FEM
Structural mass per unit length	m_c	153.7	kg/m	OF and FEM
Drag coefficient	$C_{D,c}$	1.2	-	OF and FEM
Bending stiffness	J	170	kNm^2	OF and FEM
Axial stiffness (in tension)	E_cA_c	1050000	kN	OF
Torsional stiffness	τ_c	2618	kNm^2	OF
Maximum allowable tension (straight)	T_{max}	360	kN	OF
Minimum tension (maximum compression)	T_{min}	-15	kN	OF
Maximum allowable tensional stress	σ_{max}	5354	kN/m^2	OF
Floater parameters (type: Twin Boom 600)				
Parameter:	**Symbol:**	**Magnitude:**	**Unity:**	**OF and/or FEM:**
Structural mass	m_f	6.5	kg	OF and FEM
Length (in cable parallel direction)	L_f	1.42	m	OF and FEM
Diameter air chamber	D_f	0.57	m	OF and FEM
Length air chamber	$L_{f,ac}$	1.34	m	none
Width floater (full width incl.)	$W_{f,la}$	2.15	m	none
Width between air chambers (for cable)	$W_{f,cab}$	0.57	m	none
Drag area in x-direction	$A_{D,x}$	0.51	m^2	OF
Drag area in y-direction	$A_{D,y}$	0.76	m^2	OF
Drag area in z-direction	$A_{D,z}$	1.53	m^2	OF
Drag coefficient in z,y,z-direction	$C_{D,f}$	1.1	-	OF

B

Shape functions used in the finite-element-method model

Shape functions are a mathematical tool that can assist to describe the relations between the degrees of freedom (DOF's) of one element in the finite-element-method (FEM) model. With these relations for one element, the relations between physical system properties such as mass, stiffness, buoyancy and tension and the dynamic response of the system can be made. This dynamic response is of our biggest interest, studying the behaviour of the cable-floater-system (CFS). First, the concept of shape functions is introduced in paragraph B.1 and afterwards the according shape functions are derived in paragraph B.2.

B.1. The concept of shape functions

Assume that there is a random function $\hat{f}$, dependent on one variable x. See Figure B.1.

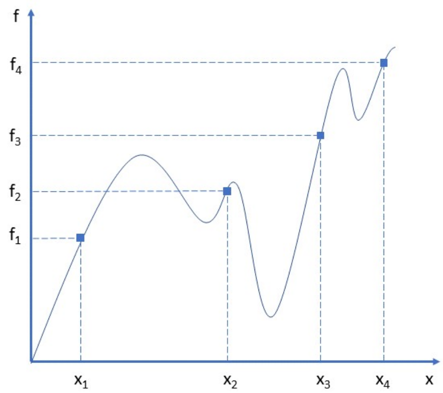

Figure B.1: Random function $\hat{f}$

The equation itself is not known, but certain data points are selected. These four points f_1,f_2, f_3 and f_4 have a relation with the function $\hat{f}$ that is described by respectively functions N_1, N_2, N_3 and N_4. With these four points f_1, f_2, f_3 and f_4 and with random functions N, function $\hat{f}$ can be described in the following way:

$$\hat{f}(x) = N_1(x)f_1 + N_2(x)f_2 + N_3(x)f_3 + N_4(x)f_4$$

The value of function $\hat{f}$ for $x = x_1$ is then equal to f_1. So:

$$\hat{f}(x = x_1) = N_1(x_1)f_1 + N_2(x_1)f_2 + N_3(x_1)f_3 + N_4(x_1)f_4 = f_1$$

If one wants to solve this equation, there is one trivial solution:

$$N_1(x_1) = 1 \qquad N_2(x_1) = 0 \qquad N_3(x_1) = 0 \qquad N_4(x_1) = 0$$

Similarly, for $x = x_2$, $x = x_3$ and $x = x_4$ respectively:

$$\begin{array}{llll} N_1(x_2) = 0 & N_2(x_2) = 1 & N_3(x_2) = 0 & N_4(x_2) = 0 \\ N_1(x_3) = 0 & N_2(x_3) = 0 & N_3(x_3) = 1 & N_4(x_3) = 0 \\ N_1(x_4) = 0 & N_2(x_4) = 0 & N_3(x_4) = 0 & N_4(x_4) = 1 \end{array}$$

This principle of setting up equations will be used also for setting up equations for the DOF's of an element in the FEM model.

B.2. Derivation of the shape functions

As mentioned at the start of this paragraph, the variables of interest are the DOF's for each element. Looking at the scale of one model element, the local dynamic system has four DOF's, see Figure 4.1:

1. Vertical displacement at left boundary: u_l
2. Angular displacement at left boundary: θ_l
3. Vertical displacement at right boundary: u_r
4. Angular displacement at right boundary: θ_r

These four DOF's are considered as the four points f_1, f_2, f_3, f_4 in Figure B.1 for which an equation needs to be formulated. The relation between vertical displacement u and angular displacement is known:

$$\theta(\hat{x}) = u'(\hat{x}) = \hat{f}'(\hat{x}) \tag{B.1}$$

Therefore the equations can be written in the following way for both boundary locations $\hat{x} = x_l$ and $\hat{x} = x_r$:

$$\begin{aligned} u(x_l) = \hat{f}(x_l) &= N_1(x_l)u_l + N_2(x_l)\theta_l + N_3(x_l)u_r + N_4(x_l)\theta_r \\ \theta(x_l) = \hat{f}'(x_l) &= N_1'(x_l)u_l + N_2'(x_l)\theta_l + N_3'(x_l)u_r + N_4'(x_l)\theta_r \\ u(x_r) = \hat{f}(x_r) &= N_1(x_r)u_l + N_2(x_r)\theta_l + N_3(x_r)u_r + N_4(x_r)\theta_r \\ \theta(x_r) = \hat{f}'(x_r) &= N_1'(x_r)u_l + N_2'(x_r)\theta_l + N_3'(x_r)u_r + N_4'(x_r)\theta_r \end{aligned}$$

This set of equations can also be written in a matrix format. Besides that the following expressions are simplified: $u(x_l) = u_l$, $\theta(x_l) = \theta_l$, $u(x_r) = u_r$ and $\theta(x_r) = \theta_r$. This gives:

$$\begin{bmatrix} u(x_l) \\ \theta(x_l) \\ u(x_r) \\ \theta(x_r) \end{bmatrix} = \begin{bmatrix} u_l \\ \theta_l \\ u_r \\ \theta_r \end{bmatrix} = \begin{bmatrix} N_1(x_l) & N_2(x_l) & N_3(x_l) & N_4(x_l) \\ N_1'(x_l) & N_2'(x_l) & N_3'(x_l) & N_4'(x_l) \\ N_1(x_r) & N_2(x_r) & N_3(x_r) & N_4(x_r) \\ N_1'(x_r) & N_2'(x_r) & N_3'(x_r) & N_4'(x_r) \end{bmatrix} \begin{bmatrix} u_l \\ \theta_l \\ u_r \\ \theta_r \end{bmatrix} \tag{B.2}$$

The left side and the last term on the right side of Equation B.2 correspond to each other. Remember the mathematical tool as described in the previous paragraph B. Equation B.2 can be rewritten into the format:

$$\begin{bmatrix} N_1(x_l) & N_2(x_l) & N_3(x_l) & N_4(x_l) \\ N_1'(x_l) & N_2'(x_l) & N_3'(x_l) & N_4'(x_l) \\ N_1(x_r) & N_2(x_r) & N_3(x_r) & N_4(x_r) \\ N_1'(x_r) & N_2'(x_r) & N_3'(x_r) & N_4'(x_r) \end{bmatrix} = \begin{bmatrix} 1 & 0 & 0 & 0 \\ 0 & 1 & 0 & 0 \\ 0 & 0 & 1 & 0 \\ 0 & 0 & 0 & 1 \end{bmatrix} \tag{B.3}$$

This matrix system, Equation B.3, can be split into four separate systems of equations, each describing one shape function $N_1(\hat{x})$, $N_2(\hat{x})$, $N_3(\hat{x})$ and $N_4(\hat{x})$:

$$\begin{bmatrix} N_1(x_l) \\ N_1'(x_l)) \\ N_1(x_r) \\ N_1'(x_r) \end{bmatrix} = \begin{bmatrix} 1 \\ 0 \\ 0 \\ 0 \end{bmatrix} \qquad \begin{bmatrix} N_2(x_l) \\ N_2'(x_l)) \\ N_2(x_r) \\ N_2'(x_r) \end{bmatrix} = \begin{bmatrix} 0 \\ 1 \\ 0 \\ 0 \end{bmatrix} \qquad \begin{bmatrix} N_3(x_l) \\ N_3'(x_l)) \\ N_3(x_r) \\ N_3'(x_r) \end{bmatrix} = \begin{bmatrix} 0 \\ 0 \\ 1 \\ 0 \end{bmatrix} \qquad \begin{bmatrix} N_4(x_l) \\ N_4'(x_l)) \\ N_4(x_r) \\ N_4'(x_r) \end{bmatrix} = \begin{bmatrix} 0 \\ 0 \\ 0 \\ 1 \end{bmatrix}$$

Each of these systems of equations contains four equations describing the shape function. Therefore the shape function can be expressed in the format of a *'piecewise cubic function'* with four variables a, b, c and d. Since there are four DOF per element, in total there are four shape functions numbered with i.

$$N_i(\hat{x}) = a_i + b_i\hat{x} + c_i\hat{x}^2 + d_i\hat{x}^3 \qquad \text{for } i = 1,2,3,4 \tag{B.4}$$

Substitute Equation B.4 for example into the system of equations of $N_1(\hat{x})$ ($i = 1$). For the derivative of the piecewise cubic function use $N_1'(\hat{x}) = b_i + 2c_i\hat{x} + 3d_i\hat{x}^2$. This gives the following system of equations:

$$\begin{bmatrix} 1 & x_l & x_l^2 & x_l^3 \\ 0 & 1 & 2x_l & 3x_l^2 \\ 1 & x_r & x_r^2 & x_r^3 \\ 0 & 1 & 2x_r & 3x^2 \end{bmatrix} \begin{bmatrix} a_1 \\ b_1 \\ c_1 \\ d_1 \end{bmatrix} = \begin{bmatrix} 1 \\ 0 \\ 0 \\ 0 \end{bmatrix} \tag{B.5}$$

In order to solve this system, the values of $\hat{x} = x_l$ and $\hat{x} = x_r$ are assumed to be known. For x_l a value of 0 is taken and for x_r a value of h is taken. The value of h is in fact the size of one system element, also called the grid size. The system can be solved for a_1, b_1, c_1 and d_1 and using Equation B.4, the shape function $N_1(\hat{x})$ is formulated. These steps are repeated for $i = 2$, $i = 3$ and $i = 4$. These give values of a_i, b_i, c_i and d_i. These values are used to formulate shape function $N_2(\hat{x})$, $N_3(\hat{x})$ and $N_4(\hat{x})$. Finally, the result is four shape functions dependent on the local $\hat{x}$ variable.

$$N_1(\hat{x}) = 1 - \frac{3}{h^2}\hat{x}^2 + \frac{2}{h^3}\hat{x}^3 \tag{B.6a}$$

$$N_2(\hat{x}) = \hat{x} - \frac{2}{h}\hat{x}^2 + \frac{1}{h^2}\hat{x}^3 \tag{B.6b}$$

$$N_3(\hat{x}) = \frac{3}{h^2}\hat{x}^2 - \frac{2}{h^3}\hat{x}^3 \tag{B.6c}$$

$$N_4(\hat{x}) = -\frac{1}{h}\hat{x}^2 + \frac{1}{h^2}\hat{x}^3 \tag{B.6d}$$

Note that these shape functions are valid for all elements of the FEM model since the local $\hat{x}$ coordinate system can used again for each element. By doing so, the shape functions are equal for each element of the CFS.

C
Mass matrix and stiffness matrix in finite-element-method model

On the next page a part of the mass matrix M, Equation C.1, and the stiffness matrix K, Equation C.2, is shown as clarification on paragraph 4.4.3, where is explained how these matrices are assembled into a full finite-element-method model. These matrices are too big to display in the text itself and are therefore attached as an appendix.

$$
\begin{bmatrix}
\nwarrow & \nwarrow & \nwarrow & \nwarrow & \nwarrow & \uparrow & \uparrow & \uparrow & \uparrow & \rightarrow \\
\nwarrow & m_{33}^{e}+m_{11}^{e+1}+m_{u,f} & m_{34}^{e}+m_{12}^{e+1} & m_{13}^{e+1} & m_{14}^{e+1} & 0 & 0 & 0 & 0 & \rightarrow \\
\nwarrow & m_{43}^{e}+m_{21}^{e+1} & m_{44}^{e}+m_{22}^{e+1}+m_{\theta,f} & m_{23}^{e+1} & m_{24}^{e+1} & 0 & 0 & 0 & 0 & \rightarrow \\
\nwarrow & m_{31}^{e+1} & m_{32}^{e+1} & m_{33}^{e+1}+m_{11}^{e+2} & m_{34}^{e+1}+m_{12}^{e+2} & m_{13}^{e+2} & m_{14}^{e+2} & 0 & 0 & \rightarrow \\
\nwarrow & m_{41}^{e+1} & m_{42}^{e+1} & m_{43}^{e+1}+m_{21}^{e+2} & m_{44}^{e+1}+m_{22}^{e+2} & m_{23}^{e+2} & m_{24}^{e+2} & 0 & 0 & \rightarrow \\
\leftarrow & 0 & 0 & m_{31}^{e+2} & m_{32}^{e+2} & m_{33}^{e+2}+m_{11}^{e+3} & m_{34}^{e+2}+m_{12}^{e+3} & m_{13}^{e+3} & m_{14}^{e+4} & \searrow \\
\leftarrow & 0 & 0 & m_{41}^{e+2} & m_{42}^{e+2} & m_{43}^{e+3}+m_{21}^{e+3} & m_{44}^{e+2}+m_{22}^{e+3} & m_{23}^{e+3} & m_{24}^{e+4} & \searrow \\
\leftarrow & 0 & 0 & 0 & 0 & m_{31}^{e+3} & m_{32}^{e+3} & m_{3}3^{e+3}+m_{11}^{e+4} & m_{34}^{e+3}+m_{12}^{e+4} & \searrow \\
\leftarrow & 0 & 0 & 0 & 0 & m_{41}^{e+3} & m_{42}^{e+3} & m_{43}^{e+3}+m_{21}^{e+4} & m_{44}^{e}e+3+m_{22}^{e+4} & \searrow \\
\downarrow & \downarrow & \downarrow & \downarrow & \downarrow & \searrow & \searrow & \searrow & \searrow & \searrow
\end{bmatrix}
\tag{C.1}
$$

$$
\begin{bmatrix}
\nwarrow & \nwarrow & \nwarrow & \nwarrow & \nwarrow & \uparrow & \uparrow & \uparrow & \uparrow & \rightarrow \\
\nwarrow & tb_{33}^{e}+tb_{11}^{e+1}+d_{u,f} & tb_{34}^{e}+tb_{12}^{e+1} & tb_{13}^{e+1} & tb_{14}^{e+1} & 0 & 0 & 0 & 0 & \rightarrow \\
\nwarrow & tb_{43}^{e}+tb_{21}^{e+1} & tb_{44}^{e}+tb_{22}^{e+1}+d_{\theta,f} & tb_{23}^{e+1} & tb_{24}^{e+1} & 0 & 0 & 0 & 0 & \rightarrow \\
\nwarrow & tb_{31}^{e+1} & tb_{32}^{e+1} & tb_{33}^{e+1}+tb_{11}^{e+2} & tb_{34}^{e+1}+tb_{12}^{e+2} & m_{13}^{e+2} & tb_{14}^{e+2} & 0 & 0 & \rightarrow \\
\nwarrow & tb_{41}^{e+1} & tb_{42}^{e+1} & tb_{43}^{e+1}+tb_{21}^{e+2} & tb_{44}^{e+1}+tb_{22}^{e+2} & tb_{23}^{e+2} & tb_{24}^{e+2} & 0 & 0 & \rightarrow \\
\leftarrow & 0 & 0 & tb_{31}^{e+2} & tb_{32}^{e+2} & tb_{33}^{e+2}+tb_{11}^{e+3} & tb_{34}^{e+2}+tb_{12}^{e+3} & tb_{13}^{e+3} & tb_{14}^{e+4} & \searrow \\
\leftarrow & 0 & 0 & tb_{41}^{e+2} & tb_{42}^{e+2} & tb_{43}^{e+3}+tb_{21}^{e+3} & tb_{44}^{e+2}+tb_{22}^{e+3} & tb_{23}^{e+3} & tb_{24}^{e+4} & \searrow \\
\leftarrow & 0 & 0 & 0 & 0 & tb_{31}^{e+3} & tb_{32}^{e+3} & tb_{e+3+tb_{11}^{e+4}} & tb_{34}^{e+3}+tb_{12}^{e+4} & \searrow \\
\leftarrow & 0 & 0 & 0 & 0 & tb_{41}^{e+3} & tb_{42}^{e+3} & tb_{43}^{e+3}+tb_{21}^{e+4} & tb_{44}^{e}e+3+tb_{22}^{e+4} & \searrow \\
\downarrow & \downarrow & \downarrow & \downarrow & \downarrow & \searrow & \searrow & \searrow & \searrow & \searrow
\end{bmatrix}
\tag{C.2}
$$

D

Possible extensions of the finite-element-method model

In paragraph 8.2.2 the possible extensions of the model were already briefly mentioned. In this appendix, in appendix D.1. a first contribution is given on how the model could be extended to take into account more DOF's. Besides that, a small start will be made on how to include external forces and compute a steady-state-response with the FEM model in appendix D.2. This appendix can be seen as a starting point for further research and extension on the FEM model.

D.1. Including more degrees of freedom

If one would like to include more DOF's, the methodology that was applied in chapter 4 can still be used but the input parameters, the equations and the resulting matrices are different. For example, if the body motions of *sway* and *yaw* are added to the model, the amount of DOF's per element increases from four to eight. Having eight DOF's per element means that eight equations of motion (EQM) are needed to solve the dynamic system for one element. In order to solve this system of eight EQM's, also eight shape functions should be formulated. In deriving the shape functions the format of a *piecewise cubic function* can no longer be used. Nonetheless, the relation of the derivative of the *heave* motion (indicated with u in chapter 4) being equal to the *pitch* motion (indicated with θ) can still be used. The relation works in the same way for the new DOF's: the *sway* motion is equal to the derivative of the *yaw* motion. Once the shape functions are formulated, the equations of motion can be formulated using the weak form of the EQM. The exact relations between the known *heave* and *pitch* motion versus the new *sway* and *yaw* motion should first be further investigated, as well as several input parameters that change. For example, besides the vertical added mass, there should now also be accounted for horizontal added mass. Concerning the different contributions of stiffness to the system: bending stiffness is most likely to be the same for the horizontal direction, as well as the axial tension stiffness. However, the discrete floater buoyancy stiffness will not be present in horizontal direction. Finally, an elemental mass matrix and stiffness matrix can be assembled with a 8x8 size (instead of 4x4). In a similar overlapping pattern, now overlapping four rows and columns, the full structure model can be build.

Computing the CFS response in time using modal superposition

In order to compute the natural frequencies and modal shapes the EQM, the mass matrix multiplied by matrix with DOF's accelerations plus the stiffness matrix multiplied by matrix with DOF's displacements, is set equal to zero. The sum of the resultant forces is zero and there is a static equilibrium. If one wants to compute the response of the FEM model in time, external forces are also taken into account. These extra forces cause the sum of the resultant forces to be no longer zero and therefore the dynamic system to be in its static equilibrium. These forces should be added on the right hand side of the EQM's. Furthermore, in order to generate accurate, trustworthy results the effects of damping also have to be taken into account. Besides that, the orthogonal properties of the stiffness and mass matrix and the principle of *modal superposition* can be used to eventually compute the displacement, velocities and accelerations at every location along the cable x_{cfs} for each moment in time t (Colomes Gene, 2021).

The eigenvectors (modal shapes) are linearly independent and stiffness and mass orthogonal. This means that the matrices are real valued and the transpose of the matrix is equal to the matrix (symmetric). Applying these properties to the general eigenvalue problem, Equation 5.3 gives:

$$\begin{cases} \phi_i^T K \phi_j = 0 \\ \phi_i^T M \phi_j = 0 \end{cases}, i \neq j \qquad\qquad \begin{cases} \phi_i^T K \phi_j = k_{ii} \\ \phi_i^T M \phi_j = m_{ii} \end{cases}, i = j \tag{D.1}$$

The orthogonal properties are used to uncouple the EQM's:

$$M_{FF}\ddot{w}_F + C_{FF}\dot{w}_F + K_{FF}w_F = F_F^{ext} - K_{FP}w_P - C_{FP}\dot{w}_P - M_{FP}\ddot{w_P}$$

The principle of modal superposition, mentioned already in 5.2, is used to replace w_F, $\dot{w}_F$ and $\ddot{w}_F$ and all terms are multiplied with Φ^T:

$$\Phi^T M_{FF}\Phi\ddot{H}(t) + \Phi^T C_{FF}\Phi\dot{H}(t) + \Phi^T K_{FF}\Phi H(t) = \Phi^T(F_F^{ext} - K_{FP}w_P - C_{FP}\dot{w}_P - M_{FP}\ddot{w_P})$$

The term on the right side in between brackets is combined in one term F^{eq}. For the mass term and the stiffness term, the orthogonality properties of Equation D.1 can be used. In order to use the same method for the damping term, often the damping term is defined as the sum of partially the mass term and partially the stiffness term. This is called *Rayleigh damping*. Applying this in the EQM:

$$C_{FF} = a_0 M_{FF} + a_1 K_{FF} \qquad \rightarrow \qquad \Phi^T C_{FF}\Phi = a_0\Phi^T M_{FF}\Phi + a_1\Phi^T K_{FF}\Phi$$

The result is then a set of N second order differential equations (EQM's) for N modes:

$$\begin{bmatrix} m_{11}\ddot{H}_1(t) \\ m_{22}\ddot{H}_2(t) \\ \vdots \\ m_{NN}\ddot{H}_N(t) \end{bmatrix} + \begin{bmatrix} c_{11}\dot{H}_1(t) \\ c_{22}\dot{H}_2(t) \\ \vdots \\ c_{NN}\dot{H}_N(t) \end{bmatrix} + \begin{bmatrix} k_{11}H_1(t) \\ k_{22}H_2(t) \\ \vdots \\ k_{NN}H_N(t) \end{bmatrix} = \begin{bmatrix} \phi_1^T F^{eq} \\ \phi_2^T F^{eq} \\ \vdots \\ \phi_N^T F^{eq} \end{bmatrix} = \begin{bmatrix} f_1^{eq} \\ f_2^{eq} \\ \vdots \\ f_N^{eq} \end{bmatrix} \tag{D.2}$$

To solve this system of equations, two initial conditions per equation are needed. The initial conditions can be formulated in the same way by using modal superposition:

$$u_F(t=0) = \sum_{i=1}^{N} \phi_i H_i(t=0) \qquad \rightarrow \qquad M_{FF}u_F(t=0) = \sum_{i=1}^{N} M_{FF}\phi_i H_i(t=0) \qquad \rightarrow$$

$$\phi_j^T M_{FF}u_F(t=0) = \sum_{i=1}^{N} \phi_j^T M_{FF}\phi_i H_i(t=0) \qquad \rightarrow \qquad \phi_j^T M_{FF}u_F(t=0) = m_{jj}H_j(t=0)$$

In a similar way this can be done for the velocity. The initial conditions then are:

$$H_j(t=0) = \frac{\phi_j^T M_{FF}u_F(t=0)}{m_{jj}} \qquad\qquad \ddot{H}_j(t=0) = \frac{\phi_j^T M_{FF}\dot{u}_F(t=0)}{m_{jj}}$$

With these initial conditions and all the EQM's in Equation D.2 can be solved giving modal responses for $H_j(t)$, $\dot{H}_j(t)$ and $\ddot{H}_j(t)$. The modal responses combined give the displacements, velocities and accelerations for time t:

$$u_F(t) = \sum_{j=1}^{M\leq N} \phi_j H_j(t) \qquad \dot{u}_F(t) = \sum_{j=1}^{M\leq N} \phi_j \dot{H}_j(t) \qquad \ddot{u}_F(t) = \sum_{j=1}^{M\leq N} \phi_j \ddot{H}_j(t)$$

E

Extra results of the parametric study on the finite-element-method model

In Figure E.1 on the next page, the plots are shown for various floater spacing values, other than those that were already shown in Figure 5.7. These additional plots where used to study how the global modal shape oscillations are slowly disappearing for an increasing floater spacing. Besides that, they were used to come up with a floater spacing that has natural frequencies outside the wave frequency spectrum (see paragraph 8.5).

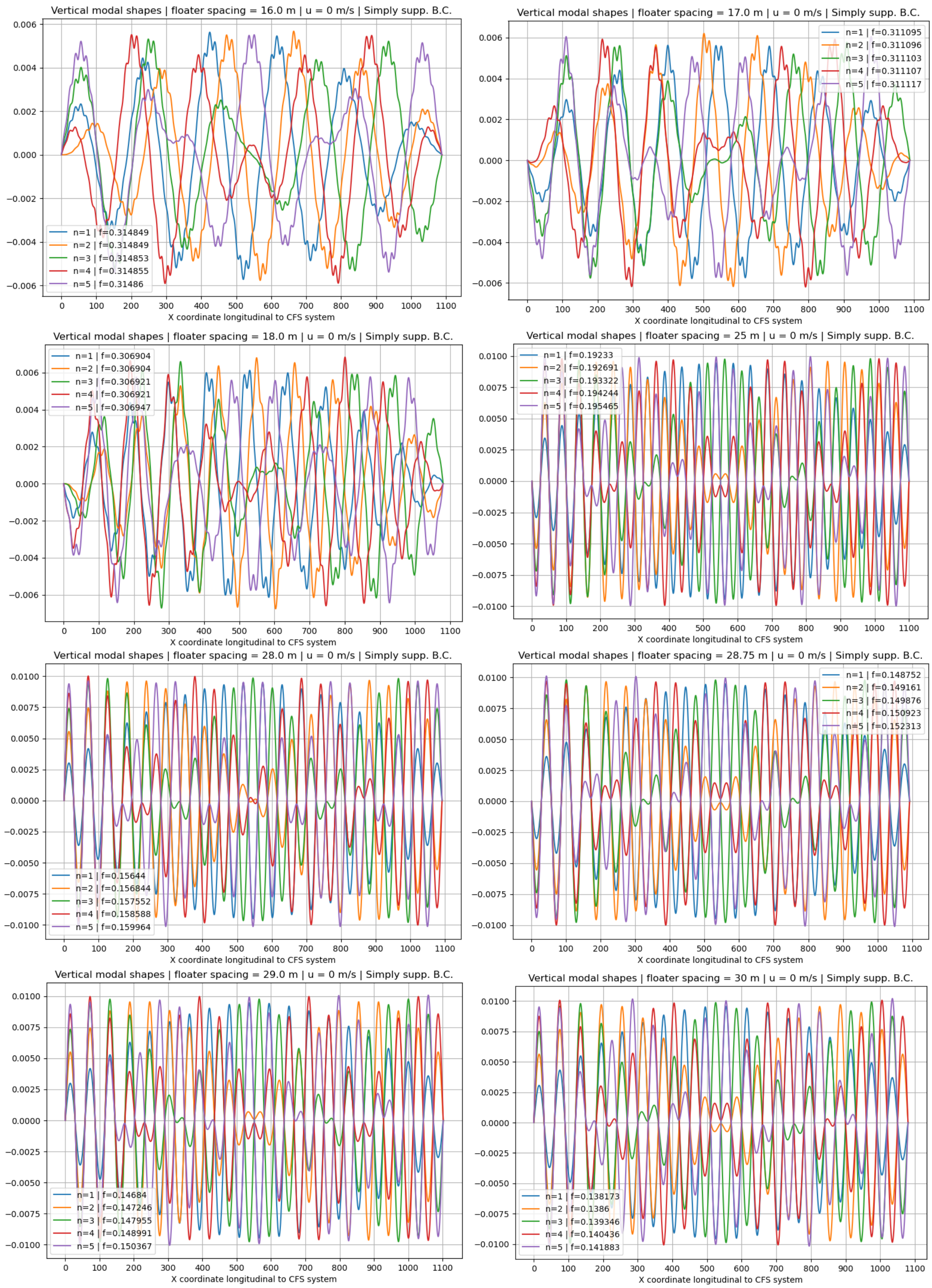

Figure E.1: The remaining plots (not shown in paragraph 5.4.2) of vertical modal shapes for case A with increasing floater spacing Δ_f

F
Extra OrcaFlex results

In this appendix more results of the OrcaFlex simulations are shown in addition to the results presented and discussed in chapter 7. These results are not accompanied with separate analyses and conclusions. However, the results plotted below are used in creating understanding on the hydrodynamic behaviour of the cable-floater-system (CFS) and used in coming up with conclusions for the report. First in appendix F.1 spectral density plots of the total displacement are shown for more arc length positions L_{arc} along the CFS. Next, in appendix F.2 the range graphs for the X, Y and Z positions between $T_{sim} = 5000$ s and $T_{sim} = 6000$ s are shown in addition to the axial cable force range graphs in Figure 7.6. Similar to this Figure, appendix F.2. includes graphs for cases without current and various wave periods $T_w = T_p$.

F.1. Spectral density plots of total displacement

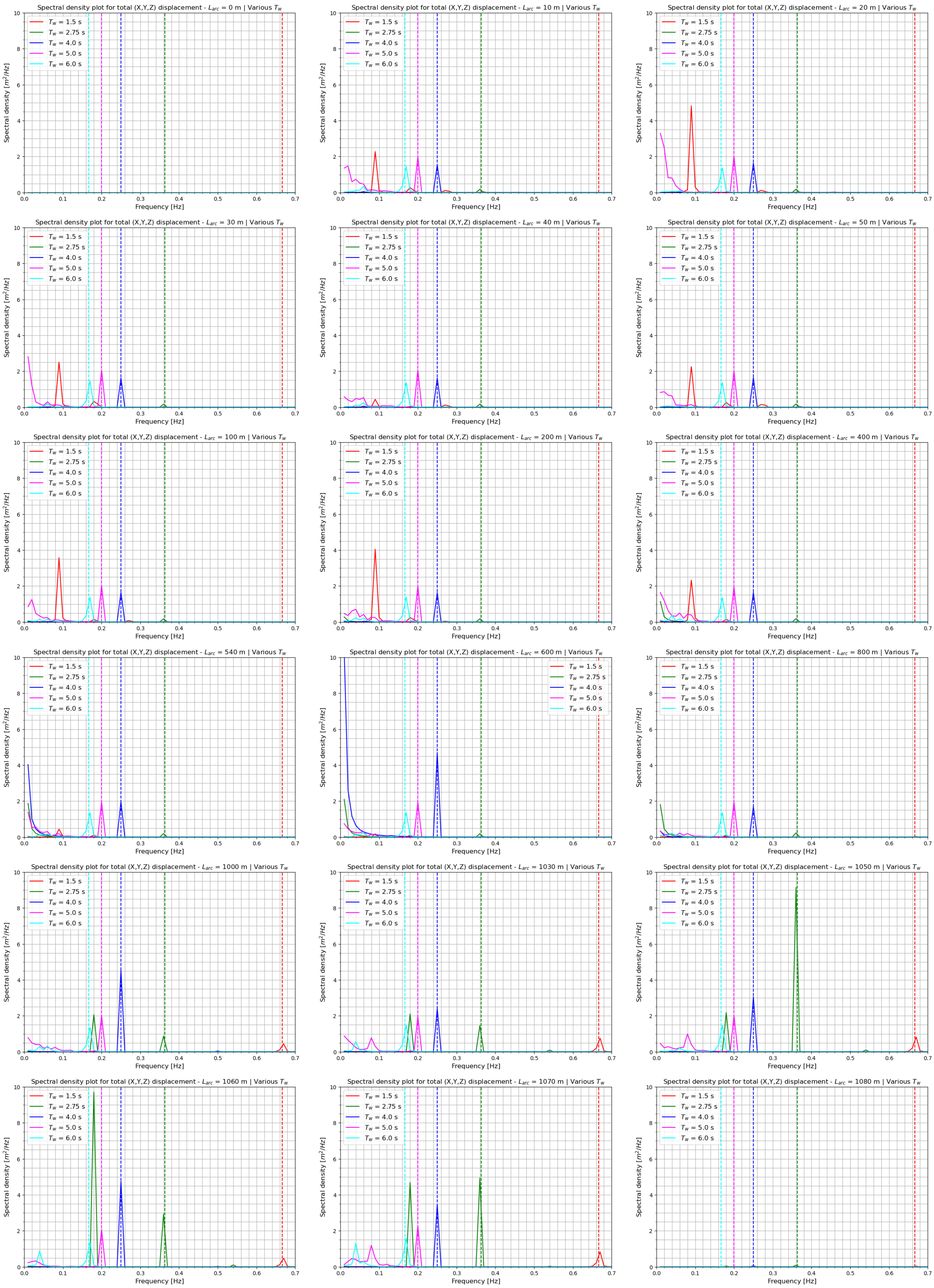

Figure F.1: Spectral density of total displacement for various T_w and a range of cable-floater-system positions L_{arc} for $5000 \leq T_{sim} \leq 6000$ s

F.2. Range graphs for X, Y, Z positions

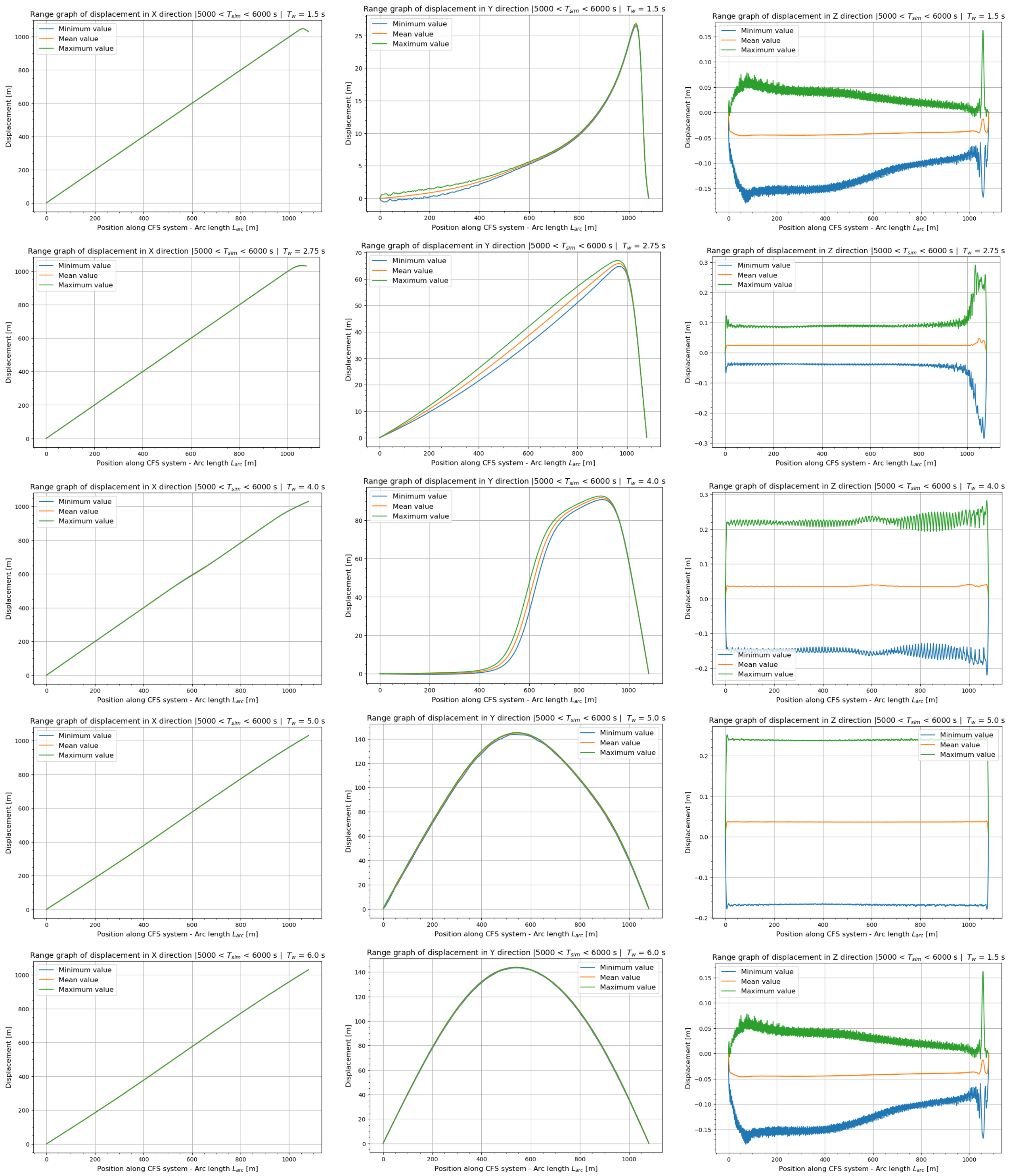

Figure F.2: Range graphs for X, Y and Z position for $5000 \leq T_{sim} \leq 6000$ s for various wave periods T_w


Delft University of Technology